Distinct effects of tubulin isotype mutations on neurite growth in *Caenorhabditis elegans*

Chaogu Zheng[a,1], Margarete Diaz-Cuadros[a,1], Susan Laura Jao[a], Ken C.Q. Nguyen[b], David H. Hall[b], and Martin Chalfie[a,*]

[a] Department of Biological Sciences, Columbia University, New York, New York, 10027, U.S.A.
[b] Department of Neuroscience, Albert Einstein College of Medicine, Bronx, NY 10461, U.S.A.

*To whom correspondence should be sent at:
Department of Biological Sciences
1012 Fairchild, MC#2446
Columbia University
1212 Amsterdam Avenue
New York, NY 10027

Phone: 212-854-8870
Fax: 212-865-8246
Email: mc21@columbia.edu.

[1] These authors contributed equally to the work.

Abstract

Eukaryotic genomes contain multiple tubulin isotypes, and their dominant missense mutations cause a range of neurodevelopmental defects. Using the *C. elegans* touch receptor neurons, we analyzed the effects of 67 missense mutations in tubulin genes on neurite growth. Three types of mutations emerged: 1) loss-of-function mutations causing mild defects in neurite growth; 2) antimorphic mutations, which map to the GTP binding site and intradimer and interdimer interfaces and significantly reduced MT stability, causing severe neurite growth defects; 3) neomorphic mutations, which map to the exterior surface and increased MT stability, causing ectopic neurite growth. Importantly, we engineered several disease-associated human tubulin mutations into *C. elegans* genes and examine their impact on neuronal development. We also discovered a MT-destabilizing α-tubulin isotype, whose loss led to the formation of hyperstable MTs and the generation of ectopic neurites; the lack of potential sites for polyamination and polyglutamination may be responsible for this destabilization.

Introduction

Microtubules (MTs) play important roles in many aspects of neurite development, including the formation, extension, guidance, and maintenance of neurites (reviewed in Dent et al. 2011; Prokop 2013; Sainath and Gallo 2015). The “search and capture” model (Mitchison and Kirschner 1984) suggests that the dynamic instability of MTs allows them to explore the growth cone periphery until they are captured by stabilized actin filaments or membrane receptors enriched at the side of the growth cone responding to a guidance cue (Tanaka et al. 1995; Challacombe et al. 1996; Schaefer et al. 2008; Qu et al. 2013). This capture transiently stabilizes MTs against catastrophe and enables MT elongation in the direction that the growth cone has turned. In addition to providing physical support for the neurite growth that follows the changes

in actin dynamics, MTs also play an instructive role for neurite guidance. Since local application of the MT-stabilizing drug paclitaxel (also known as taxol) induced growth cone attraction and of the MT-destabilizing drug nocodazole induced repulsion (Buck and Zheng 2002), signals that act by altering MT stability appear to directly initiate growth cone turning. Indeed, the guidance molecule Wnt can induce growth cone remodeling by changing the organization of MT structure through the inactivation of MT-plus end binding protein Adenomatous Polyposis Coli (Purro et al. 2008). These results indicate that the regulation of MT dynamics is crucial for neurite growth and guidance, but how MT stability is controlled either locally at specific sites of the growth cone or globally in the entire neuron is not well understood.

As the building blocks of MTs, α- and β-tubulins are crucial determinants of MT stability. Eukaryotic genomes contain multiple tubulin genes encoding different isotypes (Sullivan 1988; McKean et al. 2001) that are expressed in spatially and temporally distinct patterns (Leandro-Garcia et al. 2010). Different tubulin isotypes confer specific dynamic properties on MTs in tubulin polymerization assays *in vitro* (Panda et al. 1994) and are not functionally equivalent *in vivo* in Drosophila (Hoyle and Raff 1990) or in single-celled organisms, such as *Tetrahymena thermophile* (Pucciarelli et al. 2012). These observations support the "multi-tubulin hypothesis," which proposes that distinct tubulin isotypes impart specific properties onto MTs, so they can perform particular cellular functions (Fulton and Simpson 1976; Cleveland 1987). Moreover, tubulins also undergo a range of complex post-translational modification, which affect the dynamics of MTs and their interaction with other proteins (reviewed by Song and Brady 2015). In neurons specifically, stable axonal MTs are more detyrosinated, acetylated, and glutamylated, whereas the dynamic MTs in the growth cone are more tyrosinated (Liao and Gundersen 1998; Konishi and Setou 2009). Tubulin isotypes and modifications at the C-terminal tail also control

the velocity and processivity of MT motor proteins and microtubule depolymerization rates *in vitro* (Sirajuddin et al. 2014). Therefore, post-translational modifications on different tubulins by a set of enzymes may generate a "tubulin code" that can be read by microtubule-associated proteins (MAPs), which regulate the organization of MTs and their interaction with other cellular components (Verhey and Gaertig 2007; Yu et al. 2015).

The clinical importance of tubulin genes in the development of the nervous system has been highlighted by the recent finding that patients carrying mutations in α- and β- tubulin genes showed microcephaly, lissencephaly, pachygyria, and other cortical malformations, as well as a range of axon guidance defects, including agenesis or hypoplasia of the corpus callosum, internal capsule, commissural fibers, and corticospinal tracts, depending on the mutations (Tischfield et al. 2011). So far, based on three summaries (Bahi-Buisson et al. 2014; Liu and Dwyer 2014; Chakraborti et al. 2016), 60 point mutations in α-tubulin genes (51 in TUBA1A, 1 in TUBA3E, and 8 in TUBA4A), one splicing-affecting intronic deletion in TUBA8, 48 point mutations in β-tubulin genes (2 in TUBB2A, 24 in TUBB2B, 19 in TUBB3, and 3 in TUBB5), and one exonic deletion in TUBB2B are known to cause tubulin-related neurological disorders in heterozygous carriers (Table S4); all mutations, except for the TUBA8 deletion, appear to have dominant-negative effects. Although mutated residues are found throughout the molecules, many are found in region predicted to mediate either GTP binding, heterodimer stability, inter-dimer interaction, or association with motor proteins and other MAPs (Tischfield et al. 2011). Despite some *in vitro* studies on the effects of the mutations on tubulin folding, heterodimer assembly, and MT growth (Jaglin et al. 2009; Tian et al. 2010; Tischfield et al. 2010), very few *in vivo* studies can systematically test how these different tubulin mutations impact axon guidance and extension in

living organisms. Moreover, the complexity of the mammalian nerve system makes the analysis of the developmental consequences of these tubulin mutations very difficult.

Here, we use the morphologically simple and well-defined touch receptor neurons (TRNs) in the nematode *Caenorhabditis elegans* to model the effects of tubulin mutations on neurite growth. By analyzing a large collection of missense mutations in several tubulin genes, we found that these mutations caused three morphologically distinct defects in TRN neurite outgrowth: 1) the shortening of all TRN neurites; 2) the specific shortening of posteriorly-directed neurites; and 3) the production of ectopic posteriorly-directed neurites. The structural location of the mutated residue correlated with the resulting phenotype. Many tubulin mutations characterized in our study affect the same amino acid residue or region as the disease-causing mutations. We generated several such human mutations in *C. elegans* tubulin genes through genome editing and found that they also caused distinct neurite growth defects that fall into the above categories. Thus, our system may be used to understand the different effects of the clinically identified tubulin mutations and to facilitate their classification. Moreover, we found that null mutations in two α-tubulin genes led to very different phenotypes, supporting the hypothesis that tubulin isotypes perform specific and often non-overlapping roles in neurite development.

Results

A genetic screen for TRN neurite growth defects

The six mechanosensory TRNs (ALML/R, PLML/R, AVM, and PVM) in *C. elegans* are a useful model to study axonal outgrowth and guidance because of their well-defined morphology (Chalfie and Sulston 1981). The ALM and PLM neurons are two pairs of embryonically derived, bilaterally symmetric cells, whereas the AVM and PVM neurons arise from postembryonic lineages. All six neurons have a long anteriorly-directed neurite (AN); in

addition, the two PLM neurons have a posteriorly-directed neurite (PN), making them bipolar. Except in PVM, the AN branches at its distal end; we refer to this branch as the synaptic branch.

Previous studies had identified several components needed for proper TRN outgrowth: UNC-6/Netrin (Hedgecock et al. 1990), LIN-44/Wnt proteins (Hilliard and Bargmann 2006), and a few other signaling molecules (Du and Chalfie 2001). To systematically search for genes involved in the regulation of neurite growth, we performed an extensive genetic screen to isolate mutants with defects in TRN neurite extension. We mutagenized a strain (TU4069) carrying the *uIs134* transgene, which allows RFP expression from the TRN-specific *mec-17* promoter, and screened the progeny of individual F1 animals representing 20,200 haploid genomes. Although we focused on isolating mutants whose TRNs had morphological defects, we also obtained mutants with abnormal numbers of fluorescently labeled cells. This screen yielded 80 mutants. We identified the phenotype-causing mutations for 62 mutants; the remaining mutants either were of low penetrance (7) or did not yield a confirmable mutation (11). The characterized mutations represented 26 genes. Mutations in 8 genes caused the loss of TRN marker expression or its expression in extra cells, and mutations in 2 genes specifically affected the development of the postembryonic AVM and PVM neurons (Table S1); most of these mutant phenotypes were previous described and thus are not discussed here. Mutations in the remaining 16 genes resulted in various TRN neurite extension defects, which were organized into seven phenotypic categories (A-G, Table S2). This screen is likely to be near saturation because 1) the number of haploid genomes examined is 10 times the reciprocal of the average mutation rate (5×10^{-4}) for null alleles (Brenner 1974); and 2) nine of the ten genes represented by multiple alleles had three or more alleles.

The 16 genes whose products regulate neurite outgrowth and guidance (Table S2) encode proteins that affect either extracellular signaling to the TRNs, intracellular signaling, or effectors that are directly involved in cytoskeleton rearrangement and growth cone movement. Molecules affecting extracellular signaling include the guidance protein LIN-44/Wnt and its receptor LIN-17/Frizzled, and three proteins, UNC-23, MUA-3, and SUP-26 not acting within the TRNs. PLM neurites in *lin-44* and *lin-17* mutants failed to navigate towards the anterior (category D) because of the repellent activity of the Wnt signal (Hilliard and Bargmann 2006; Zheng et al. 2015a). *unc-23* (category G) and *mua-3* (category B) are only expressed in muscle cells (Bercher et al. 2001; Papsdorf et al. 2014), and their mutant phenotypes could not rescued by TRN-specific expression of the wild-type gene. Similarly, mutations in *sup-26* (category B), which encodes a RNA-binding protein and is expressed in most somatic cells (Mapes et al. 2010), could not be rescued by TRN-specific expression of the wild-type gene. We have not investigated how these molecules affect neurite outgrowth and guidance in a non-cell autonomous manner.

Genes encoding molecules that are presumably involved with intracellular signaling include *unc-51*, *mec-15*, *dsh-1*, *egl-5*, *unc-73*, and *tiam-1*. *unc-51* encodes a serine/threonine-protein kinase; mutation of *unc-51* caused general outgrowth and guidance defects (category A; Du and Chalfie 2001). *mec-15*, which is needed for touch sensitivity (Au and Chalfie, 1989), encodes a F-box protein with WD repeats and so is likely to mediate ubiquitination and protein degradation (category E; Bounoutas et al. 2009b). Mutation of *mec-15* caused shortening of both PLM neurites. We previously reported that DSH-1/Dishevelled (category B) negatively modulates the activity of Wnt signaling to allow posterior outgrowth against the Wnt gradients (Zheng et al. 2015a) and that *egl-5* (category B), which encodes a Abd-B-like Hox transcription factor, promotes PLM differentiation by inducing the growth of PLM-PN and at least one

downstream effector (Zheng et al. 2015b). We also identified guanine nucleotide exchange factors (GEFs) [UNC-73/Trio (category E) and TIAM-1 (category B)], which controls neurite extension towards the anterior and posterior, respectively (Zheng et al. 2016).

In this study, we describe the role of the downstream effectors of directional neurite outgrowth, the presumed targets of extracellular and intracellular signaling: primarily tubulin isotypes (MEC-7/β-tubulin, MEC-12/α-tubulin, and TBA-7/α-tubulin) and kinesin motor proteins (KLP-7 and KLP-11). MEC-7 and MEC-12 are expressed at high levels in the TRNs (Hamelin et al. 1992; Mitani et al. 1993), which contain large diameter (15-protofilament, 15-p) MTs instead of the typical 11-protofilament (11-p) MTs found in all other cells (Chalfie and Thomson 1979; Savage et al. 1994). Combining the alleles isolated in our screen, created through genome editing, and previously obtained by our lab (Savage et al. 1994) and the million mutation project (Thompson et al. 2013), we collected in total 78 alleles representing 48 different missense mutations in *mec-7* and 19 in *mec-12* (Table 1) and found that these mutations led to various outgrowth defects (category A, B, and C defined in Table S2).

mec-7/β-tubulin, but not _mec-12_/α-tubulin, is needed to form 15-p MTs

Previous studies suggested that the α-tubulin MEC-12 and the β-tubulin MEC-7 form the TRN-specific 15-p MTs that assemble into bundles to fill up the TRN neurites and are required for the mechanosensory functions of TRNs (Chalfie and Thomson 1979; Chalfie and Au 1989; Savage et al. 1994; Bounoutas et al. 2009a). We first examined the MT structures of the *mec-12(tm5083)* and *mec-7(ok2152)* deletion alleles using electron microscopy (EM; Figure 1A and S1). *mec-12* and *mec-7* knockout animals had on average 7 and 6 MTs, respectively, in a cross section of the ALM neurite compared to 31 MTs in the wild type animals (Figure 1B). MTs in *mec-12(tm5083)* animals had the same diameter as the 15-p MTs in the wild-type animals,

whereas the diameter of MTs in *mec-7(ok2152)* animals was much smaller (16.6 nm; Figure 1). These results suggest that although the abundance of MTs is dependent on both MEC-12 and MEC-7, the formation of 15-p MTs requires MEC-7 but not MEC-12; other α-tubulin genes may compensate for the loss of MEC-12. In the absence of MEC-7, however, the 15-p MTs in TRNs are replaced by smaller, presumably 11-p, MTs.

The *mec-7* result is similar to our previous observations on *mec-7(e1506)* animals (the *e1506* mutation alters the start codon and results in no detectable mec-7 mRNA; Chalfie and Thomson 1982; Savage et al. 1994). In contrast, the *mec-12* result was unexpected, because the *mec-12[(e1607* (G144S)*]* allele, which was regarded as the null allele in several previous studies (Bounoutas et al. 2009a; Bounoutas et al. 2011; Hsu et al. 2014), had very few (~2) MTs, all of which had the small diameter (Chalfie and Au 1989; also this study). We found that *e1607* and several previously characterized missense alleles were in fact antimorphic (*anti*) gain-of-function alleles and their phenotypes in neurite growth was also different from the *mec-12* loss-of-function (*lf*) mutants (see below).

Loss-of-function mutations in *mec-7*/β-tubulin but not *mec-12*/α-tubulin cause defects in posteriorly directed neurite growth

To test whether MEC-12 and MEC-7 were needed for neurite growth, we examined the outgrowth in animals with *mec-12* and *mec-7* null alleles. No defects in TRN outgrowth were found in animals mutant for four presumably null *mec-12* alleles [the knockout allele (*tm5083*) and three frameshift mutations (*u1026*, *u1027*, and *u1028*; Figure S1A)] (Figure 2). These results suggest that MTs made without MEC-12 can still respond normally to guidance cues and support neurite morphogenesis. Because *C. elegans* genome contains nine α-tubulin genes, other tubulin isotypes may compensate for the loss of MEC-12. One such candidate is TBA-7/α-tubulin,

which is expressed and functions in TRNs (see below); however, *mec-12; tba-7* double mutants were still capable of forming and growing normal TRN neurites, suggesting further genetic redundancy.

Null mutations in *mec-7* (*ok2152*, *u156*, and *u440*; Figure S1B) only slightly affected the growth of anteriorly-directed neurites but markedly shortened the PLM-PN (Figure 2B). This result suggests that PLM-AN and PLM-PN, which arise at the same time in the embryo, have different tubulin requirements. Normally the PLM-AN extends anteriorly past the vulva to within 50 μm of ALM cell body. Lockhead et al. (2016) reported that the gap between the end of PLM and ALM cell body was wider in *mec-7 lf* mutants due to the shortening of the PLM-AN (Lockhead et al. 2016). We also found a similar modest widening of the gap in *mec-7(ok2152)* animals, but 92% of the PLM-ANs still extended beyond the vulva (Figure 2B and D). Moreover, no shortening of the ALM-AN was seen. A more penetrant and striking defect, however, was the fact that 78% of PLM-ANs in *mec-7(ok2152)* lacked a synaptic branch, which normally arises posterior to the vulva (Figure 2A and S2). In our analysis, 12 missense mutations (Table 1), including the newly isolated *u1020* (G34S) allele, caused a similar *mec-7* null phenotype.

The above results and EM data suggest that 1) the reduction of MT numbers in *mec-12 lf* mutants does not affect neurite development; 2) the smaller, generic 11-p MTs in *mec-7 lf* mutants are capable of supporting general neurite growth in TRNs; 3) the presence of 15-p MTs is essential for the normal extension of PLM-PN.

In addition to neurite growth, MTs are important for many other functions in TRNs, which were studied before using a few *mec-12* and *mec-7* missense alleles (Bounoutas et al. 2009a; Hsu et al. 2014). In this study, we systematically confirmed their phenotypes using the knockout mutants and also compared the null alleles with *gf* alleles for those phenotypes (Figure

3). Deletion of either *mec-12* or *mec-7* resulted in touch insensitivity, defects in the localization of pre-synaptic vesicles, and severe loss of MT acetylation, a mark for stable MTs. Since MEC-12 is the only α-tubulin isotype that contains the acetylation site (lysine 40) in *C. elegans*, the TRN-specific 15-p MTs are likely the only MTs that can be acetylated. The loss of *mec-7* and *mec-12* also induced a global reduction in protein levels through a mechanism dependent on the dual leucine zipper-bearing kinase DLK-1 (Bounoutas et al. 2011). Interestingly, mutations in *dlk-1* restored the normal protein expression in *mec-7* and *mec-12* null mutants but failed to rescue the PLM-PN growth defects in *mec-7(ok2152)* animals (Figure 3D). Therefore, this PLM-PN defect is most likely a direct effect of the loss of MEC-7 and not the result of secondary changes in protein levels.

Several *mec-12* partial *lf* mutations affected only a subset of MT functions. *mec-12(e1605)* animals carrying the H192Y missense mutation were defective in mechanosensation but had retained normal 15-p MT structures, tubulin acetylation, axonal transport, protein levels, and neurite growth patterns (Figure S3; Bounoutas et al. 2009a). Similarly, *mec-12* mutants carrying the *u63* (E415K) or *gm379* (G416E) alleles were partially touch-insensitive but kept the large dimeter MTs; however, these animals showed mistargeting of synaptic vesicles presumably because alterations in the EEGE (amino acid 414-417) motif increased affinity with the motor dynein (Hsu et al. 2014). *u63* and *gm379* mutations also caused a slight decrease in tubulin acetylation and a partial reduction in protein production; *gm379* allele led to very mild defects in the growth of PLM-PN (Figure S3). These mutations may be useful in understanding some specific aspects of MT functions.

Antimorphic mutations in *mec-7*/β-tubulin led to severe, general defects in neurite outgrowth

We identified 19 strong *mec-7*(*anti*) gain-of-function missense mutations (Table 1) that caused severe shortening of all TRN neurites (Figure 2B); the ALM-AN did not reach the pharynx, the PLM-AN terminated before reaching the PVM cell body and the PLM-PN was shortened (Figure 2D). We also identified 4 weak *mec-7(anti)* mutants (Table 1), in which ALM-AN did not extend beyond the nerve ring and PLM-AN did not reach the vulva. All of these alleles, except the recessive *u430* (A97V) mutation, were either dominant or semi-dominant. Early studies of one of the dominant *mec-7* alleles, *e1343* (P171L), found that the mutants contained very few (2.8 ± 0.5 in a cross section) MTs (Chalfie and Thomson 1982), which suggests that the *anti* mutations may block MT polymerization and thereby cause the severe neurite outgrowth defects. In fact, when compared to the *mec-7(ok2152)* null allele, these *anti* mutations caused stronger defects not only in neurite outgrowth, but also in touch sensitivity, synaptic vesicle transport, tubulin acetylation, and protein expression levels (Figure 3). Mutations in *dlk-1* could block the reduction in global expression but failed to rescue the neurite growth defects (Figure 3D).

The amino acid residues mutated in the antimorphs are located in three regions on the structure of an αβ tubulin dimer determined by electron crystallography (Nogales et al. 1998): 1) the GTP/GDP binding pocket, 2) the intradimer interface, and 3) the lateral or longitudinal interdimer interface. All of which are important for tubulin polymerization. For example, *u430* (A97V), *u911* (P171S), *u957* (P171L), and *u262* (N226Y) mutations alter amino acids in direct contact with the GTP molecule, and *u48* (S176F) and *u449* (V179A) change amino acids in the B5 (the fifth β-strand)-to-H5 (the fifth α-helix) loop, which is crucial for forming the GTP/GDP binding pocket (Figure 4C). Two other mutations *u445* (M300V) and *u98* (M300T) substitute

M300, which is located in a loop near the GTP binding site and may participate in positioning H7 (the seventh α-helix) with its critical N226, and thus indirectly affect GTP binding.

The second group of mutated residues in *mec-7(anti)* alleles is located in the intradimer interface, where β-tubulin makes contact with α-tubulin to form the heterodimer (red residues in Figure 4D). *u283* (P243L), *u958* (G244S), *n434* (N247I), and *u162* (D249N) mutations all affect the residues on the H7-to-H8 loop, which interacts extensively with residues on H1 and H2 of α-tubulin. Two other dominant mutations *gk286000* (A314V) and *u955* (A352T) changed residues that located on B8 and B9, respectively, which are physically adjacent to the H7-to-H8 loop at the interface. In addition, two prolines mutations, *u910* (P357L) and *u956* (P358L) possibly disrupted the B9-to-B10 loop (a.a. 356-361) critical for the positioning of B9.

The third group of *mec-7(anti)* alleles include *e1527* (V286D), *u18* (A393T), and *gk285997* (A393V), which affect residues involved in the lateral (V286) and longitudinal (A393) interdimer interaction between one α/β-tubulin heterodimer and the neighboring one on the MTs. These mutations may interfere with the interaction between tubulin dimers.

Overall, the above β-tubulin antimorphs act as dominant-negative mutants by forming a poisonous α/β dimer, whose incorporation into MTs could terminate MT polymerization and induce instability; the mutated β-tubulin either cannot properly bind to GTP (the first group) or form misshaped α/β heterodimers that block the growing end of MTs (the second group) or disrupt the stacking of tubulin dimers (the third group). Therefore, changes in tubulin structure led to compromised MT elongation, which caused severe defects in neurite outgrowth, highlighting the importance of functional MTs in neuronal morphogenesis.

Antimorphic mutations in *mec-12*/α-tubulin led to specific defects in posteriorly directed neurite growth

Similar to the *mec-7(anti)* mutations, we identified 5 *mec-12(anti)* mutations that also mapped to the GTP binding pocket [*u76* (D69N), *u950* (S140F), and *u1021* (G144S); labeled in red in Figure 4B], the intradimer interface [*u1016* (E97K); Figure 4D], or the interdimer interface [*u1019* (G354E)]. However, these *mec-12* antimorphs are mostly recessive, except for *u1019*, and did not cause strong, general defects in TRN neurite outgrowth. Instead, these mutations led to the specific shortening of PLM-PN, similar to the defects observed in *mec-7* null animals. Electron microscopy studies revealed that the *mec-12(anti)* mutants have very few small diameter MTs (*e.g.* ALM neurons in *u1021* animals had on average 2.7 MTs in a cross section and 15% of the 72 sections examined had no MTs; the diameter of MTs was 17.9 nm on average; Figure 1B). Therefore, *mec-12(anti)* mutations have distinct phenotypes from the *lf* alleles, which retained 15-p MTs and had no defects in neurite formation. The *e1607* (G144S) allele, which was previously thought to be a null allele, had the same molecular lesion as antimorph *u1021* and caused the shortening of PLM-PN (Figure 2E) and the loss of 15-p MTs (Chalfie and Au 1989); these results further confirm that *e1607* should not be regarded as a *lf* allele.

In addition, the *mec-12* antimorphs also resulted in touch insensitivity, reduction in tubulin acetylation, synaptic vesicle mistargeting, and decrease in TRN protein levels; these phenotypes were much stronger than the phenotypes of *mec-12* null alleles and were comparable to those produced by *mec-7* null mutations but not *mec-7 anti* mutations (Figure 3). One possible explanation for this phenotype is that MEC-12/α-tubulin preferentially or exclusively binds to MEC-7/β-tubulin, and MEC-12 mutant proteins could only sequester and disable MEC-7 but not other β-tubulin isotypes. As a result, either *anti* mutations in *mec-12* or *lf* mutations in *mec-7* could eliminate the specialized, large diameter, stable MTs that require the MEC-12/MEC-7 heterodimer, but neurite growth could still be supported by regular MTs formed with other α-

and β-tubulin isotypes. Consistent with this hypothesis, *mec-7(lf); mec-12(anti)* double mutants did not show additive effects with regards to the neurite growth defects compared to either single mutant (Figure 2E).

The specific shortening of PLM-PN in *mec-7* null mutants and *mec-12* antimorphs may be caused by higher sensitivity of the posteriorly neurites to changes in microtubule stability compared to the anteriorly directed neurites. The normal 15-p MTs exist in great numbers and form bundles, which may provide stronger support for neurite growth than the few 11-p MTs found in the mutants. In fact, treatment with the MT-destabilizing drug colchicine (1mM) led to a similar shortening of the PLM-PN, phenocopying these mutations (Figure S4).

Neomorphic mutations in *mec-7* and *mec-12* resulted in the growth of ectopic neurites

A third category of *mec-7*/β-tubulin mutations resulted in novel phenotypes, different from the effects of either *mec-7 lf* or *anti* mutations; these neomorphic (*neo*) alleles caused the growth of an extra posteriorly directed neurite in ALM neurons, as well as the overextension of the PLM-PN. Three such alleles [*u170* (E407K), *u278* (C303Y), and *ky852* (P220S)] were previously reported (Savage et al. 1994; Kirszenblat et al. 2013), and three more [*gk895768* (T149I), *gk286003* (R162Q), and *u1017* (L377F)] were identified in this study. L377 and E407 are located on the H11 and H12 helices, respectively, both of which are on the exterior side of MTs and may, therefore, bind motor proteins and other MAPs (Figure 4E). R162 on the H4-to-B5 loop and C303 on the H9-to-B8 loop are also exposed on the MT surface, whereas T149 and P220 are located inside the tubulin structure and may be important for the folding of the protein. Among these six alleles, *u278* (C303Y) produced the strongest phenotype; the ectopic posterior neurite of ALM neurons often extended posteriorly to the PLM cell body (Figure 2B).

Interestingly, the C303S mutation in allele *gk286001* did not lead to similar excessive growth (Table 1), suggesting that tyrosine's bulky phenolic ring may be responsible for the phenotype.

We also found four *mec-12*/α-tubulin *neo* alleles [*gk170196* (P32S), *gk915672* (E196K), *u917* (V260I), *gk515972* (V323I)], which generated similar but less severe phenotypes than the *mec-7(neo)* alleles, since the ectopic ALM-PN was shorter in the *mec-12* mutants than in the *mec-7* mutants (Figure 2F). This observation supports the notion that MEC-12 may be less critical than MEC-7 in controlling MT dynamics and neurite growth. E196 and V260 are located on loops on the exterior surface, whereas P32 and V323 may be involved in protein folding (Figure 4F).

The production of the ectopic ALM-PN requires both *mec-7* and *mec-12*. The *mec-12* null alleles suppressed the ALM posterior outgrowth in *mec-7(neo)* mutants, and *mec-7 lf* mutation similarly suppressed the effect of *mec-12(neo)* alleles (Figure 6A). We also conducted a suppressor screen to search for mutations that can suppress the strong phenotype of ALM-PN growth in *mec-7(u278 neo)* mutants. After screening 16,000 haploid genomes, we isolated three suppressors: 1) an intragenic mutation in *mec-7* [*u1040* (G98E)], 2) a *lf* mutation in *mec-12* [*u1041* (G246E)], and 3) a *lf* mutation in *mec-15* [*u1042* (R27*)]. The identification of *mec-7* and *mec-12* mutations as suppressors suggests that the incorporation of the MEC-7/MEC-12 heterodimers into the MTs is required for the generation of the excessive neurite; the role of *mec-15*, which codes for an F-box protein with WD repeats, is described below.

Neomorphic mutations in *mec-7* and *mec-12* increase MT stability

These neomorphic tubulin mutations appeared to increase the stability of MTs, as first suggested by KIRSZENBLAT *et al.* (2013) for *mec-7*. Supporting this hypothesis, pharmacological stabilization of MTs with paclitaxel induced the growth of ALM-PN, although at a low

frequency (Kirszenblat et al. 2013), and destabilizing MTs with colchicine can partially suppress this ectopic growth in *mec-7(ky852)* mutants (Kirszenblat et al. 2013) and in *mec-7(u278)*, *mec-7(u1017)*, and *mec-12(u917)* animals (Figure 6A). Moreover, these mutants also showed increased tubulin acetylation (Figure 3C), an indication of stable MTs (Song and Brady 2015). *mec-7(u278)* and *mec-7(u170)* mutants had large diameter MTs (slightly larger than in wild-type cells), but fewer of them (Figure 1B). Moreover, the MT bundles in the mutants are more closely spaced than the wild type and are not surrounded by the electron-lucent region seen in the wild type (Savage et al. 1994); we quantified these differences by showing that the distance between two closest center points of MTs is smaller in *mec-7* neomorph compared to the wild type and that MTs occupied a bigger proportion of the cross-sectional area of the neurite in the mutants (Figure 1B). In fact, the TRN neurite in these mutants is about 50% thinner than the wild type animals. The observation that tightly packed 15-p MT bundles filled up most of the space in the TRN neurites is consistent with increased MT stability, which presumably allowed the excessive neurite growth towards the posterior, overcoming the normal inhibition of this growth in the wild-type ALM neurons.

Another line of evidence indicating higher stability of MTs in *mec-7* and *mec-12* neomorphs came from their increased resistance to colchicine. This MT-destabilizing drug caused the similar level of reduction in both touch insensitivity and PLM-PN length at a higher concentration in the *neo* mutants than in the wild type animals (Figure S4). Because the majority of the altered residues in the *neo* alleles are located on the exterior surface of MTs, these mutations may interfere with the binding of motor proteins or MAPs to the MTs and therefore cause changes in MT stability.

The *mec-7* and *mec-12 neo* alleles also caused some of the same phenotypes that *lf* mutations do, such as touch insensitivity, synaptic vesicle mistargeting, and reduced TRN protein levels, suggesting that an optimal stability of MTs is needed for their proper functions. Furthermore, the fact that these phenotypes can occur in conjunction with either impaired (in *anti* mutants) or excessive (in *neo* mutants) neurite growth support to the hypothesis that the role of MTs in regulating neurite development is genetically separable from other MT functions.

Modeling the effects of tubulin mutations using the TRN neurites

Our genetic analysis shows that missense mutations in tubulin genes can have distinct effects on MT stability and neurite growth pattern, and those different phenotypes appear to correlate with the positions of the altered residues in the tubulin structure. Such structure-function analyses were carried out before for yeast α-tubulin TUB1 and for Drosophila testis-specific β-tubulin βTub85D (Fackenthal et al. 1995; Richards et al. 2000) but not for tubulins in the nervous system. Moreover, recent discovery of over a hundred missense mutations in tubulin genes in patients with a range of neurological disorders prompted us to examine the cellular impact of specific tubulin mutations on neurons. Combining the convenience of genome editing in *C. elegans* and the ease of observing TRN morphology as the readout of MT stability and neurite growth, we could systematically study the effects of those human tubulin mutations. To provide proof of concept, we generated five clinically observed β-tubulin mutations (S172P, P173L, A302T, P380S, and E410K) in *mec-7* through CRISPR/Cas9-mediated gene editing (Materials and Methods; Figure 5A) and found that these mutations indeed caused distinct phenotypes on TRN morphogenesis.

S172P and P173L mutations in human TUBB3 were found in heterozygous patients with microcephaly, polymicrogyria, cortical dysplasia, and agenesis of the corpus callosum, which are

defects in neuronal migration and axon growth (Jaglin et al. 2009; Poirier et al. 2010; Bahi-Buisson et al. 2014). *In vitro* studies found that tubulin heterodimer containing the β-tubulin S172P mutant could not be incorporated into MTs (Jaglin et al. 2009), indicating that the mutated protein is nonfunctional. Consistent with these findings, the *u1056* (S172P) mutation of *mec-7* led to a recessive *loss-of-function* Mec-7 phenotype in the TRNs, which showed significantly shortened PLM-PN and slightly shortened PLM-AN with branching defects (Figure 5B). Surprisingly, the *u1057* (P173L) allele did not cause any TRN morphological or functional defects. The difference between the mutant phenotypes in humans and worms is puzzling, since both S172 and P173 are located on the GTP binding B5-to-H5 loop (Figure 4C), which is identical in *C. elegans* MEC-7 and human TUBB3 (Figure S5). Perhaps the differences arise from differences in MT structure and organization: the *C. elegans* TRNs have 15-p MTs that are bundled, whereas human neurons have 13-p MTs that are not bundled.

Heterozygous A302T and R380C mutations in human TUBB3, which affect residues on the external surface of the MTs, were associated with moderate congenital fibrosis of the extraocular muscles 3 (CEFOM3), anterior commissure hypoplasia, and corpus callosum hypoplasia. Mutation of A302 and R380 in yeast led to the formation of highly stable, benomyl-resistant MTs (Tischfield et al. 2010). Consistent with these observations, we found that the same mutations of MEC-7 produced a *neo* phenotype (the generation of an ectopic ALM-PN; Figure 5B).

TUBB3 E410K mutation was also found in patients with severe CEFOM3 and hypoplasia of anterior commissure and corpus callosum, but these patients also suffer from facial weakness and progressive axonal sensorimotor polyneuropathy (Tischfield et al. 2010). In yeast, MTs containing β-tubulin with the E410K substitution were less stable and less resistant to benomyl

and had markedly decreased plus-end accumulation of kinesin-like motor proteins, compared to MTs with A302T and R380C mutations (Tischfield et al. 2010). In *C. elegans*, MEC-7(E410K) produced a distinct neurite growth phenotype: ALM-AN and PLM-AN, but not PLM-PN were significantly shortened, which indicates reduced MT stability; but the PLM-PN was not affected, making the phenotype also different from that of the *mec-7* antimorphs, which cause general defects in MT polymerization (Figure 5B). Since E410 is also exposed to the exterior of MTs like A302 and R380 (Figure 4E), these results suggest that the cellular impact of the missense mutations would depend on the specific amino acid change instead of the location of the affected residues alone.

The loss of *tba-7/α*-tubulin also caused excessive posterior neurite growth

C. elegans genome contains nine α-tubulin genes (*mec-12*, *tba-1*, *tba-2*, and *tba-4* through *tba-9*) and six β-tubulin genes (*ben-1*, *mec-7*, *tbb-1*, *tbb-2*, *tbb-4*, and *tbb-6*). Our screen yielded mutants in only three of these genes: *mec-7*, *mec-12*, and *tba-7*. The missense *tba-7* allele *u1015* (G92D) caused the growth of an ectopic ALM posterior neurite, resembling the phenotype of *mec-7* and *mec-12 neo* alleles. This *tba-7* allele is likely a *lf* allele, because it failed to complement with *gk787939* (Q230*), which is presumably a null and produced similar phenotype as *u1015* (Figure S1C). We also examined mutants of other tubulin isotypes, and did not find morphological defects in the TRNs (we did not test for redundancy among the genes; Table S3).

tba-7 was expressed in the TRNs, and the excessive growth phenotype of *tba-7(u1015)* could be rescued by expressing *tba-7(+)* from the TRN-specific *mec-17* promoter, indicating that TBA-7 acts cell-autonomously in the TRNs (Figure S6). *tba-7 lf* mutants did not exhibit touch insensitivity, synaptic vesicle mistargeting, or reduced protein levels, suggesting that the general

function of TRN MTs was not affected and that the primary function of TBA-7 is to regulate neurite growth (Figure S7). We hypothesized that the loss of TBA-7 led to the formation of hyperstable MTs, similar to the *mec-7* and *mec-12 neo* mutations. Supporting this hypothesis, electron microscopy studies revealed that, like *mec-7(neo)* mutants, *tba-7(u1015)* animals retained the large diameter 15-p MTs and have closely packed MT bundles, which occupied a larger-than-normal area of a neurite cross-section (Figure 1). *tba-7 lf* mutants also retained normal tubulin acetylation levels (Figure S7C) and had increased resistance to colchicine (Figure S4), which confirmed the presence of stable MTs. Treatment with 1 mM colchicine fully suppressed in the growth of ALM-PN in *tba-7(u1015)* animals, and either *lf* or *gf* mutations in *mec-7* or *mec-12* could do so as well (Figure 6A).

The amino acids sequences of α-tubulin TBA-7 and MEC-12 are 82% identical and 94% similar; they mainly differ in a N-terminal region and the C-terminal tail (Figure 6C). Domain swapping experiments showed that changing L31 of TBA-7 to Q found in MEC-12 or replacing the C-terminal DANDNGD (a.a. 435-441 in TBA-7) sequence with MEDNGEEG (a.a. 440-447 in MEC-12) partially impaired the function of TBA-7 proteins to restrict excessive neurite growth; and TBA-7 proteins with both L31Q mutation and the C-terminal replacement completely lost the ability to rescue the *tba-7 lf* phenotype (Figure 6D). Q31 in MEC-12 is a potential site for polyamination (Song et al. 2013) and E445 of the GEE motif (a.a. 444-446 in MEC-12, but absent in TBA-7) is a target for polyglutamination (Edde et al. 1990). Post-translational modifications at these two sites could increase the stability of neuronal MTs (Song and Brady 2015). Interestingly, replacing the a.a. 35- 47 region of TBA-7 with the sequence from MEC-12 that contains lysine 40 (the site for α-tubulin acetylation) did not affect the TBA-7

function (Figure 6D), suggesting that MT acetylation level was not responsible for the ectopic neurite growth.

Since TBA-7 lacks some modification sites (e.g. Q31 and E445) that could stabilize MTs, our results suggest that TBA-7 may be a MT-destabilizing tubulin isotype, as compared to MEC-12. In wild-type animals, TBA-7 incorporation into the 15-p MTs with MEC-7 and MEC-12 may reduce MT stability; when TBA-7 is not available, more MEC-12 and possibly other α-tubulin isotypes replace TBA-7 and this replacement alters MT dynamics to produces hyperstable MTs.

The *tba-7(u1015 lf); mec-7(u1017 neo)* double mutant had an ALM-PN that was similar in length to that in *mec-7(u1017)* single mutants (Figure 6A), but the double mutant additionally produced up to 4 and 5 short ectopic neurites sprouting from the ALM and PLM cell bodies, respectively; this phenotypes was rarely observed in *mec-7(u1017)* animals (Figure 6E and F). These results suggest that an additive effect occurs in the double mutant. Treating *tba-7(u1015)* and *mec-7(u1017)* single mutants with paclitaxel did not produce the double mutant phenotype, probably because the effect of paclitaxel on neurite growth is weak (Kirszenblat et al. 2013).

Mutations in MT-associated Kinesins affect TRN neurite growth

Since motor proteins and MAPs regulate MT dynamics (Akhmanova and Steinmetz 2015), we expected mutations in MAP genes to cause similar phenotype to those of some of the tubulin mutations. Indeed, Ghosh-Roy et al. (2012) found and we have confirmed that the loss of the MT-depolymerizing kinesin *klp-7* induced the growth of an ectopic posterior neurite in ALM neurons (Figure 6B). KLP-7 belongs to the kinesin-13 family of catastrophe factors that bind to MT plus-ends and promotes depolymerization, thus generating dynamic microtubules (Han et al. 2015). Importantly, as with the tubulin neomorphs, we found that the growth of the ectopic ALM-PN in *klp-7* mutants was suppressed by *mec-7* and *mec-12 lf* mutations but not enhanced

by *mec-7 neo* mutations. These results suggest that the mutated MEC-7 proteins may render MTs hyperstable by reducing their interaction with KLP-7 or by making the MTs insensitive to the action of KLP-7.

Our screen yielded a mutation in a second kinesin gene, *klp-11*. The putative *klp-11* null allele *u1024* (Q53*) caused a moderate shortening of ALM-AN and PLM-AN without affecting PLM-PN; in the mutants, ALM-AN failed to extend beyond the metacorpus of the pharynx and PLM-AN did not reach the vulva (Figure S8). A *klp-11* deletion allele, *tm374*, gave the same phenotype. *klp-11* codes for a homolog of human KIF3B, a subunit of the plus end-directed kinesin-II motor complex. Kinesin-II functions in fast, anterograde axonal transport of vesicles and is thus needed for neurite building (Takeda et al. 2000). These data are consistent with KLP-11 being a positive regulator of neurite growth in TRNs. The selectivity of the *klp-11* effect on the ANs and not the PNs may relate to the polarity of the MTs they contain. MTs in the anterior neurites of TRNs have uniform polarity with all the plus ends oriented outward from the cell body, whereas the MTs in the PLM-PN have mixed polarity, containing both minus-end-out and plus-end-out MTs (Chalfie and Thomson 1979; Hsu et al. 2014). Thus, the use of minus end-directed motor proteins could support the growth of PLM-PN in the absence of KLP-11. Moreover, the moderate shortening of the ANs also suggests redundancy among the kinesin motor proteins. These results support the hypothesis that MTs promote TRN neurite growth by serving as tracks for the transport of membrane-bound vesicles.

The F-box containing protein MEC-15 is required for tubulin neomorphic phenotype

The putative *mec-15* null allele *u1008* (Q194*) was isolated from our main screen because the mutation caused the shortening of both PLM-AN and PLM-PN. Another null allele *u75* (Q118*) caused the same phenotype (Figure 7A). *mec-15* encodes a protein that contains a

F-box at the N-terminus and four WD-40 repeats in the middle. Previous work from our lab found that *mec-15* is required for touch sensitivity and chemical synapse development in TRNs (Bounoutas et al. 2009b). We found that the ALM-AN and PLM-AN in *mec-15* mutants could not fully extend the synaptic branch (Figure 7A), which may have caused the defects in synaptic development.

From the screen for suppressors of *mec-7(u278)* neomorph, we identified another *mec-15* null allele *u1024* (R27*), which strongly suppressed the growth of ectopic ALM-PN in *mec-7(u278 neo)* animals. This suppression is cell-autonomous and depends on the F-box of MEC-15; the expression of the wild-type MEC-15 from the TRN-specific *mec-18* promoter in *mec-15*(*lf*); *mec-7(u278 neo)* double mutants restored the ectopic ALM-PN, but the expression of MEC-15 proteins that lacked or had a truncated the F-box domain could not (Figure 7C and D). Since F-box is the substrate recognition subunit of the Skp, Cullin, F-box containing E3 ubiquitin ligase complex (known as the SCF complex), our results suggest that ubiquitination is involved in stabilizing the MTs in *mec-7(neo)* mutants. One hypothesis is that some unidentified MT-destabilizing molecule is normally ubiquitinated and targeted for degradation in a MEC-15-dependent manner. This unknown protein would be abnormally accumulated in TRNs to reduce MT stability, which caused the shortening of the main neurites and their branches in *mec-15(lf)* single mutants and the suppression of ALM-PN in *mec-15(lf)*; *mec-7(u278 neo)* double mutants; the double mutants no longer have the hyperstable MTs. We also observed similar suppression of the ectopic growth of ALM-PN in *mec-15(lf); mec-7(u1017 neo)*, *mec-15(lf); tba-7(lf)*, and *mec-15(lf); klp-7(lf)* double mutants (Figure 7D), supporting the hypothesis that MEC-15-dependent ubiquitination is needed for the increase of MT stability in the regulation of neurite growth.

Tubulin mutations induce excessive neurite growth independent of MEC-17/α-TAT

Our lab previously reported that the α-tubulin acetyl-transferase (α-TAT) MEC-17, which acetylates MEC-12 in the MTs, is required for the formation of 15-p MTs, as well as MT bundling and organization (Topalidou et al. 2012). Although the loss of MEC-17 does not significantly reduce MT acetylation due to the redundancy with its paralog ATAT-2, *mec-17* null mutants showed defects in touch sensitivity, neurite growth and morphology, and vesicle transport; these defects were rescued by expressing a catalytically inactive version of MEC-17, indicating that non-enzymatic activity of MEC-17 is responsible for normal neurite formation (Topalidou et al. 2012; Neumann and Hilliard 2014).

Although the ALM neurons in *mec-17*(*lf)* mutants also grew an ectopic posterior neurite, the Mec-17 phenotype is quite different from the phenotypes of the *mec-7* or *mec-12 neo* mutants in the following ways. 1) the ALM-PN in *mec-17* animals grows beginning at the L4 stage, whereas it was present as early as the L1 stage in *mec-7* and *mec-12 neo* mutants, and *tba-7* and *klp-7 lf* mutants; 2) the ALM-PN in *mec-17* null mutants was longer at 25 °C than at 15 °C, whereas the opposite was seen in tubulin neomorphs, which have a longer ALM-PN at 15 °C than at 25 °C (Figure 8A); 3) excessive swelling and looping of the TRN neurites were observed in *mec-17* mutants (Topalidou et al. 2012) but not the other mutants; 4) *mec-17* mutants had twice as many actively growing MTs as the wild-type animals, indicating increased dynamics (Neumann and Hilliard 2014), whereas the other mutants presumably caused the formation of hyperstable MTs. Interestingly, treatment with paclitaxel, which decreases MT dynamics, partially suppressed the growth of ALM-PN in *mec-17(lf)* mutants but not in *mec-7* and *mec-12 neo* mutants or *tba-7* or *klp-7 lf* animals (Figure 8B). Moreover, when we combined the *mec-17(ok2109 lf)* allele with the *mec-7(u1017 neo)* allele or *tba-7(u1015 lf)* allele, additive effects were observed for the length of both ALM-PN and PLM-PN (Figure 8C). Together, our data

indicate that the loss of MEC-17 and the mutations in tubulin isotypes may induce excessive, posteriorly directed neurite growth through different mechanisms.

One such difference in mechanism is the differential dependency on the guanine nucleotide exchange factor TIAM-1, which promotes the growth of a posteriorly directed neurite in the bipolar PLM neurons (Zheng et al. 2016). *tiam-1* null mutations suppressed the growth of ALM-PN in *mec-17(lf)* mutants but not in *mec-7* and *mec-12 neo* mutants and *tba-7(lf)* mutants (Figure 8D). Because TIAM-1 promotes neurite extension through the Rac1 GTPase, which presumably regulates the dynamics of actin cytoskeleton (Zheng et al. 2016), the loss of MEC-17 may activate TIAM-1 and induce actin remodeling, whereas the MT-stabilizing tubulin mutations do not evoke TIAM-1 to promote posterior outgrowth.

Discussion

Neuronal morphogenesis requires an optimal MT stability

MTs both support and regulate neurite growth. As the building block of MTs, α- and β-tubulins determine the structural properties of MTs and also mediate their interaction with motor proteins and MAPs. As a result, any alteration in the tubulin proteins can potentially lead to changes in MT dynamics, which then affects neurite formation, guidance, and extension. In this study, we analyzed the effects of 67 tubulin missense mutations on neurite development in *C. elegans* touch receptor neurons. Based on the phenotypes, we categorized these mutations into three classes: loss-of-function (*lf*), antimorphic (*anti*), and neomorphic (*neo*) mutations. 1) *lf* mutations cause only mild neurite growth defects by reducing MT stability moderately; 2) *anti* mutations block MT polymerization and cause severe neurite growth defects; 3) *neo* mutations cause excessive neurite growth by inducing hyperstable MTs (Figure 9). The directionality of the

excessive neurite in ALM reflects its potential to grow towards the posterior. In fact, about 30% of the adult ALM neurons have a very short (less than one cell body length) posterior protrusion, and manipulation of cellular signaling (e.g. activating the small GTPase Rac or altering the recycling endosome pathway) can induce the production of ALM-PN (Zheng et al. 2015b; Zheng et al. 2016). Thus, the ectopic growth of ALM-PN can serve as an indication for globally increased cytoskeletal stability.

The correlation between the amount of neurite growth and the stability of MTs suggests that MT structure and dynamics are major determinants of neurite growth. Given the great number of proteins involved in both positively and negatively regulating MT assembly and disassembly (Mimori-Kiyosue 2011), our results support that an optimal level of MT stability is required for proper neuronal morphogenesis. This hypothesis is further supported by the finding that negative regulators of MT stability, such as the α-tubulin isotype TBA-7 and the MT-destabilizing kinesin-13 KLP-7, prevent excessive TRN neurite growth.

We suspect that other MT destabilizers are also important for TRN neurite development and that these destabilizing proteins are, in turn, regulated by the F-box containing protein MEC-15, perhaps by its involvement in ubiquitination and protein degradation. Loss of *mec-15* results in TRNs with shorter ANs and PNs. Since *mec-15(lf)* is epistatic with regard to neurite growth to the mec-7(*neo)*, *mec-12(neo)*, *tba-7(lf)*, and *klp-7(lf)* mutations, MEC-15 is likely to reduce the amount of, as yet, unknown MT destabilizers.

Structure-function analysis of tubulin mutations

The large number of missense mutations analyzed in this study allowed us to perform structure-function analysis of neuronal tubulin proteins in living animals. Mapping the altered amino acid residues onto the *Bos taurus* tubulin α/β heterodimer structure 1JFF (Nogales et al.

1998), we found that *lf* mutations mostly affect residues located in the interior of the structure and possibly disrupt protein folding. *anti* mutations affect residues that participate in GTP binding, intradimer interaction, or interdimer interactions. *neo* mutations mostly alter residues on the exterior surface and probably perturb the association of motor proteins and MAPs with MTs (Figure 4 and 9).

Although similar structure-function relationship studies were conducted before in yeast α-tubulin *TUB1* and β-tubulin *TUB2* and Drosophila testis-specific *β2*-tubulin (Reijo et al. 1994; Fackenthal et al. 1995; Richards et al. 2000), our work provides another model to study the properties of tubulin proteins. In fact, our findings are consistent with those previous studies. For example, yeast *TUB1* mutations that caused supersensitivity to the MT-destabilizing drug benomyl mainly altered amino acids involved in GTP binding (e.g. D70) and intradimer (e.g. E98) and interdimer interaction; the change of equivalent residues in MEC-12 (D69 and E97) were identified in *mec-12 anti* mutants. Similarly, some Drosophila *β2*-tubulin mutations (S25L and G96E) that made MTs less stable (Fackenthal et al. 1995) affected the same or the adjacent residue in *mec-7* antimorphs [*u319* (S25F) and *u430* (A97V)]. On the other hand, yeast *TUB1* mutations that conferred benomyl-resistance mostly affect the residues exposed to the outer surface of the MTs (Richards et al. 2000), and *mec-7 neo* mutations similarly led to increased resistance to colchicine. Therefore, comparative studies using the three different organisms can help identify key residues in the tubulin structure responsible for various MT functions.

Modeling the effects of neuronal tubulin mutations

We have used the *C. elegans* TRNs as a model to study neuronal MTs, which are much more stable and have different types of post-translational modification than the MTs in dividing cells (Baas et al. 2016). Clinical studies in the past five years identified more than 100 missense

mutations in tubulin genes that cause a wide spectrum of neurodevelopmental disorders, such as microcephaly, lissencephaly, polymicrogyria, and cortical malformation, along with severe defects in axon guidance and growth, including the complete or partial absence of corpus callosum, defects in commissural fiber tracts, and degeneration of motor and sensory axons (Tischfield et al. 2011; Chakraborti et al. 2016). Patients carrying different tubulin mutations often display distinct symptoms, but the complexity of the human nervous system makes it difficult to analyze the impact of specific mutations at the cellular level.

Combining CRISPR/Cas9-mediated genome editing with *in vivo* examination of TRN morphology, we were able to create several disease-causing human β-tubulin mutations in the *C. elegans mec-7* gene and examined their effects on neurite growth at a single neuron resolution. Our phenotypic evaluation was largely consistent with previous characterization of those mutations, suggesting that the TRN system could be instrumental to model the effects of human tubulin mutations identified in the clinic.

In fact, many disease-causing tubulin mutations alter amino acids that are physically adjacent to or located in the same region as the ones affected in our mutants, suggesting that they may affect MT stability in similar ways. By mapping 51 TUBA1A, 24 TUBB2B, and 19 TUBB3B mutations that were clinically identified onto the tubulin structure, we could correlate the location of some of the affected residues with the resulting clinical manifestation (Table S4). For example, 7/8 (87.5%) mutations that alter residues involved in GTP binding caused complete agenesis of corpus callosum, an indication of severe defects in axonal growth, whereas only 5/23 (21.7%) changes of residues in the interior of the structure and 10/32 (31.2%) mutations of residues involved in MAP binding did so (Table S4).

However, position of the mutated residues alone could not determine the effects of the missense mutation; each specific mutation should be evaluated individually. For example, the B5-to-H5 loop of β-tubulin (from V170 to V179) is in contact with the GTP molecule and four strong *mec-7 anti* mutations (P171S, P171L, S176F, and V179A) were mapped to this loop. Unexpectedly, S172P mutation led to a *lf* phenotype and P173L mutation caused no defects in TRNs. One possible explanation is that S172 and P173 are further away from the GTP binding site and thus are less important than P171 and S176.

The identity of the residue replacing the wild type one also plays a critical role. For instance, *u278* (C303Y) was the strongest *mec-7* neomorph, but *gk286001* (C303S) had no effect at all; since both tyrosine and serine have the polar hydroxyl group, the bulky phenyl group of the tyrosine may be responsible for disrupting some MT functions. Moreover, the *u1058* (A302T) mutation also caused a strong *mec-7(neo)* phenotype. A302 and C303 on the H9-to-B8 loop are exposed to the exterior of MTs but are not located on the major landing surface (H11 and H12) for motor protein and MAPs. Our results suggest that A302 and C303 may represent a previously unrecognized site of interaction between the MTs and their associated proteins. Even for residues located on H11 and H12, the effects of their mutation can be different. *u1059* (R380S) is a *mec-7* neomorph, whereas *u1060* (E410K) allele produced an antimorph-like phenotype, suggesting that the impact of the missense mutation depends on how the interaction of MTs with the motor proteins or MAP is affected by the amino acid change.

MT-destabilizing tubulin isotype and "multi-tubulin hypothesis"

The presence of multiple tubulin genes in eukaryotic genomes, their subtle differences in the protein sequences, and their functional differences led to the "multi-tubulin hypothesis." In multicellular organism, the tubulins may have distinct expression patterns, *e.g.* Drosophila *β2*-

tubulin is only expressed in the male germline (Kemphues et al. 1980); human TUBB3B is highly enriched in the nervous system, whereas TUBB2B is expressed in many tissues (Sullivan and Cleveland 1986). In single-cell organisms like *Tetrahymena*, different β-tubulin isotypes are spatially separated; some are only used to make the nuclear MTs of the mitotic apparatus, and some are only detected in the MTs of somatic cilia and basal bodies (Pucciarelli et al. 2012). Our studies, however, found that two distinct α-tubulin isotypes (MEC-12 and TBA-7) could have different functions when both incorporated into the same MTs in the same neurons; MEC-12 promotes stability and TBA-7 promotes instability.

The abundance of large diameter 15-p MTs in the TRNs requires MEC-12, but the role of TBA-7 is to increase MT dynamics and to prevent the ectopic growth of posteriorly directed neurites in ALMs. Thus, TBA-7 is a MT-destabilizing tubulin isotype, and this destabilizing activity depends on the absence of potential polyamination and polyglutamination sites that could increase MT stability. Our results are consistent with early *in vitro* experiments suggesting that TUBB3 (also known as β_{III}) also promotes MT dynamics; removal of TUBB3 from the brain extract resulted in a tubulin mixture that assembled much more rapidly than the unfractionated control (Banerjee et al. 1990), and MTs assembled from the purified $\alpha\beta_{III}$ heterodimers were considerably more dynamic than MTs made from the $\alpha\beta_{II}$ and $\alpha\beta_{IV}$ dimers (Panda et al. 1994). However, the long-standing question is whether some tubulin isotypes do destabilize MTs *in vivo*. Our findings suggest the answer is yes. A balanced incorporation of multiple tubulin isotypes into the same MT structure is critical to generate MTs with the optimal stability.

The absence of post-translational modification sites in tubulin isotypes may lead to functional diversity. In addition to TBA-7, among the other eight *C. elegans* α-tubulin isotypes, TBA-8 and TBA-5 also lack the Q31 for polyamination, and TBA-6 lacks the E445 for

polyglutamination; all nine human α-tubulins have Q31, but TUBAL3 has a short C-terminal tail and does not contain potential polyglutamination sites (Figure S9). The incorporation of those tubulin isotypes may be a general regulatory mechanism to control MT stability.

Moreover, *mec-12* and *tba-7* do not appear to be redundant, because the *tba-7 lf* mutation alone produced uncontrolled growth. Moreover, both *mec-12 lf* mutants and *mec-12; tba-7* double *lf* mutants retained the ability to grow out a normal amount of neurites, suggesting strong genetic redundancy among the α-tubulins with regards to supporting neurite growth.

Different contributions of tubulin isotypes to MT dynamics were also observed in *C. elegans* embryogenesis (Honda et al. 2017). The spindle MTs required two β-tubulins (TBB-1 and TBB-2), but TBB-2 was incorporated into the MTs twice as much as TBB-1; the loss of TBB-2 caused a dramatic decrease in MT growth rate and an increase in catastrophe frequency, leading to highly unstable MTs, whereas the loss of TBB-1 only slightly reduced growth rate. These data support the "multi-tubulin concept" that different tubulin isotypes have distinct functions in the same cells.

Materials and Methods

Strains and genetic screens

C. elegans wild type (N2) and mutant strains were maintained at 20 °C as previously described (Brenner 1974). Alleles listed in Table S1 and S2 were isolated by visually screening for mutants with TRN differentiation defects using TU4069, which carries *uIs115 [mec-17p::RFP]* for the visualization of the TRNs, as the starter strain and ethyl methanesulfonate as the mutagen. Mutants were outcrossed with wild type, and the phenotype-causing mutations were identified as previously described by whole-genome resequencing (Zheng et al. 2013) or by

complementation tests with reference alleles. *mec-7* alleles *e1343*, *e1505*, *e1527*, *e1522*, *n434*, *u10*, *u18*, *u22*, *u48*, *u58*, *u98*, *u127*, *u129*, *u162*, *u170*, *u223*, *u225*, *u278*, *u234*, *u249*, *u262*, *u275*, *u283*, *u305*, *u319*, *u428*, *u429*, *u430*, *u433*, *u449*, and *u445*, and *mec-12* alleles *e1605*, *e1607*, *u50*, *u63*, *u76*, and *u241* were previously isolated (Chalfie and Sulston 1981; Chalfie and Au 1989; Savage et al. 1994) and re-examined in this study.

u1056 to *u1060* alleles were created through CRISPR/Cas9-mediated homologous recombination (Dickinson et al. 2013). Guide RNAs were designed according to the target sequence closest to the desired codon change (Figure 5A). Recombination templates were created by cloning the *mec-7* coding region and 466 bp 3'UTR sequence into the SalI and BamHI sites of pBlueScript II SK (+) vector and then introducing the desired missense mutation (red in Figure 5A), along with synonymous mutations (blue in Figure 5A) that change the guide RNA target sites, using the Q5 Site-Directed Mutagenesis Kit from New England Biolabs (NEB; Ipswich, MA). pDD162 constructs expressing Cas9 and specific guide RNAs were injected together with the corresponding recombination template and marker *myo-2p::RFP* into TU4069 animals. F1s expressing RFP in the muscle were singled out and genotyped to identify heterozygotes with successful edits, and F2s carrying homozygous mutations were then isolated and examined for TRN morphology.

The *gk* alleles of *mec-7* and *mec-12* listed in Table 1 were generated in the million mutation project (Thompson et al. 2013) and obtained from the Caenorhabditis Genetics Center, which is funded by NIH Office of Research Infrastructure Programs (P40 OD010440). *klp-7(tm2143)*, *klp-11(tm374)*, and *mec-12(tm5083)* were generated by the National Bioresource Project of Japan, and *mec-12(gm379)* was kindly provided by Dr. Chun-Liang Pan at the National Taiwan University.

Additional *mec-12* null alleles (*u1026*, *u1027*, and *u1028*) were generated by CRISPR/Cas9-mediated genome editing targeting 5'-GAAGTAATTTCGATTCACATCGG-3' in exon 2 of *mec-12* as described above (Dickinson et al. 2013). Frameshift-causing mutations were identified by sequencing the *mec-12* locus (Figure S1).

A second screen was conducted using TU4879 [*mec-7 (u278); uIs115 (mec-17p::RFP)*] as the starter strain, and mutants with significantly shortened ALM-PN were isolated. *mec-7* [*u1040* (G98E)], *mec-12* [*u1041* (G246E)], and *mec-15* [*u1042* (R26*)] were obtained from this screen as suppressors of *mec-7[u278* (C303Y) *neo]* mutants.

Constructs and Transgenes

A *tba-7::GFP* reporter (TU#1632) was made by cloning a 1.2 kb *tba-7* promoter and the entire coding region from the genomic DNA to wild-type genomic DNA into the Gateway pDONR221 P4-P1r vector; the resulting entry vector, together with the pENTR-GFP, pENTR-*unc-54*-3'UTR, and destination vector pDEST-R4-R3 were used in the LR reaction to create the final expression vectors. *mec-17p::tba-7(+)* (TU#1629) was created by cloning a 1.9 kb *mec-17* promoter and the *tba-7* coding sequence into pDONR221 P4-P1r and pDONR221 vectors, respectively, and assembling these entry vectors with pENTR-*unc-54*-3'UTR and the destination vector. Details about the Gateway cloning method by Life Technologies can be found at www.invitrogen.com/site/us/en/home/Products-andServices/Applications/Cloning/Gateway-Cloning.html. *tba-7(+)* locus, including the 1.2 kb promoter, coding region, and a 911-bp 3'UTR, was cloned using SalI and NotI into pBlueScript II SK(+) vector; NEB Q5 site-directed mutagenesis kit was then used to generate constructs expressing the TBA-7 variants shown in Figure 6D.

To rescue the *mec-15* mutants, we amplified the *mec-15(+)* locus that includes a 3.2 kb promoter, coding region, and a 951 bp downstream region and injected the purified PCR product to perform the rescue experiments. We used previously described TU#891 *[mec-18p::mec-15(+)]* construct (Bounoutas et al. 2009b) to perform cell-specific rescue and to generate constructs that express truncated MEC-15 proteins shown in Figure 7C.

Transgenes *uIs31[mec-17p::GFP]* III, *uIs115[mec-17p::RFP]* IV, and *uIs134[mec-17p::RFP]* V were used to visualize TRN morphology (Zheng et al. 2015a). *jsIs821[mec-7p::GFP::RAB-3]* was used to assess synaptic vesicle localization (Bounoutas et al. 2009b).

Electron microscopy

We re-analyzed previously collected cross-section images of ALM neurites from wild type animals (N501, N631, N933, and N934 from the Hall lab collection) and from *mec-7* neomorphic mutants *u170* and *u278* (Savage et al. 1994). The wild type animals had been fixed by either chemical immersion fixation without tannic acid (samples N501, N631; Hall 1995) or by high-pressure freezing/freeze substitution (HPF/FS) including tannic acid (samples N933, N934; Topalidou et al. 2012). The *mec-7* neomorphic alleles had also been fixed by chemical immersion, without tannic acid.

For this study, we fixed *mec-7 lf (ok2152)*, *mec-12 lf (tm5083)*, and *tba-7 lf (u1015)* adults using an HPF/FS protocol that included a first fixation in 0.5% glutaraldehyde + 0.1% tannic acid and a second fix in 2% osmium tetroxide + 0.1% uranyl acetate (UAc), both at -90 °C, followed by staining in 1% UAc in acetone at 0 °C. We also fixed adults of *mec-12(anti)* mutants, *u950*, *u76*, and *u1021*, using HPF/FS using a similar protocol, but without tannic acid. Eighty-nanometer transverse sections were collected at multiple positions along the ALM anterior

neurite and post-stained with uranium acetate and lead citrate. A Philips CM10 electron microscope with an attached Morada digital camera (Olympus) was used to acquire the images.

For each animal, we counted the number of MTs in the ALMs and measured the MT diameter on sections collected from at least five different positions along the ALM-AN; data from ALML and ALMR were combined. For each strain, we examined sections from at three different animals. For wild-type animals, *tba-7 lf* mutants, and *mec-7* neomorphs, we used at least ten sections to measure the distance between two closest MT centers and the proportion of MT-occupied area to the cross-sectional area of the neurite.

Phenotype Scoring and Statistical Analysis

We measured the length of TRN neurites in at least 30 fourth stage larvae or young adults grown at 20° C, except where otherwise stated. Relative length of posteriorly directed neurites was calculated by dividing the neurite length by the diameter of the cell body. Defects in TRN anterior neurite length were assessed by counting the percentage of cells whose neurites failed to reach the vulva (for PLM) or the posterior pharyngeal bulb (for ALM); at least 50 cells were examined for each strain.

Fluorescence intensity of the RFP expressed from the *uIs134* transgene in the ALM cell body was used to measure TRN protein levels; intensity was calculated after manual background subtraction using ImageJ as previously described (Chen and Chalfie 2015). Synaptic vesicle localization was quantified by calculating the percentage of animals in each of the four phenotypical categories: 1) normal localization to the PLM synaptic branch; 2) reduced intensity of the synaptic marker at the synapses as partial defect; 3) complete loss of normal localization to the synapse as complete defect; 4) localization to the PLM-PN as mistargeting. At least 50 adult animals were examined.

Acetylated α-tubulin staining using antibody [6-11B-1] (abcam, Cambridge, MA) was performed and analyzed as previously described (Topalidou et al. 2012). For colchicine treatment, animals were grown in standard NGM agar plates containing different concentrations (from 0.06 mM to 2 mM) of colchicine before phenotypic analysis as described before (Bounoutas et al. 2009a). Similarly, 100 nM paclitaxel was added to the NGM agar plates, L1 animals were placed onto the plates, and young adults were examined for TRN morphology. PyMOL (Schrodinger 2015) was used to view the structure of α/β tubulin dimer (1jff.pdb; Nogales et al. 1998) and to label affected residues in *mec-7* and *mec-12* mutants,.

For statistical analysis, ANOVA and the post hoc Dunnett's test or Tukey-Kramer test were used to identify significant difference between the mutants and wild type animals in multiple comparisons. Student's *t* test was used to find significant difference between two samples in paired comparisons. Single and double asterisks indicated $p < 0.05$ and $p < 0.01$, respectively. The χ^2 test was used for the categorical data to find significant difference between different strains.

Acknowledgements

We thank Dan Dickinson, Chun-Liang Pan, and Andrew Chisholm for sharing reagents. This work was supported by NIH Grant GM30997 (to M.C.) and OD 010943 (to D.H.H.). Core facilities for electron microscopy were supported by NICHD P30 HD71593 for the RFK-IDDRC at Albert Einstein College of Medicine.

References

Akhmanova A, Steinmetz MO. 2015. Control of microtubule organization and dynamics: two ends in the limelight. *Nat Rev Mol Cell Biol* **16**: 711-726.

Baas PW, Rao AN, Matamoros AJ, Leo L. 2016. Stability properties of neuronal microtubules. *Cytoskeleton (Hoboken)* **73**: 442-460.

Bahi-Buisson N, Poirier K, Fourniol F, Saillour Y, Valence S, Lebrun N, Hully M, Bianco CF, Boddaert N, Elie C et al. 2014. The wide spectrum of tubulinopathies: what are the key features for the diagnosis? *Brain* **137**: 1676-1700.

Banerjee A, Roach MC, Trcka P, Luduena RF. 1990. Increased microtubule assembly in bovine brain tubulin lacking the type III isotype of beta-tubulin. *The Journal of biological chemistry* **265**: 1794-1799.

Bercher M, Wahl J, Vogel BE, Lu C, Hedgecock EM, Hall DH, Plenefisch JD. 2001. mua-3, a gene required for mechanical tissue integrity in Caenorhabditis elegans, encodes a novel transmembrane protein of epithelial attachment complexes. *J Cell Biol* **154**: 415-426.

Bounoutas A, Kratz J, Emtage L, Ma C, Nguyen KC, Chalfie M. 2011. Microtubule depolymerization in Caenorhabditis elegans touch receptor neurons reduces gene expression through a p38 MAPK pathway. *Proceedings of the National Academy of Sciences of the United States of America* **108**: 3982-3987.

Bounoutas A, O'Hagan R, Chalfie M. 2009a. The multipurpose 15-protofilament microtubules in C. elegans have specific roles in mechanosensation. *Current biology : CB* **19**: 1362-1367.

Bounoutas A, Zheng Q, Nonet ML, Chalfie M. 2009b. mec-15 encodes an F-box protein required for touch receptor neuron mechanosensation, synapse formation and development. *Genetics* **183**: 607-617, 601SI-604SI.

Brenner S. 1974. The genetics of Caenorhabditis elegans. *Genetics* **77**: 71-94.

Buck KB, Zheng JQ. 2002. Growth cone turning induced by direct local modification of microtubule dynamics. *The Journal of neuroscience : the official journal of the Society for Neuroscience* **22**: 9358-9367.

Chakraborti S, Natarajan K, Curiel J, Janke C, Liu J. 2016. The emerging role of the tubulin code: From the tubulin molecule to neuronal function and disease. *Cytoskeleton (Hoboken)* **73**: 521-550.

Chalfie M, Au M. 1989. Genetic control of differentiation of the Caenorhabditis elegans touch receptor neurons. *Science* **243**: 1027-1033.

Chalfie M, Sulston J. 1981. Developmental genetics of the mechanosensory neurons of Caenorhabditis elegans. *Developmental biology* **82**: 358-370.

Chalfie M, Thomson JN. 1979. Organization of neuronal microtubules in the nematode Caenorhabditis elegans. *J Cell Biol* **82**: 278-289.

-. 1982. Structural and functional diversity in the neuronal microtubules of Caenorhabditis elegans. *J Cell Biol* **93**: 15-23.

Challacombe JF, Snow DM, Letourneau PC. 1996. Actin filament bundles are required for microtubule reorientation during growth cone turning to avoid an inhibitory guidance cue. *J Cell Sci* **109 (Pt 8)**: 2031-2040.

Chen X, Chalfie M. 2015. Regulation of mechanosensation in C. elegans through ubiquitination of the MEC-4 mechanotransduction channel. *The Journal of neuroscience : the official journal of the Society for Neuroscience* **35**: 2200-2212.

Cleveland DW. 1987. The multitubulin hypothesis revisited: what have we learned? *J Cell Biol* **104**: 381-383.

Dent EW, Gupton SL, Gertler FB. 2011. The growth cone cytoskeleton in axon outgrowth and guidance. *Cold Spring Harb Perspect Biol* **3**.

Dickinson DJ, Ward JD, Reiner DJ, Goldstein B. 2013. Engineering the Caenorhabditis elegans genome using Cas9-triggered homologous recombination. *Nature methods* **10**: 1028-1034.

Du H, Chalfie M. 2001. Genes regulating touch cell development in Caenorhabditis elegans. *Genetics* **158**: 197-207.

Edde B, Rossier J, Le Caer JP, Desbruyeres E, Gros F, Denoulet P. 1990. Posttranslational glutamylation of alpha-tubulin. *Science* **247**: 83-85.

Fackenthal JD, Hutchens JA, Turner FR, Raff EC. 1995. Structural analysis of mutations in the Drosophila beta 2-tubulin isoform reveals regions in the beta-tubulin molecular required for general and for tissue-specific microtubule functions. *Genetics* **139**: 267-286.

Fulton C, Simpson FA. 1976. Selective synthesis and utilization of flagellar tubulin: the multi-tubulin hypothesis. in *Cell Motility* (eds. R Goldman, T Pollard, J Rosenbaum), pp. 987-1005. Cold Spring Harbor Publications, New York.

Ghosh-Roy A, Goncharov A, Jin Y, Chisholm AD. 2012. Kinesin-13 and tubulin posttranslational modifications regulate microtubule growth in axon regeneration. *Developmental cell* **23**: 716-728.

Hall DH. 1995. Electron microscopy and three-dimensional image reconstruction. *Methods Cell Biol* **48**: 395-436.

Hamelin M, Scott IM, Way JC, Culotti JG. 1992. The mec-7 beta-tubulin gene of Caenorhabditis elegans is expressed primarily in the touch receptor neurons. *The EMBO journal* **11**: 2885-2893.

Han X, Adames K, Sykes EM, Srayko M. 2015. The KLP-7 Residue S546 Is a Putative Aurora Kinase Site Required for Microtubule Regulation at the Centrosome in C. elegans. *PLoS One* **10**: e0132593.

Hedgecock EM, Culotti JG, Hall DH. 1990. The unc-5, unc-6, and unc-40 genes guide circumferential migrations of pioneer axons and mesodermal cells on the epidermis in C. elegans. *Neuron* **4**: 61-85.

Hilliard MA, Bargmann CI. 2006. Wnt signals and frizzled activity orient anterior-posterior axon outgrowth in C. elegans. *Developmental cell* **10**: 379-390.

Honda Y, Tsuchiya K, Sumiyoshi E, Haruta N, Sugimoto A. 2017. Tubulin isotype substitution revealed that isotype composition modulates microtubule dynamics in C. elegans embryos. *J Cell Sci*.

Hoyle HD, Raff EC. 1990. Two Drosophila beta tubulin isoforms are not functionally equivalent. *J Cell Biol* **111**: 1009-1026.

Hsu JM, Chen CH, Chen YC, McDonald KL, Gurling M, Lee A, Garriga G, Pan CL. 2014. Genetic analysis of a novel tubulin mutation that redirects synaptic vesicle targeting and causes neurite degeneration in C. elegans. *PLoS genetics* **10**: e1004715.

Jaglin XH, Poirier K, Saillour Y, Buhler E, Tian G, Bahi-Buisson N, Fallet-Bianco C, Phan-Dinh-Tuy F, Kong XP, Bomont P et al. 2009. Mutations in the beta-tubulin gene TUBB2B result in asymmetrical polymicrogyria. *Nat Genet* **41**: 746-752.

Kemphues KJ, Raff EC, Raff RA, Kaufman TC. 1980. Mutation in a testis-specific beta-tubulin in Drosophila: analysis of its effects on meiosis and map location of the gene. *Cell* **21**: 445-451.

Kirszenblat L, Neumann B, Coakley S, Hilliard MA. 2013. A dominant mutation in mec-7/beta-tubulin affects axon development and regeneration in Caenorhabditis elegans neurons. *Mol Biol Cell* **24**: 285-296.

Konishi Y, Setou M. 2009. Tubulin tyrosination navigates the kinesin-1 motor domain to axons. *Nature neuroscience* **12**: 559-567.

Leandro-Garcia LJ, Leskela S, Landa I, Montero-Conde C, Lopez-Jimenez E, Leton R, Cascon A, Robledo M, Rodriguez-Antona C. 2010. Tumoral and tissue-specific expression of the major human beta-tubulin isotypes. *Cytoskeleton (Hoboken)* **67**: 214-223.

965 Liao G, Gundersen GG. 1998. Kinesin is a candidate for cross-bridging microtubules and intermediate
966 filaments. Selective binding of kinesin to detyrosinated tubulin and vimentin. *The Journal of*
967 *biological chemistry* **273**: 9797-9803.
968 Liu G, Dwyer T. 2014. Microtubule dynamics in axon guidance. *Neurosci Bull* **30**: 569-583.
969 Lockhead D, Schwarz EM, O'Hagan R, Bellotti S, Krieg M, Barr MM, Dunn AR, Sternberg PW, Goodman
970 MB. 2016. The tubulin repertoire of C. elegans sensory neurons and its context-dependent role
971 in process outgrowth. *Mol Biol Cell*.
972 Mapes J, Chen JT, Yu JS, Xue D. 2010. Somatic sex determination in Caenorhabditis elegans is modulated
973 by SUP-26 repression of tra-2 translation. *Proceedings of the National Academy of Sciences of*
974 *the United States of America* **107**: 18022-18027.
975 McKean PG, Vaughan S, Gull K. 2001. The extended tubulin superfamily. *J Cell Sci* **114**: 2723-2733.
976 Mimori-Kiyosue Y. 2011. Shaping microtubules into diverse patterns: molecular connections for setting
977 up both ends. *Cytoskeleton (Hoboken)* **68**: 603-618.
978 Mitani S, Du H, Hall DH, Driscoll M, Chalfie M. 1993. Combinatorial control of touch receptor neuron
979 expression in Caenorhabditis elegans. *Development* **119**: 773-783.
980 Mitchison T, Kirschner M. 1984. Dynamic instability of microtubule growth. *Nature* **312**: 237-242.
981 Neumann B, Hilliard MA. 2014. Loss of MEC-17 leads to microtubule instability and axonal degeneration.
982 *Cell Rep* **6**: 93-103.
983 Nogales E, Wolf SG, Downing KH. 1998. Structure of the alpha beta tubulin dimer by electron
984 crystallography. *Nature* **391**: 199-203.
985 Panda D, Miller HP, Banerjee A, Luduena RF, Wilson L. 1994. Microtubule dynamics in vitro are regulated
986 by the tubulin isotype composition. *Proceedings of the National Academy of Sciences of the*
987 *United States of America* **91**: 11358-11362.
988 Papsdorf K, Sacherl J, Richter K. 2014. The balanced regulation of Hsc70 by DNJ-13 and UNC-23 is
989 required for muscle functionality. *The Journal of biological chemistry* **289**: 25250-25261.
990 Poirier K, Saillour Y, Bahi-Buisson N, Jaglin XH, Fallet-Bianco C, Nabbout R, Castelnau-Ptakhine L,
991 Roubertie A, Attie-Bitach T, Desguerre I et al. 2010. Mutations in the neuronal ss-tubulin subunit
992 TUBB3 result in malformation of cortical development and neuronal migration defects. *Hum Mol*
993 *Genet* **19**: 4462-4473.
994 Prokop A. 2013. The intricate relationship between microtubules and their associated motor proteins
995 during axon growth and maintenance. *Neural Dev* **8**: 17.
996 Pucciarelli S, Ballarini P, Sparvoli D, Barchetta S, Yu T, Detrich HW, 3rd, Miceli C. 2012. Distinct functional
997 roles of beta-tubulin isotypes in microtubule arrays of Tetrahymena thermophila, a model
998 single-celled organism. *PLoS One* **7**: e39694.
999 Purro SA, Ciani L, Hoyos-Flight M, Stamatakou E, Siomou E, Salinas PC. 2008. Wnt regulates axon
1000 behavior through changes in microtubule growth directionality: a new role for adenomatous
1001 polyposis coli. *The Journal of neuroscience : the official journal of the Society for Neuroscience* **28**:
1002 8644-8654.
1003 Qu C, Dwyer T, Shao Q, Yang T, Huang H, Liu G. 2013. Direct binding of TUBB3 with DCC couples netrin-1
1004 signaling to intracellular microtubule dynamics in axon outgrowth and guidance. *J Cell Sci* **126**:
1005 3070-3081.
1006 Reijo RA, Cooper EM, Beagle GJ, Huffaker TC. 1994. Systematic mutational analysis of the yeast beta-
1007 tubulin gene. *Mol Biol Cell* **5**: 29-43.
1008 Richards KL, Anders KR, Nogales E, Schwartz K, Downing KH, Botstein D. 2000. Structure-function
1009 relationships in yeast tubulins. *Mol Biol Cell* **11**: 1887-1903.
1010 Sainath R, Gallo G. 2015. Cytoskeletal and signaling mechanisms of neurite formation. *Cell Tissue Res*
1011 **359**: 267-278.

Savage C, Xue Y, Mitani S, Hall D, Zakhary R, Chalfie M. 1994. Mutations in the Caenorhabditis elegans beta-tubulin gene mec-7: effects on microtubule assembly and stability and on tubulin autoregulation. *J Cell Sci* **107 (Pt 8)**: 2165-2175.

Schaefer AW, Schoonderwoert VT, Ji L, Mederios N, Danuser G, Forscher P. 2008. Coordination of actin filament and microtubule dynamics during neurite outgrowth. *Developmental cell* **15**: 146-162.

Schrodinger, LLC. 2015. The PyMOL Molecular Graphics System, Version 1.8.

Sirajuddin M, Rice LM, Vale RD. 2014. Regulation of microtubule motors by tubulin isotypes and post-translational modifications. *Nature cell biology* **16**: 335-344.

Song Y, Brady ST. 2015. Post-translational modifications of tubulin: pathways to functional diversity of microtubules. *Trends Cell Biol* **25**: 125-136.

Song Y, Kirkpatrick LL, Schilling AB, Helseth DL, Chabot N, Keillor JW, Johnson GV, Brady ST. 2013. Transglutaminase and polyamination of tubulin: posttranslational modification for stabilizing axonal microtubules. *Neuron* **78**: 109-123.

Sullivan KF. 1988. Structure and utilization of tubulin isotypes. *Annu Rev Cell Biol* **4**: 687-716.

Sullivan KF, Cleveland DW. 1986. Identification of conserved isotype-defining variable region sequences for four vertebrate beta tubulin polypeptide classes. *Proceedings of the National Academy of Sciences of the United States of America* **83**: 4327-4331.

Takeda S, Yamazaki H, Seog DH, Kanai Y, Terada S, Hirokawa N. 2000. Kinesin superfamily protein 3 (KIF3) motor transports fodrin-associating vesicles important for neurite building. *J Cell Biol* **148**: 1255-1265.

Tanaka E, Ho T, Kirschner MW. 1995. The role of microtubule dynamics in growth cone motility and axonal growth. *J Cell Biol* **128**: 139-155.

Thompson O, Edgley M, Strasbourger P, Flibotte S, Ewing B, Adair R, Au V, Chaudhry I, Fernando L, Hutter H et al. 2013. The million mutation project: a new approach to genetics in Caenorhabditis elegans. *Genome Res* **23**: 1749-1762.

Tian G, Jaglin XH, Keays DA, Francis F, Chelly J, Cowan NJ. 2010. Disease-associated mutations in TUBA1A result in a spectrum of defects in the tubulin folding and heterodimer assembly pathway. *Hum Mol Genet* **19**: 3599-3613.

Tischfield MA, Baris HN, Wu C, Rudolph G, Van Maldergem L, He W, Chan WM, Andrews C, Demer JL, Robertson RL et al. 2010. Human TUBB3 mutations perturb microtubule dynamics, kinesin interactions, and axon guidance. *Cell* **140**: 74-87.

Tischfield MA, Cederquist GY, Gupta ML, Jr., Engle EC. 2011. Phenotypic spectrum of the tubulin-related disorders and functional implications of disease-causing mutations. *Curr Opin Genet Dev* **21**: 286-294.

Topalidou I, Keller C, Kalebic N, Nguyen KC, Somhegyi H, Politi KA, Heppenstall P, Hall DH, Chalfie M. 2012. Genetically separable functions of the MEC-17 tubulin acetyltransferase affect microtubule organization. *Current biology : CB* **22**: 1057-1065.

Verhey KJ, Gaertig J. 2007. The tubulin code. *Cell Cycle* **6**: 2152-2160.

Yu I, Garnham CP, Roll-Mecak A. 2015. Writing and Reading the Tubulin Code. *The Journal of biological chemistry* **290**: 17163-17172.

Zheng C, Diaz-Cuadros M, Chalfie M. 2015a. Dishevelled attenuates the repelling activity of Wnt signaling during neurite outgrowth in Caenorhabditis elegans. *Proceedings of the National Academy of Sciences of the United States of America* **112**: 13243-13248.

-. 2015b. Hox Genes Promote Neuronal Subtype Diversification through Posterior Induction in Caenorhabditis elegans. *Neuron* **88**: 514-527.

-. 2016. GEFs and Rac GTPases control directional specificity of neurite extension along the anterior-posterior axis. *Proceedings of the National Academy of Sciences of the United States of America* **113**: 6973-6978.

Zheng C, Karimzadegan S, Chiang V, Chalfie M. 2013. Histone methylation restrains the expression of subtype-specific genes during terminal neuronal differentiation in Caenorhabditis elegans. *PLoS genetics* **9**: e1004017.

Figure legends

Figure 1. MT structures in tubulin mutants. (A) Cross sectional images of ALM-AN in wild type and, *mec-12(tm5083 lf)*, *mec-7(ok2152 lf)*, *tba-7(u1015 lf) mec-12[u950* (S140F) *anti]* and *mec-12[u1021* (G144S) *anti]* mutants. MT structures in *mec-7(anti)* mutants were analyzed by Chalfie and Thomson (1982). Insets in the lower right corner of *mec-12(lf)*, *mec-7(lf)*, and *tba-7(lf)* animals show the protofilament structure of tannic acid stained MTs (4-fold enlarged). Scale bar = 100 nm. (B) Measures of MT structure and organization. Numbers of observations are shown in parentheses, and a Dunnett's test was performed to compare the mutants with the wild type. Throughout the figures, one asterisk represents a statistical significance of $p < 0.05$ and two asterisks indicate $p < 0.01$. [Note: Our earlier studies found that wild-type TRN MTs had much larger diameters than we find here (29.6 ± 0.4 nm; (Chalfie and Thomson 1979). We could not explain the discrepancy between these and our current results. We are, nonetheless, very confident in the current calibration.]

Figure 2. *mec-7* and *mec-12* mutations affect TRN neurite length. (A) Schematic diagram of ALM and PLM morphology in *mec-7* and *mec-12 lf*, *anti*, and *neo* mutants. (B) On the left panel, compared to the wild-type animals, *mec-7(ok2152 lf)* animals showed an increased gap between PLM-AN and ALM cell body (dashed line) and significantly shortened PLM-PN (arrows). PLM-AN still extends beyond the position of the vulva indicated by the triangle. The middle panel showed PLM posterior neurites in the various animals. Arrows pointed to the shortened PLM-PN. The right panel displayed the TRN morphologies in *mec-12[u1019* (G354E) *anti]*, *mec-7[u957* (P171L) *anti]*, and *mec-7[u958* (G244S) *anti]* animals. (C) TRN morphology of *mec-12[u917* (V260I) *neo]*, *mec-7[u278* (C303Y) *neo]*, and *mec-7[u1017* (C377F) *neo]* animals. Arrows point to the ectopic ALM-PN. (D) The percentage of ALM and PLM cells that had significantly shortened anterior neurites (ALM-AN not reaching the posterior pharyngeal bulb and PLM-AN not extending beyond the vulva). Amino acid changes in the alleles can be found in Table 1. A χ^2 test for categorical data was used to compare mutants with the wild type. (E-F) The relative length of PLM-PN or ALM-PN in *mec-7*and *mec-12 lf*, *anti*, and *neo* mutant animals, as well as the double mutants of *mec-7(ok2151 lf)* with *mec-12 neo* alleles. Dunnett's test was used to analyze the data.

Figure 3. Effects of *mec-7* and *mec-12* mutations on TRN development and functions. (A) The average number of anterior touch responses of *mec-7* and *mec-12 lf*, *anti*, and *neo* mutants at the anterior side. (B) Defective targeting of the synaptic vesicle marker RAB-3::GFP in *mec-7* and *mec-12* mutant PLM

neurons. RAB-3::GFP signal is found in patches where PLM-AN branches synapse onto target neurons in the wild-type ventral nerve cord. This targeting was partially or completely lost in many of the mutants; this loss in *mec-7(lf)* and *mec-12(anti)* mutants could be partly caused by the lack of PLM synaptic branch. In *mec-7(u278*; C303Y*)* mutants, however, the marker was mistargeted to the distal end of PLM-PN (arrow). (C) Immunofluorescent intensity of antibody labeling of acetylated α-tubulin. (D) Fluorescent intensity of the TRN marker *uIs134 [mec-17p::RFP]* in various *mec-7* and *mec-12* mutants and their doubles with *dlk-1 lf (ju476)* allele. Dunnett's tests were performed to compare the mutants with the wild type animals, and *t* tests with Bonferroni correction were used to identify significant difference between the tubulin single mutants and *dlk-1; mec-7* or *dlk-1; mec-12* double mutants.

Figure 4. Position of amino acid residues changed in *mec-7* and *mec-12* mutants. (A) The structure of the α/β tubulin dimer (1jff.pdb) visualized using PyMOL. α-tubulin is in wheat, and β-tubulin is in cyan, magenta, and pink, which labels α-helices, β-sheets, and loops, respectively. GTP is labeled in green. (B-C) Amino acid changes around the GTP binding pocket in *mec-7* (red) and *mec-12* (pink) antimorphs. P173L and S172P (blue) are disease-associated mutations found in human TUBB3 that were engineered in *mec-7* to test their effects. (D) *mec-7* (red) and *mec-12* (pink) *anti* mutations mapped to intradimer interface. (E-F) Amino acid alterations in *mec-7* (E, yellow) and *mec-12* (F, yellow) *neo* alleles. A302T, R380S, and E410K (orange) were clinically identified TUBB3 mutations. E415 and G416 (green), mutated in *mec-12* partial *lf* alleles, are located at the exterior surface of α-tubulin.

Figure 5. Modeling human tubulin mutations in *C. elegans* TRNs. (A) Sequence changes designed to introduce TUBB3 missense mutations in *mec-7* gene. For each mutation, the line with an arrow underscores the 20 bp DNA sequence for the guide RNA target, and the directionality of the arrow indicates the strand of the target. The bottom DNA sequence contains the desired nonsynonymous (red) and synonymous mutations (blue) on the homologous repair template. Amino acids sequence with the positional information was shown on the top. (B) TRN morphologies of animals carrying the engineered missense mutations. For *u1056*, dashed line, triangle, and the arrow indicate the gap from PLM-AN to ALM cell body, the position of the vulva, and the shortened PLM-PN, respectively. For *u1058* and *u1059*, arrows point to the ectopic ALM-PN. For *u1060*, the arrow points to the severely shortened PLM-AN.

Figure 6. Mutations in *mec-7*, *mec-12*, *tba-7*, and *klp-7* result in the growth of ectopic ALM posterior neurites. (A) The length of ALM-PN in *tba-7(u1015 lf)* and *mec-7* and *mec-12* neomorphic alleles and the effect of 1 mM colchicine and *mec-7(ok2152 lf)*, *mec-7(u957 anti*), *mec-12(tm5083 lf)*, and *mec-12(u1016 anti)* mutations. (B) The length of ALM-PN in *klp-7 lf (tm2143)* mutants and their double mutants with *mec-7(ok2152 lf)*, *mec-7(u957 anti*), *mec-12(tm5083 lf)*, and *mec-7(u1017 neo)*. (C) The differences between the TBA-7 and MEC-12 amino acid sequences in the alignment were labeled in color. (D) The

length of ALM-PN in *tba-7(u1015 lf)* carrying the transgene expressing the wild type or mutant TBA-7 proteins. TBA-7 (CT SWAP) had DANDNGD (a.a. 435-441) replaced by MEDNGEEG, TBA-7 (NT SWAP) had TSMEPDGNSGSLG (a.a. 35-47) replaced by QMPSDKSLGGSDDSFS, and TBA-7 (L31Q + CT SWAP) carried both mutations. (E) Sprouting of neurites from the ALM and PLM cell bodies in *tba-7(u1015 lf)*; *mec-7(u1017 neo)* double mutants. (F) The average number of neurites emanating from the cell bodies in *tba-7(u1015 lf)* and *mec-7(u1017 neo)* single mutants and their double mutants.

Figure 7. F-box protein MEC-15 promotes neurite growth. (A) TRN morphology in *mec-15(u75 lf)* mutants (i; scale bar = 100 μm). PLM-AN was shortened and did not extend beyond PVM (ii); PLM-PN was also significantly shortened (iii). Synaptic branches of ALM-AN (iv) and PLM-AN (v) could not fully extend in *mec-15* mutants. Scale bar = 20 μm in (ii) through (v). (B) The growth of ALM-PN (arrows) in *mec-7(u278 neo)* mutants was suppressed by *mec-15(lf)* mutations and was restored in the double mutants by expressing wild-type MEC-15 under a TRN-specific *mec-18* promoter. (C) Protein structures of the wild type MEC-15 and F-Box mutants. F-Box and the four WD-40 repeats (WD) were labeled in green and blue, respectively. (D) The length of ALM-PN in various strains. Asterisks indicate significant difference in Tukey-Kramer test.

Figure 8. *mec-17 lf* mutations and tubulin *neo* mutations induce the growth of ectopic ALM-PN through different mechanisms. (A) The length of ALM-PN in *mec-17(ok2109 lf)* and tubulin *neo* mutants grown at 15°C and 25°C. Data for the rest of the figure were collected from animals grown at 20°C. (B) The length of ALM-PN in *mec-17(ok2109 lf)*, *mec-7(u278 neo)*, *mec-12(u917 neo)*, *tba-7(u1015 lf)*, and *klp-7(tm2143 lf)* animals treated with or without 100 nM paclitaxel. (C) *mec-17(ok2109 lf)* mutants and their double mutants with *mec-7(ok2152 lf)*, *mec-7(u957 anti*), *mec-12(tm5083 lf)*, *mec-12(u1016 anti)*, and *mec-7(u1017 neo)*. (D) The length of ALM-PN in *mec-17(ok2019 lf)*, *mec-7(u278 neo)*, *mec-12(u917 neo)*, and *tba-7(u1015 lf)* mutants and their double mutants with *tiam-1(u914 lf)*. Asterisks indicate significant difference in Tukey-Kramer test.

Figure 9. A model for the effect of MT dynamics on neurite development. (A) In wild-type animals, 15-p MTs are mostly made of MEC-12/α-tubulin and MEC-7/β-tubulin. Another α-tubulin TBA-7 is also incorporated into the MTs, probably to increase the dynamics. (B) In the absence of MEC-7, the abundant 15-p MTs are replaced by a few 11-p MTs, which use other β-tubulins for polymerization and can still support neurite growth. Whether those β-tubulins are normally incorporated into the MTs is unclear. (C) *mec-7(anti)* mutations produce dominant-negative MEC-7 proteins with defects in the GTP binding pocket or the intradimer or interdimer interfaces. Such MEC-7 mutants can either sequester all α-tubulin or form toxic heterodimers that can terminate MT elongation upon incorporation. Thus, MT polymerization is blocked and neurite growth is disrupted in *mec-7(anti)* animals. (D) *mec-7(neo)*

mutations mostly map to the exterior facing surface of the tubulin structure. When incorporated into the MTs, those MEC-7 mutant proteins may affect the binding of MAPs or motor proteins (e.g. Kinesin 13 family protein KLP-7) by either binding poorer to destabilizing proteins or better to stabilizing proteins. The net result would be hyperstable MTs. The loss of TBA-7 presumably allowed more MEC-12 to be incorporated into the MTs, which led to increased MT stability. Abnormally elevated MT stability caused excessive neurite growth.

Supplemental Figure legends

Figure S1. Gene structures for *mec-12*, *mec-7*, and *tba-7* and the molecular lesions in various putative null alleles. *u1026*, *u1027*, and *u1028* were created using CRISPR/Cas9-mediated genome editing and guide RNAs designed to target exon 2 of *mec-12*. Frameshift-causing deletions were identified by genotyping. The *tm5083* mutation deletes part of exon 3 and intron 3 of *mec-12* and also causes a frameshift.

Figure S2. The loss of MEC-7 causes PLM-AN branching defects. (A) In the wild-type animals, PLM-AN extends beyond the vulva (asterisk) and sends out a synaptic branch at a position posterior to the vulva; the branch extends to reach the ventral nerve cord. (B-C) PLM-AN is slightly shorter in *mec-7 (ok2152lf)* animals, although it still extends beyond the vulva (triangle). However, PLM-AN fails to form a synaptic branch (B) or could not fully extend the branch at the correct position (C).

Figure S3. *mec-12* alleles that specifically affect touch sensitivity or synaptic vesicle transport. (A) Anterior touch response (out of five stimuli) of the *mec-12* alleles. (B) Percentage of PLM cells showing transport defects or mistargeting of the presynaptic marker RAB-3::GFP. (C) Immunofluorescent intensity of staining using anti-acetylated α-tubulin antibodies. (D) Fluorescent intensity of RFP expressed from the transgene *uIs134[mec-17p::RFP]* crossed into the *mec-12* mutants. Arbitrary units were used in C and D. (E) The length of the PLM-PN in some *mec-12* mutants. Asterisks indicate significant differences ($p < 0.01$) from the wild type animals.

Figure S4. *mec-7(neo)* and *mec-12(neo)*, *tba-7(lf)*, and *klp-7(lf)* mutants have increased resistance to colchicine. (A) Anterior touch response of adult animals grown on plate containing different concentrations of colchicine from the first larval (L1) stage. (B) The normalized length of PLM-PN of adults grown on plates with colchicine from the L1 stage. PLM-PN lengths of animals treated with 0.06 mM colchicine (9.0 for wild type, 13.3 for *u278*, 10.0 for *u1017*, 10.1 for *u917*, 11.0 for *u1015*, and 10.5 for *tm2143*) were used to set as the reference for the normalization. Asterisks indicate the differences

among the means were statistically significant in ANOVA tests (one asterisk indicates $p < 0.05$ and two for $p < 0.01$).

Figure S5. Sequence alignment of MEC-7 with human TUBB3 and TUBB2B (A) and alignment between MEC-12 and TUBA1A (B). Regions predicted to be α-helices (H1 to H12) or β-strands (B1 to B10) by the α/β tubulin dimer structure (1jff.pdb; Nogales et al. 1998) were labeled. Amino acids that were changed in *mec-7* or *mec-12* antimorphs and neomorphs were labeled in red and blue, respectively.

Figure S6. TBA-7 is expressed and acts cell-autonomously in the TRNs. (A) A schematic representation of the *tba-7::GFP* reporter, containing a 1.2 kb promoter and the entire coding region. (B) The expression of *tba-7::GFP* in the TRNs, which are also labeled by *mec-17p::RFP*. Arrows point to the cell bodies of TRNs. The posterior intestine also showed strong GFP signal (the rightmost panel). (C) The length of ALM-PN in *tba-7(u1015 lf)* mutants that carried a rescuing array that expressed wild-type *tba-7* in the TRNs specifically.

Figure S7. Touch sensitivity, presynaptic vesicle localization, tubulin acetylation level, and protein expression level of *tba-7(u1015 lf)* and *klp-7(tm2143 lf)* mutants. No significant differences between these mutants and wild type were found.

Figure S8. Moderate shortening of ALM-AN and PLM-AN in *klp-11[u1024* (Q53*) *lf]* mutants. In (B), arrows point to the ends of the anterior neurites, and triangles indicate the position of the vulva. ALM-AN did not extend as far as the procorpus of the pharynx and PLM-AN failed to reach the vulva in *klp-11* mutants.

Figure S9. Sequence alignment of all *C. elegans* α-tubulin proteins (A) and all human α-tubulin proteins (B). Only the N-terminal and C-terminal sequences were shown. The arrow points to Q31 residue.

Gene	Allele	Mutation	Structural function	Classification	Morphological defects	Touch sensitivity	Expression
mec-7	*u319*	S25F	Tubulin folding	weak antimorph	moderately shortened neurites	-	semidominant
	u305, u1020	G34S	Lumen-facing loop	lf	short PLM-PN	±	recessive
	gk906464	G38E	Lumen-facing loop	N/A	no defects	+	N/A
	u58, u223	P61L	Lateral interaction	weak antimorph	moderately shortened neurites	−	semidominant
	u249	P61S	Lateral interaction	weak antimorph	moderately shortened neurites	−	semidominant
	gk337318	V64I	Tubulin folding	N/A	no defects	+	N/A
	u430	A97V	GTP binding	antimorph	short TRN neurites	−	recessive
	u222	G109E	Lateral interaction	weak antimorph	moderately shortened neurites	−	semidominant
	u429, u433	G141E	Tubulin folding	lf	short PLM-PN	−	recessive
	gk595364	G141R	Tubulin folding	lf	short PLM-PN	−	recessive
	u275	G148R	Tubulin folding	lf	short PLM-PN	−	recessive
	gk895768	T149I	Tubulin folding	neomorph	ectopic ALM-PN	±	recessive
	gk286003	R162Q	MAP binding	neomorph	ectopic ALM-PN	±	recessive
	u911	P171S	GTP binding	antimorph	short TRN neurites	−	dominant
	u957, u127, e1343	P171L	GTP binding	antimorph	short TRN neurites	−	semidominant
	u1056	S172P*	GTP binding	lf	short PLM-PN	−	recessive
	u1057	P173L*	GTP binding	N/A	no defects	+	N/A
	u48	S176F	GTP binding	antimorph	short TRN neurites	−	semidominant
	u449	V179A	GTP binding	antimorph	short TRN neurites	−	semidominant
	u10	S188F	Tubulin folding	lf	short PLM-PN	±	recessive
	u225	T214P	Tubulin folding	lf	short PLM-PN	±	recessive
	ky852	P220S	Tubulin folding	neomorph	ectopic ALM-PN	−	semidominant
	u262	N226Y	GTP binding	antimorph	short TRN neurites	−	semidominant
	gk286002	P243S	Intradimer interaction	lf	short PLM-PN	±	recessive
	u283	P243L	Intradimer interaction	antimorph	short TRN neurites	−	dominant
	u129, u958	G244S	Intradimer interaction	antimorph	short TRN neurites	−	dominant
	n434	N247I	Intradimer interaction	antimorph	short TRN neurites	−	dominant
	u162	D249N	Intradimer interaction	antimorph	short TRN neurites	−	dominant
	e1505	G269D	Tubulin folding	lf	short PLM-PN	±	recessive
	e1527	V286D	Lateral interaction	antimorph	short TRN neurites	−	dominant
	u445	M300V	Tubulin folding	antimorph	short TRN neurites	−	semidominant
	u98	M300T	Tubulin folding	antimorph	short TRN neurites	−	semidominant
	u1058	A302T*	MAP binding	neomorph	ectopic ALM-PN	±	semidominant
	u278	C303Y	MAP binding	neomorph	ectopic ALM-PN	−	semidominant
	gk286001	C303S	MAP binding	N/A	no defects	+	N/A
	gk286000	A314V	Tubulin folding	antimorph	short TRN neurites	−	semidominant
	e1522	F317I	Tubulin folding	lf	short PLM-PN	±	recessive
	u234	R318Q	Tubulin folding	lf	short PLM-PN	±	recessive
	u955	A352T	Intradimer interaction	antimorph	short TRN neurites	−	dominant
	u910, gk373602	P357L	Tubulin folding	antimorph	short TRN neurites	−	dominant

	u956	P358L	Tubulin folding	antimorph	short TRN neurites	−	dominant
	u428	G369E	Tubulin folding	lf	short PLM-PN	−	recessive
	u1017	L377F	MAP binding	neomorph	the growth of ectopic ALM-PN	±	recessive
	u1059	R380S*	MAP binding	neomorph	the growth of ectopic ALM-PN	±	recessive
	u18	A393T	Longitudinal interaction	antimorph	short TRN neurites	−	dominant
	gk285997	A393V	Longitudinal interaction	antimorph	short TRN neurites	−	dominant
	u170	E407L	MAP binding	neomorph	the growth of ectopic ALM-PN	±	recessive
	u1060	E410K*	MAP binding	antimorph	shortened TRN-ANs	−	semidominant
mec-12	*gk170196*	P32S	Lumen-facing loop	neomorph	the growth of ectopic ALM-PN	±	recessive
	gk170195	S50N	Lumen-facing loop	N/A	no defects	+	N/A
	gk636747	R60H	Lumen-facing loop	N/A	no defects	+	N/A
	u76	D69N	GTP binding	antimorph	short PLM-PN	−	recessive
	u1016	E97K	Intradimer interaction	antimorph	short PLM-PN	−	recessive
	u950, gk672907	S140F	GTP binding	antimorph	short PLM-PN	−	recessive
	gk600523	G142E	GTP binding	lf	no defects	±	recessive
	u1021, e1607	G144S	GTP binding	antimorph	short PLM-PN	−	recessive
	gk583647	L152F	Tubulin folding	N/A	no defects	+	N/A
	u50, e1605	H192Y	MAP binding	partial lf	no defects	−	recessive
	gk915672	E196K	MAP binding	neomorph	the growth of ectopic ALM-PN	±	recessive
	u1041	G246E	Tubulin folding	lf	no defects	±	recessive
	u917	V260I	MAP binding	neomorph	the growth of ectopic ALM-PN	±	recessive
	gk854211	P307L	MAP binding	N/A	no defects	+	N/A
	gk515972	V323I	Longitudinal interaction	neomorph	the growth of ectopic ALM-PN	±	recessive
	u241, u1019	G354E	Longitudinal interaction	antimorph	short PLM-PN	−	recessive
	gk341552	G365E	Lumen-facing loop	N/A	no defects	+	N/A
	u63	E415K	MAP binding	partial lf	no defects	±	recessive
	gm379	G416E	MAP binding	partial lf	no defects	±	recessive

Table Legends

Table 1. The *mec-7* and *mec-12* mutations analyzed in this study. Several mutations are represented by multiple alleles, whose phenotypes were found to be similar. For touch sensitivity, + indicate the average response to 5 anterior stimuli is above 4; ± indicate the average is between 4 and 1; − indicate the average is below 1. Partial *lf* alleles of *mec-12* showed some but not all of the *lf* phenotypes (see the text). Asterisks indicate that the mutation was originally found in humans and was created in *mec-7* gene through CRISPR/Cas9-mediated genome editing. Mapping of the amino acid residues to the structural domains was done according to Tischfield *et al.* (2011).

A

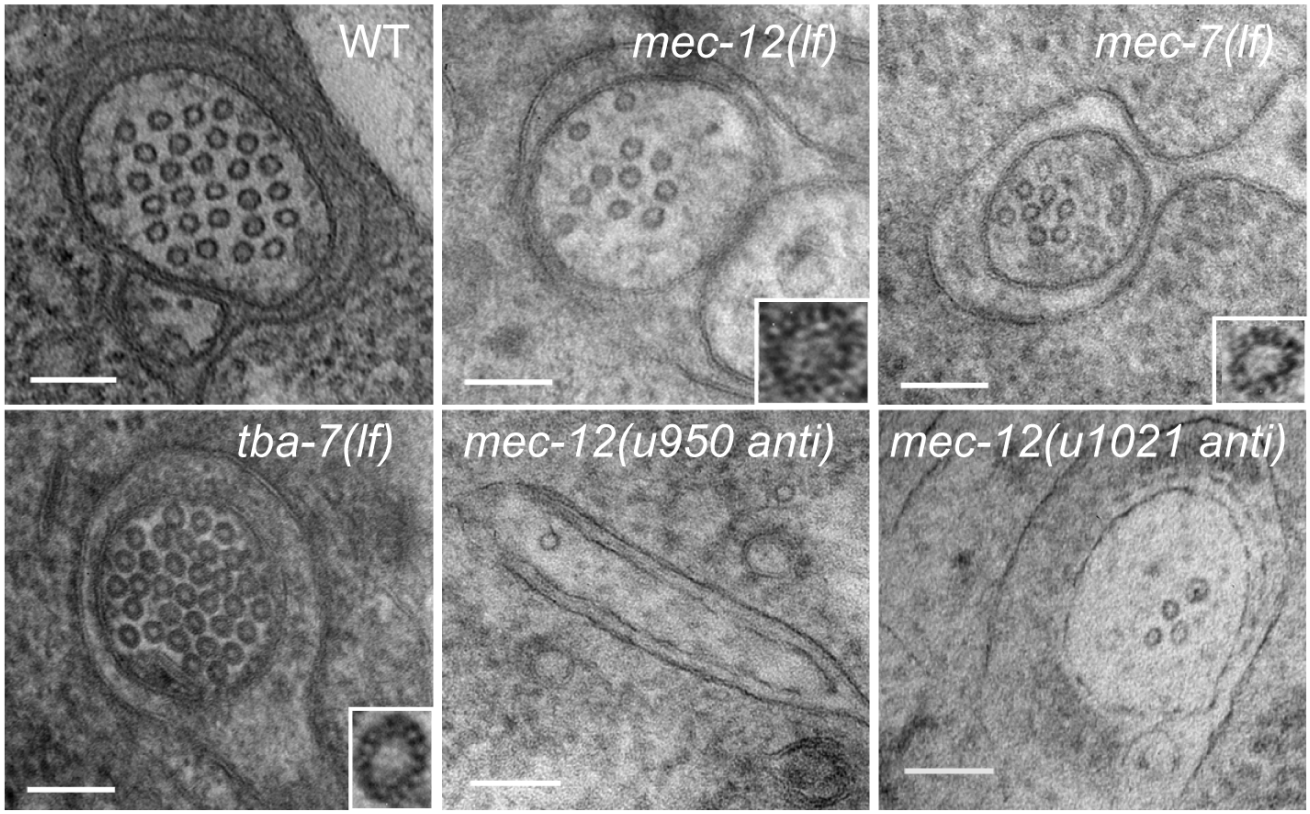

B

Genotype	Number of MTs	MT diameters (nm)	Center-center distance (nm)	MT-occupied area (%)
wild type	31.1 ± 7.3 (79)	21.5 ± 1.6 (126)	34.4 ± 1.0 (320)	46.7 ± 5.5 (38)
mec-7(ok2152 lf)	6.0 ± 2.2 (52)**	16.6 ± 1.4 (123)**		
mec-12(tm5083 lf)	7.4 ± 2.4 (36)**	21.3 ± 2.0 (103)		
tba-7(u1015 lf)	27.0 ± 10.1 (109)	22.4 ± 1.8 (248)**	32.3 ± 2.1 (278)**	57.2 ± 10.1 (74)**
mec-7(u170 neo)	18.0 ± 5.8 (25)**	22.7 ± 2.2 (192)**	31.7 ± 2.3 (148)**	58.6 ± 5.2 (20)**
mec-7(u278 neo)	20.6 ± 6.8 (23)**	22.5 ± 1.9 (176)**	32.9 ± 1.5 (164)**	59.0 ± 8.1 (18)**
mec-12(u76 anti)	1.6 ± 1.5 (52)**	17.6 ± 2.6 (53)**		
mec-12(u950 anti)	2.5 ± 2.1 (40)**	18.0 ± 2.0 (75)**		
mec-12(u1021 anti)	2.7 ± 2.4 (72)**	17.9 ± 1.8 (114)**		

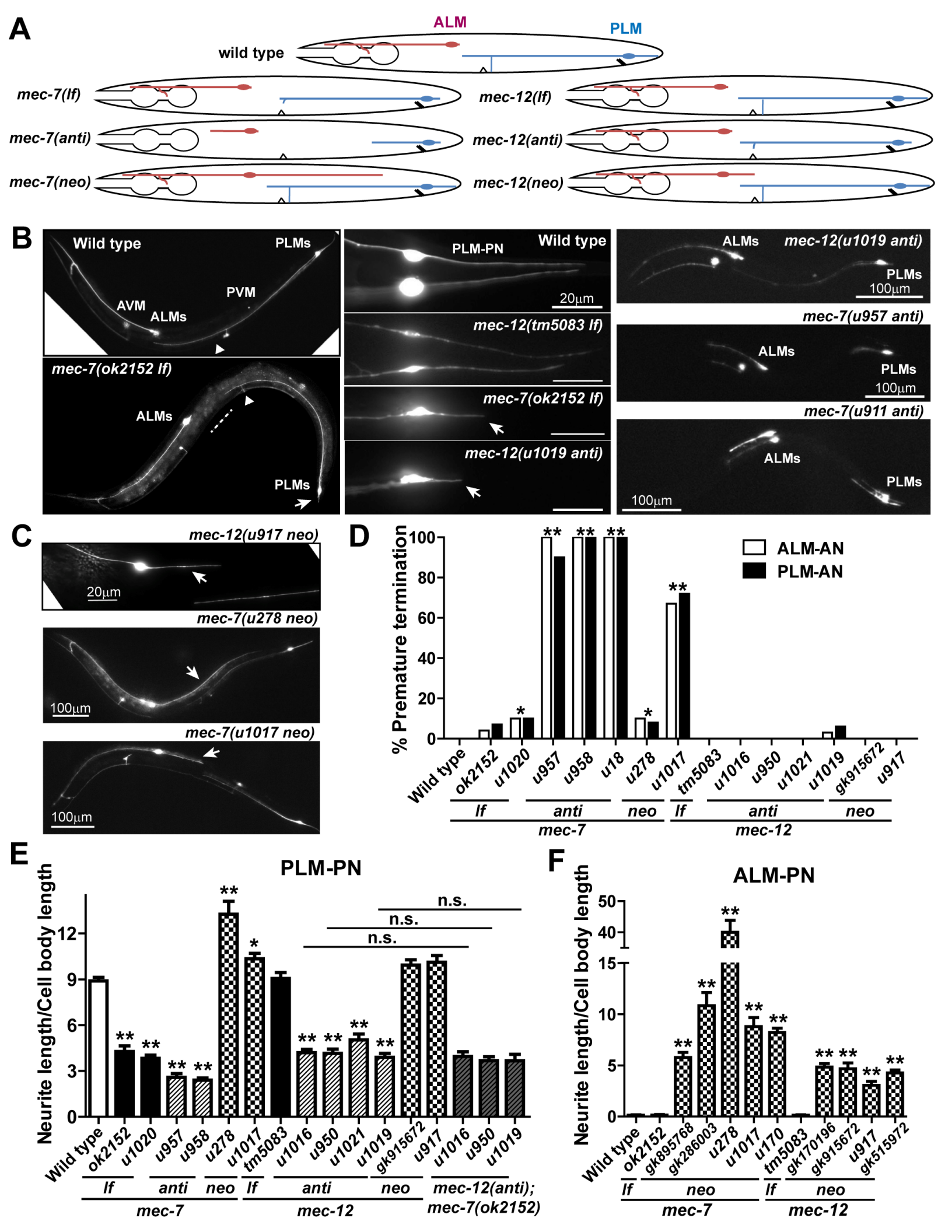
A
ALM
PLM
wild type
mec-7(lf)
mec-7(anti)
mec-7(neo)
mec-12(lf)
mec-12(anti)
mec-12(neo)
B
Wild type
PLMs
AVM
ALMs
PVM
mec-7(ok2152 lf)
ALMs
PLMs
PLM-PN
Wild type
20μm
mec-12(tm5083 lf)
mec-7(ok2152 lf)
mec-12(u1019 anti)
ALMs
mec-12(u1019 anti)
PLMs
100μm
mec-7(u957 anti)
ALMs
PLMs
100μm
mec-7(u911 anti)
ALMs
PLMs
100μm
C
mec-12(u917 neo)
20μm
mec-7(u278 neo)
100μm
mec-7(u1017 neo)
100μm
D
% Premature termination
ALM-AN
PLM-AN
Wild type
ok2152
u1020
u957
u958
u18
u278
u1017
tm5083
u1016
u950
u1021
u1019
gk915672
u917
lf
anti
neo
lf
anti
neo
mec-7
mec-12
E
PLM-PN
Neurite length/Cell body length
n.s.
n.s.
n.s.
Wild type
ok2152
u1020
u957
u958
u278
u1017
tm5083
u1016
u950
u1021
u1019
gk915672
u917
u1016
u950
u1019
lf
anti
neo
lf
anti
neo
mec-12(anti);
mec-7(ok2152)
mec-7
mec-12
F
ALM-PN
Neurite length/Cell body length
Wild type
ok2152
gk895768
gk286003
u278
u1017
u170
tm5083
gk170196
gk915672
u917
gk515972
lf
neo
lf
neo
mec-7
mec-12

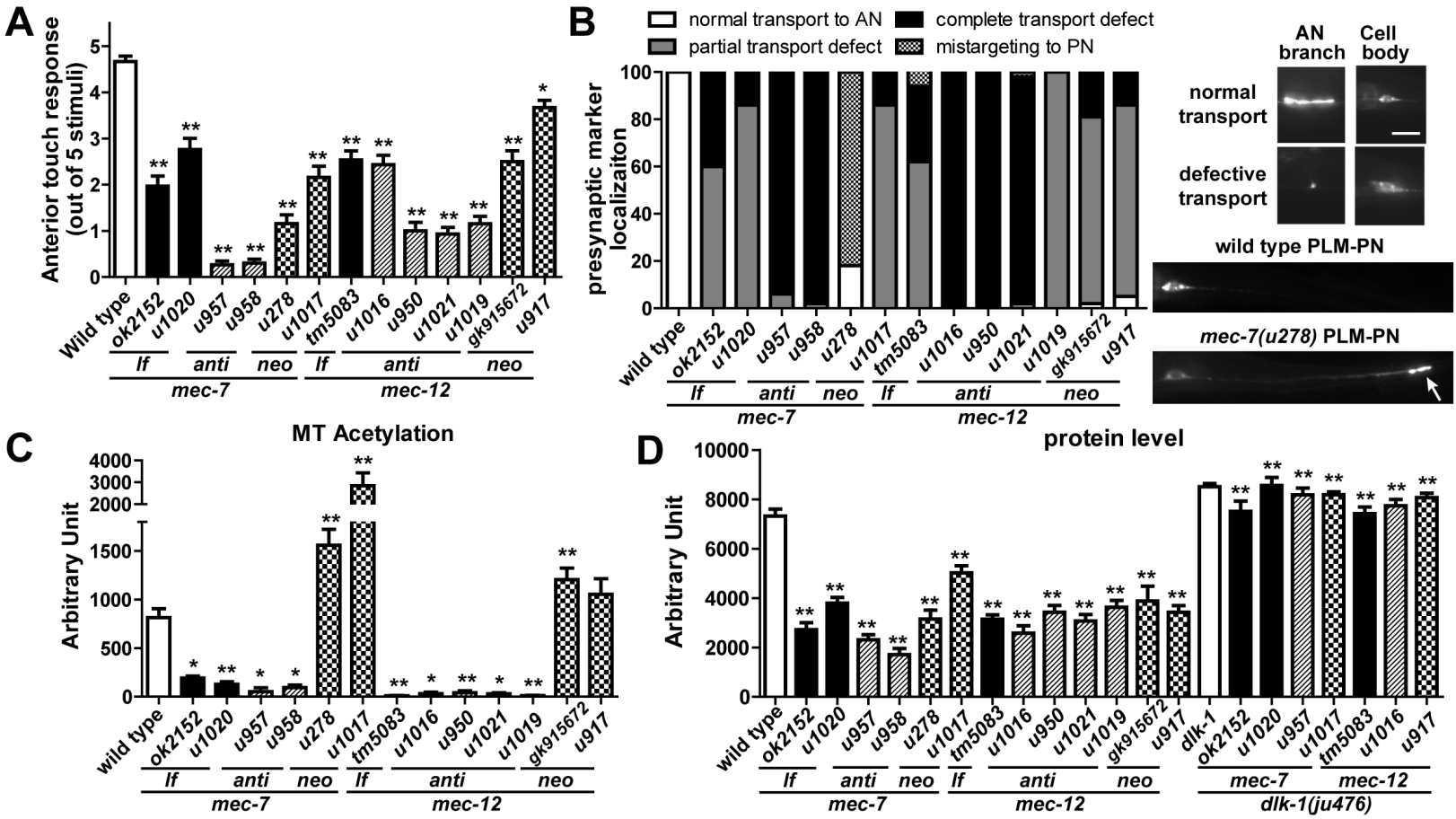
A
Anterior touch response (out of 5 stimuli)
Wild type
ok2152
u1020
u957
u958
u278
u1017
tm5083
u1016
u950
u1021
u1019
gk915672
u917
lf
anti
neo
mec-7
mec-12
B
normal transport to AN
partial transport defect
complete transport defect
mistargeting to PN
presynaptic marker localizaiton
AN branch
Cell body
normal transport
defective transport
wild type PLM-PN
mec-7(u278) PLM-PN
C
MT Acetylation
Arbitrary Unit
D
protein level
Arbitrary Unit
dlk-1
dlk-1(ju476)

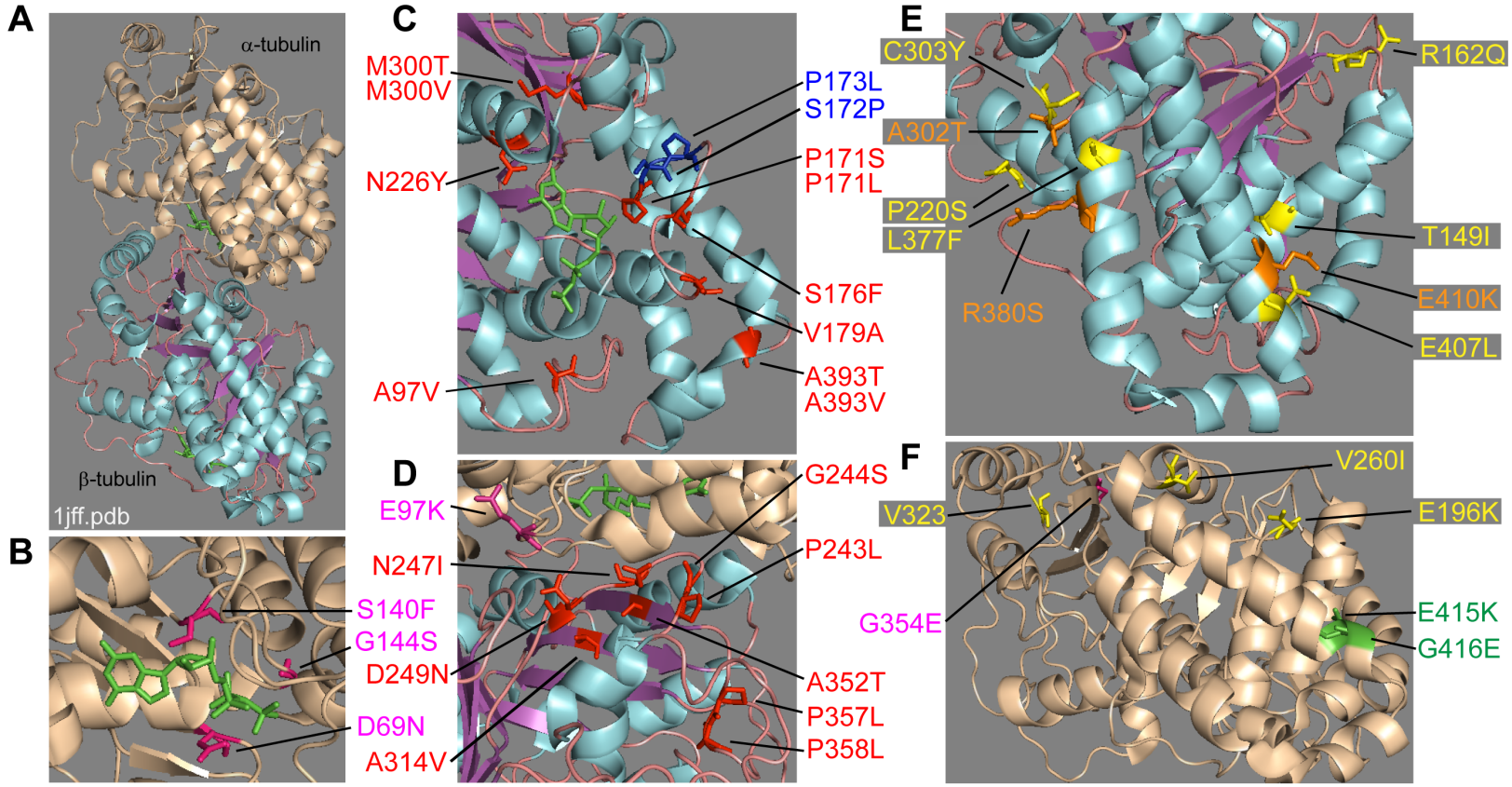
A
α-tubulin
β-tubulin
1jff.pdb
B
S140F
G144S
D69N
C
M300T
M300V
N226Y
A97V
P173L
S172P
P171S
P171L
S176F
V179A
A393T
A393V
D
E97K
N247I
D249N
A314V
G244S
P243L
A352T
P357L
P358L
E
C303Y
A302T
P220S
L377F
R380S
R162Q
T149I
E410K
E407L
F
V323
G354E
V260I
E196K
E415K
G416E

A

S172P

169 V V P S P K V S D T V V E P Y 183

GTAGTTCCAAGTCCAAAAGTATCCGACACTGTAGTCGAACCCTAC

GTAGTTCCACCTCCAAAGGTCTCCGACACTGTAGTGCTTGGGATC

P173L

169 V V P S P K V S D T V V E P Y 183

GTAGTTCCAAGTCCAAAAGTATCCGACACTGTAGTCGAACCCTAC

GTAGTTCCAAGTCTGAAGGTCTCCGACACTGTAGTGCTTGGGATC

A302T

296 A K N M M A A C D P R H G R Y 310

GCAAAGAACATGATGGCTGCATGCGATCCAAGACATGGACGTTAT

GCAAAGAACATGATGGCTACTTGTGACCCTAGACATGGACGTTAT

R380S

369 G N S T A I Q E L F K R I S E 383

GGAAACTCCACCGCCATTCAAGAGCTCTTTAAGAGAATCTCAGAG

GGAAACTCCACCGCCATACAGGAACTGTTCAAGAGTATCTCAGAG

E410K

402 G M D E M E F T E A E S N M N 416

GGAATGGACGAGATGGAATTCACTGAGGCGGAGAGCAACATGAAC

GGAATGGACGAGATGGAGTTTACCAAAGCGGAGAGCAACATGAAC

B

***u1056* (S172P)**

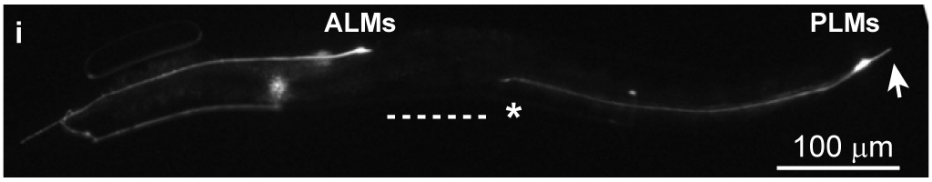

***u1059* (R380S)**

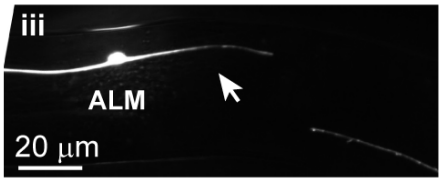

***u1057* (P173L)**

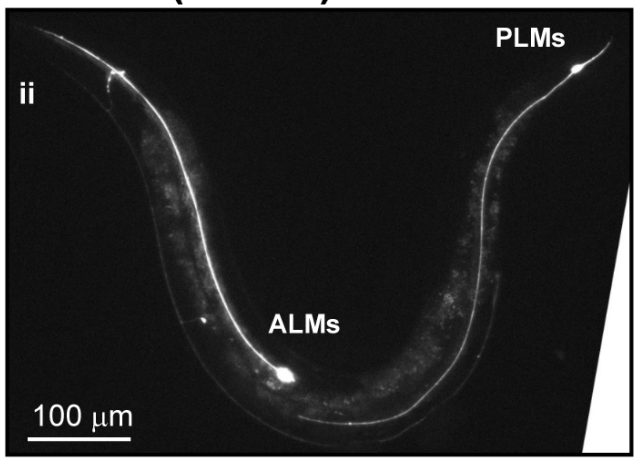

***u1058* (A302T)**

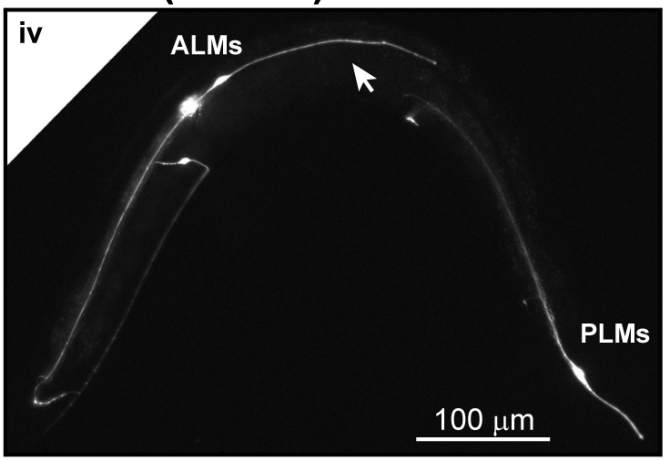

***u1060* (E410K)**

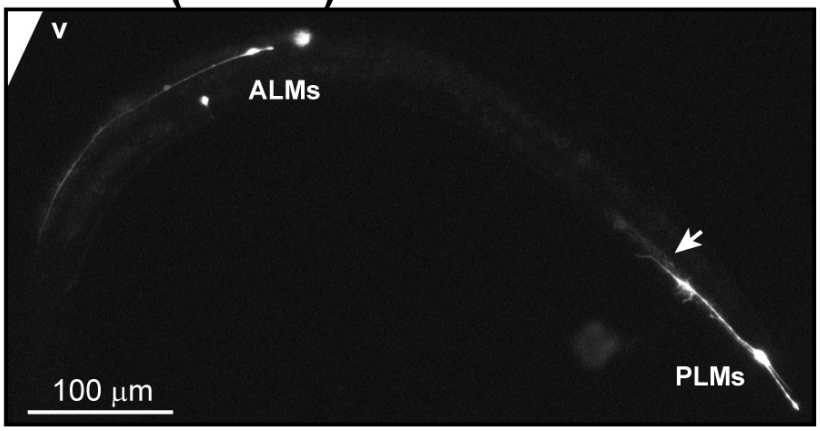

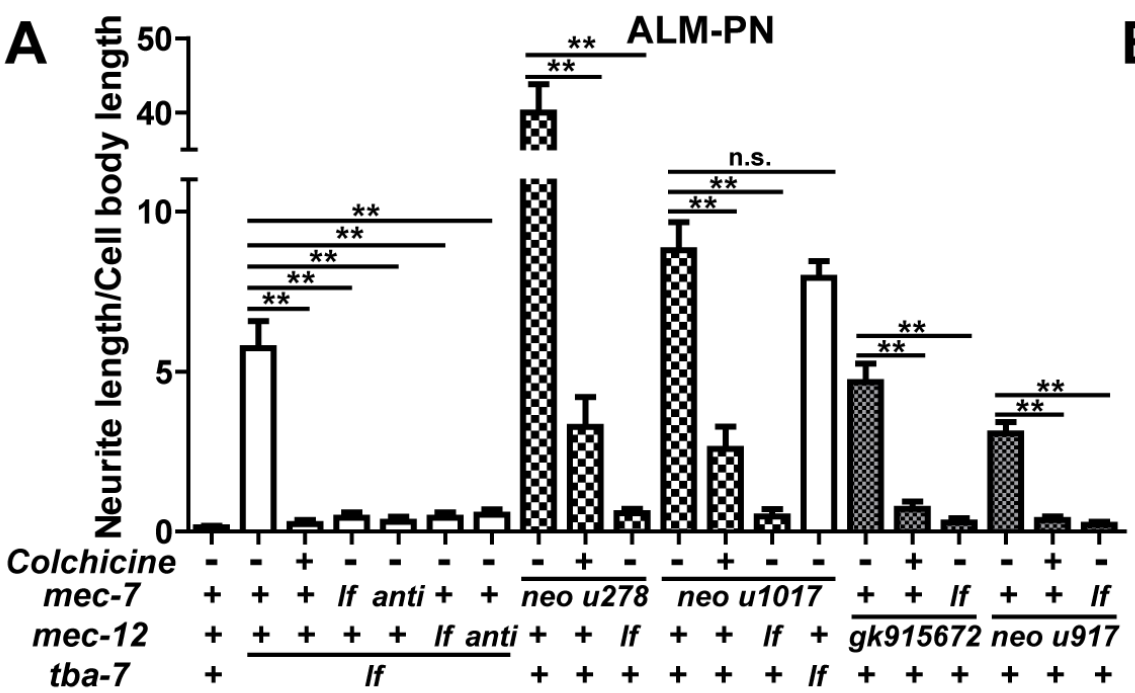

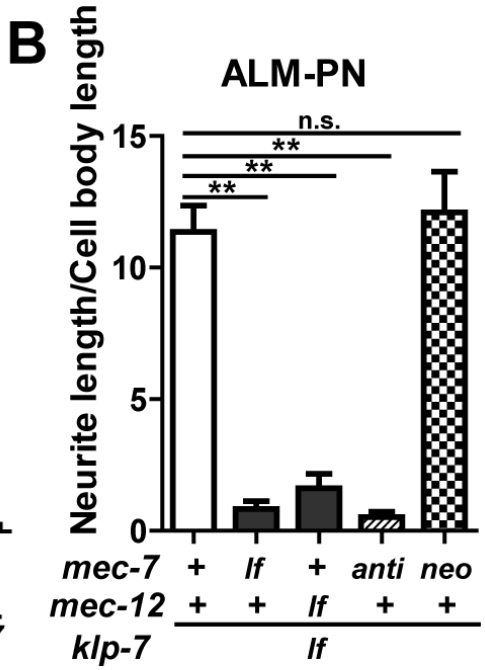

C

```
TBA-7    26 LEHGILPDGTSMEP---DGNSGSLGTFF 50
MEC-12   26 LEHGIQPDGQMPSDKSLGGSDDSFSTFF 53

TBA-7   418 EDLAALEKDYEEVGADSDANDN-GDDEY 444
MEC-12  423 EDLAALEKDYEEVGVDSMEDNGEEGDEY 450
```

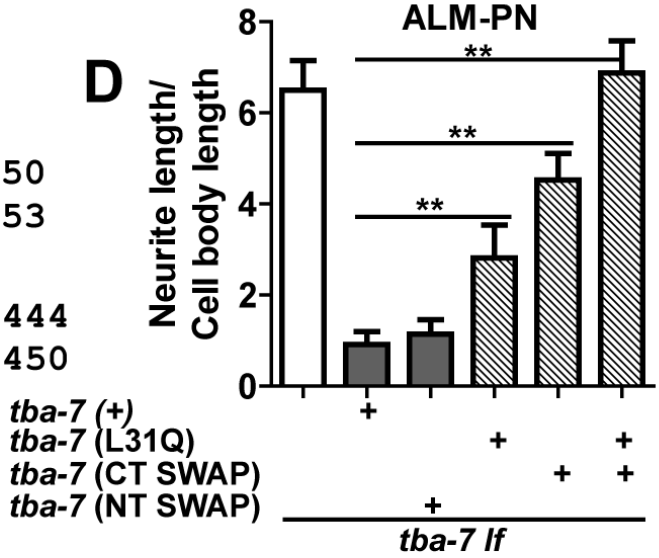

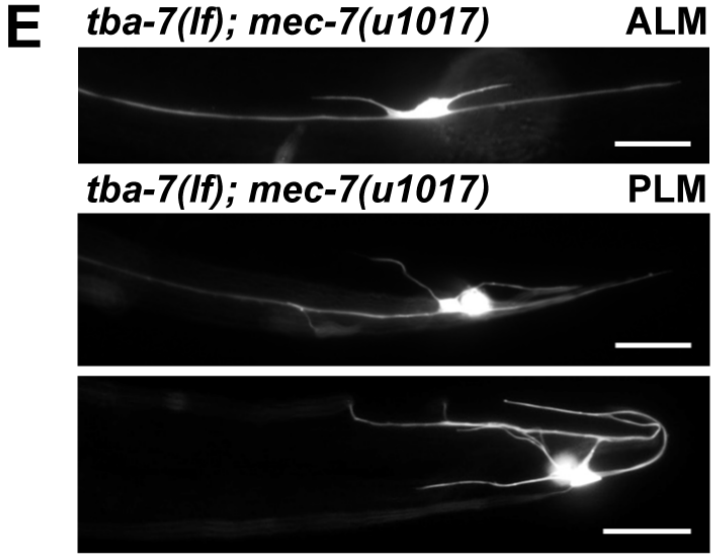

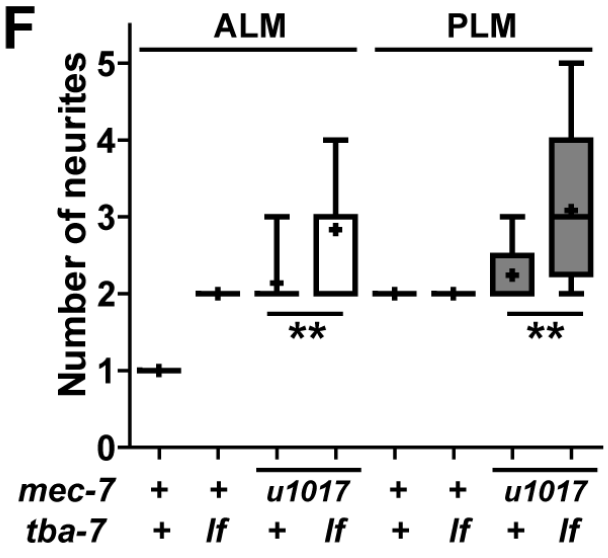

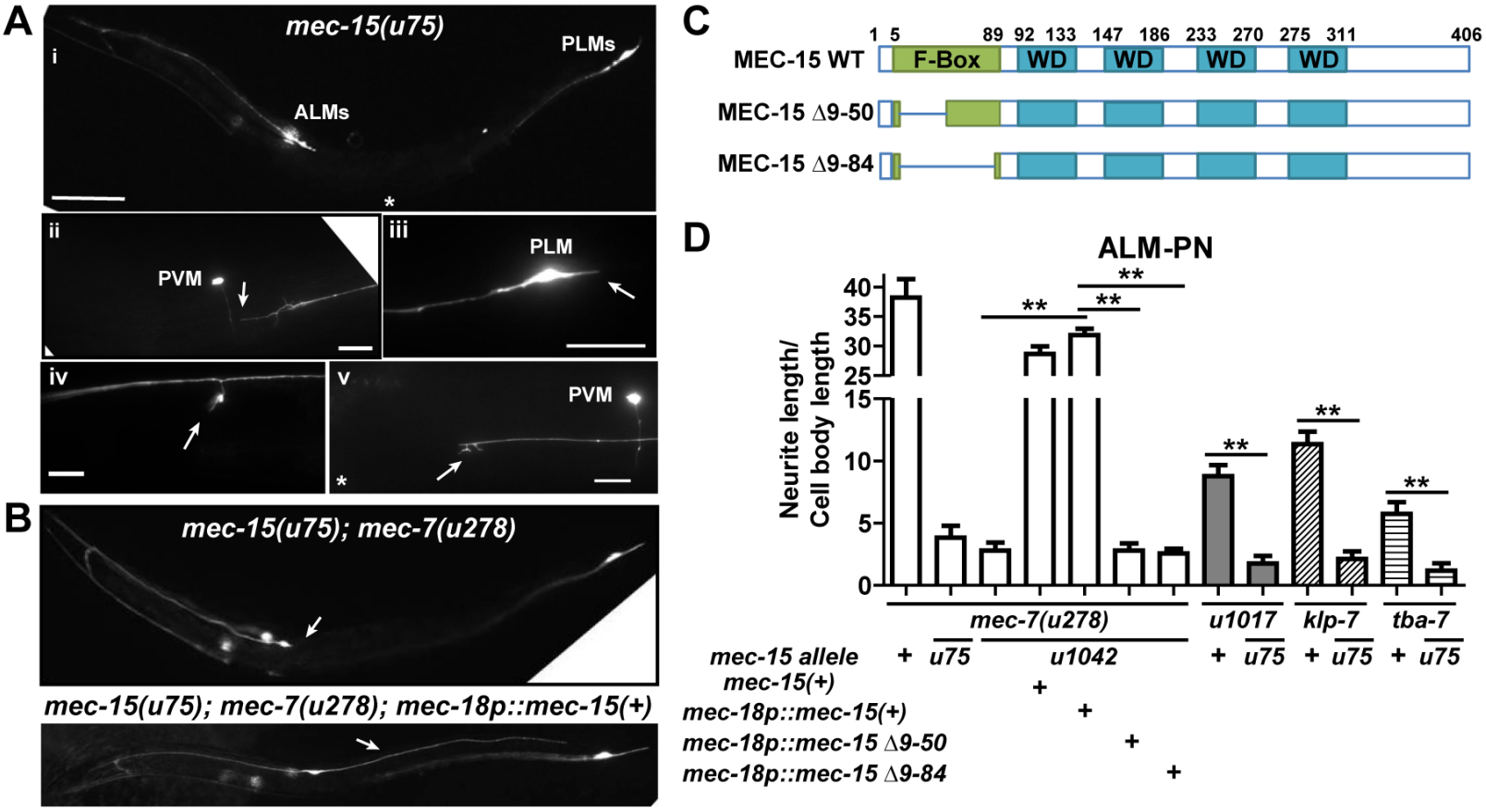
A
mec-15(u75)
i
PLMs
ALMs
*
ii
PVM
iii
PLM
iv
v
PVM
*
B
mec-15(u75); mec-7(u278)
mec-15(u75); mec-7(u278); mec-18p::mec-15(+)
C
1 5 89 92 133 147 186 233 270 275 311 406
MEC-15 WT
F-Box
WD
WD
WD
WD
MEC-15 Δ9-50
MEC-15 Δ9-84
D
ALM-PN
Neurite length/
Cell body length
40
35
30
25
15
10
5
0
**
**
**
**
**
**
mec-7(u278)
u1017
klp-7
tba-7
mec-15 allele
+
u75
u1042
+
u75
+
u75
+
u75
mec-15(+)
+
mec-18p::mec-15(+)
+
mec-18p::mec-15 Δ9-50
+
mec-18p::mec-15 Δ9-84
+

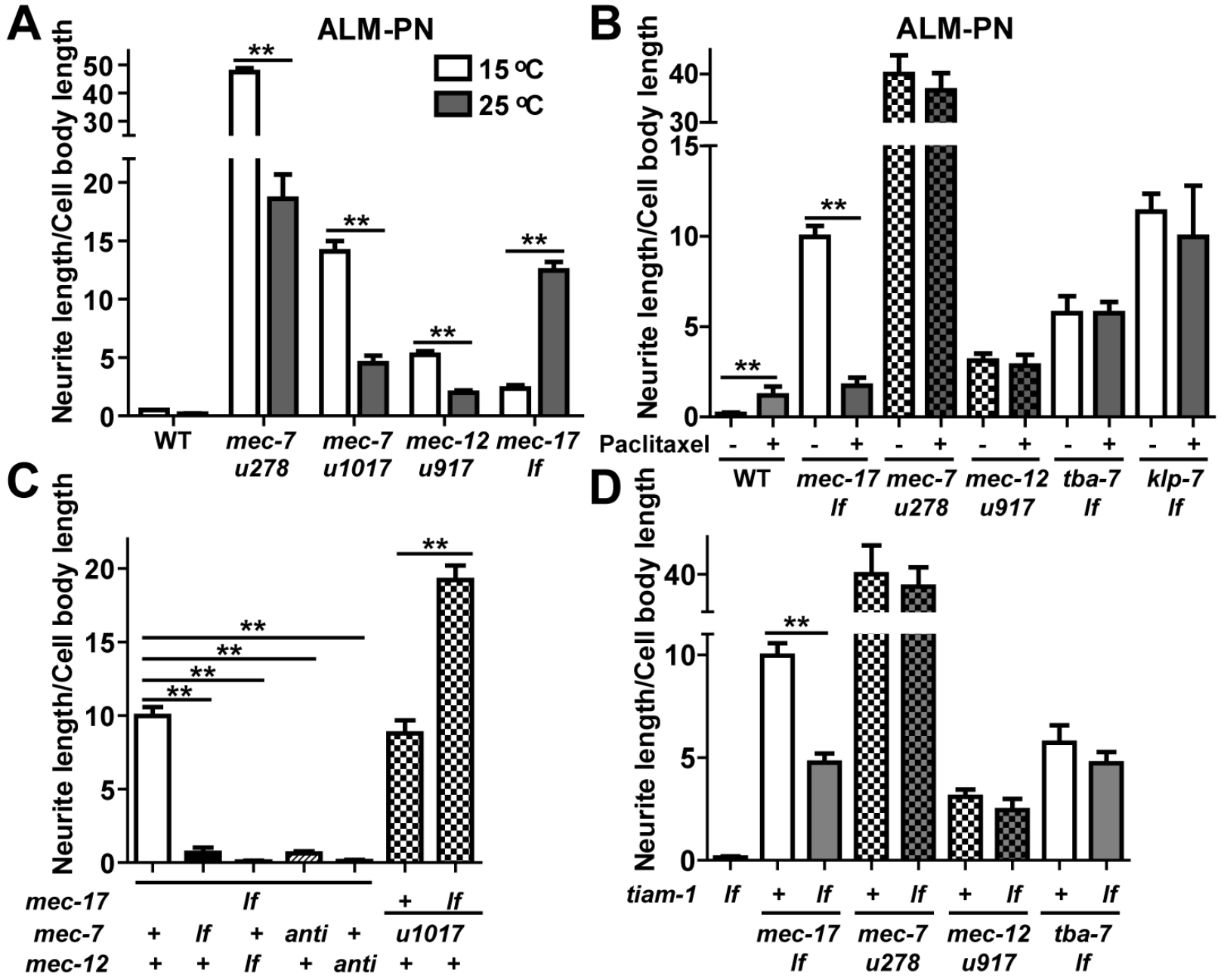
A
ALM-PN
Neurite length/Cell body length
15 ºC
25 ºC
**
WT
mec-7 u278
mec-7 u1017
mec-12 u917
mec-17 lf
B
ALM-PN
Neurite length/Cell body length
Paclitaxel
WT
mec-17 lf
mec-7 u278
mec-12 u917
tba-7 lf
klp-7 lf
C
Neurite length/Cell body length
mec-17
mec-7
mec-12
lf
anti
u1017
D
Neurite length/Cell body length
tiam-1
mec-17 lf
mec-7 u278
mec-12 u917
tba-7 lf

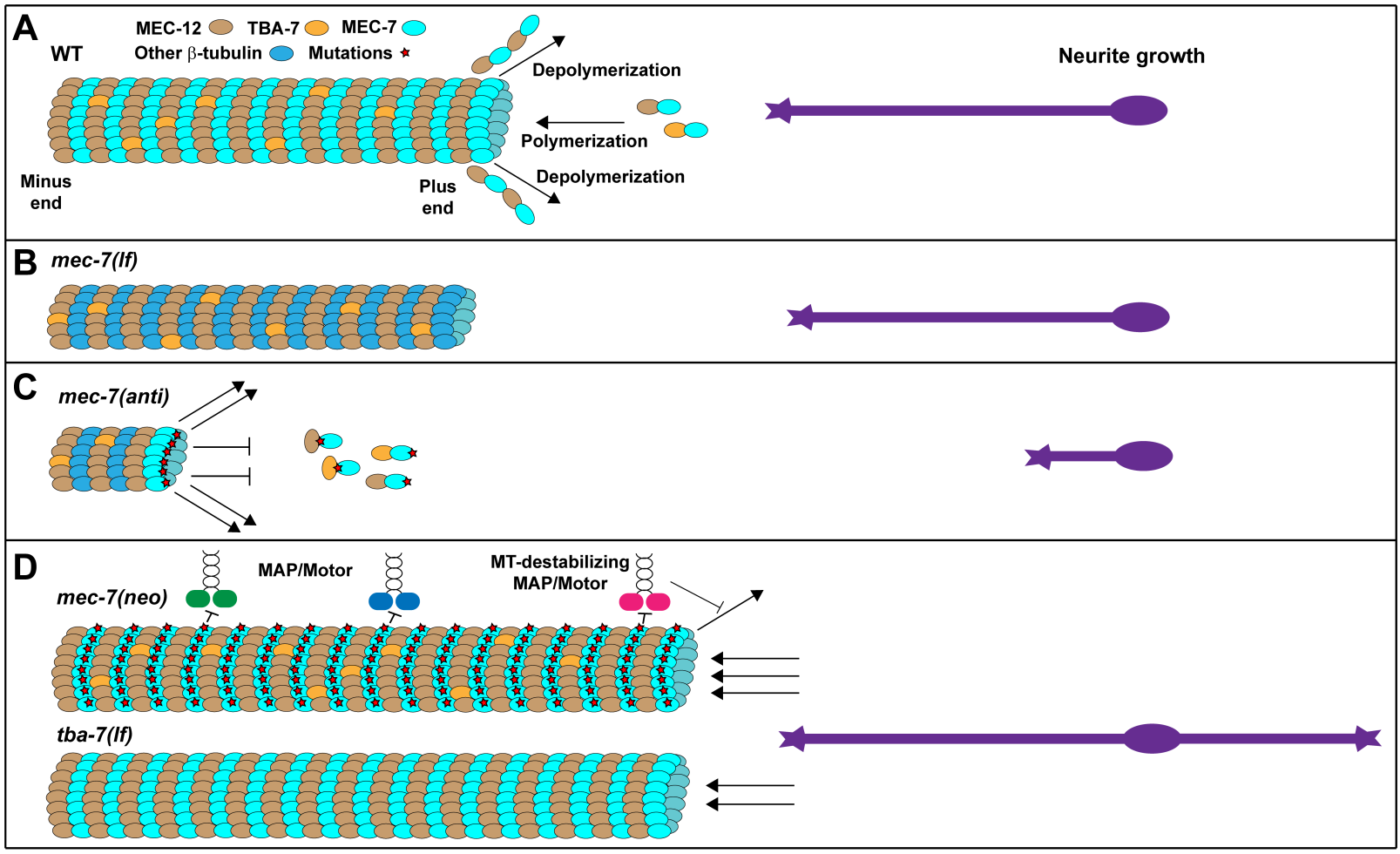
A
WT
MEC-12
TBA-7
MEC-7
Other β-tubulin
Mutations
Depolymerization
Polymerization
Depolymerization
Minus end
Plus end
Neurite growth
B
mec-7(lf)
C
mec-7(anti)
D
mec-7(neo)
MAP/Motor
MT-destabilizing MAP/Motor
tba-7(lf)

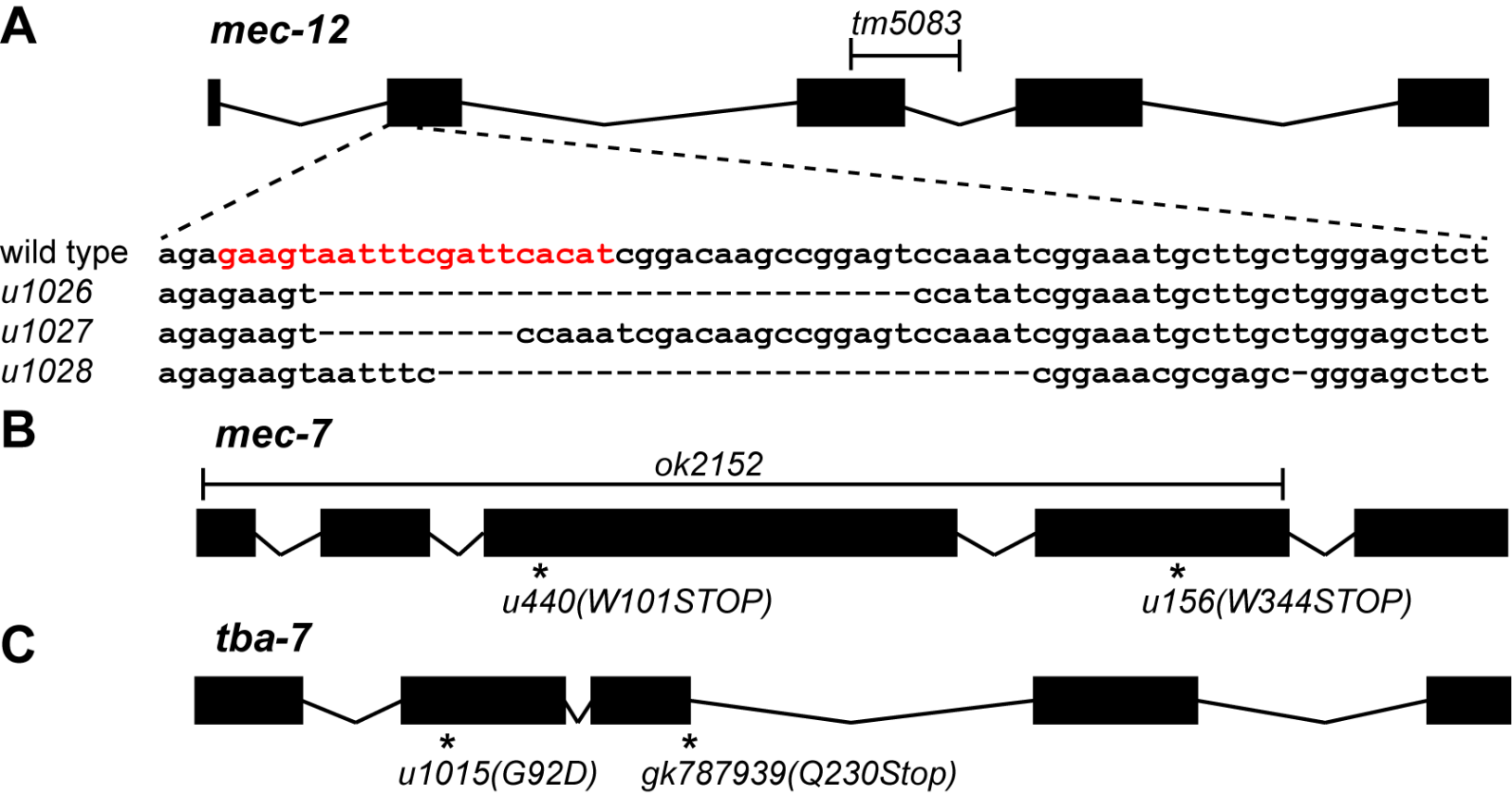
A
mec-12
tm5083
wild type agagaagtaatttcgattcacatcggacaagccggagtccaaatcggaaatgcttgctgggagctct
u1026 agagaagt----------ccatatcggaaatgcttgctgggagctct
u1027 agagaagt----------ccaaatcgacaagccggagtccaaatcggaaatgcttgctgggagctct
u1028 agagaagtaatttc----------cggaaacgcgagc-gggagctct
B
mec-7
ok2152
u440(W101STOP)
u156(W344STOP)
C
tba-7
u1015(G92D)
gk787939(Q230Stop)

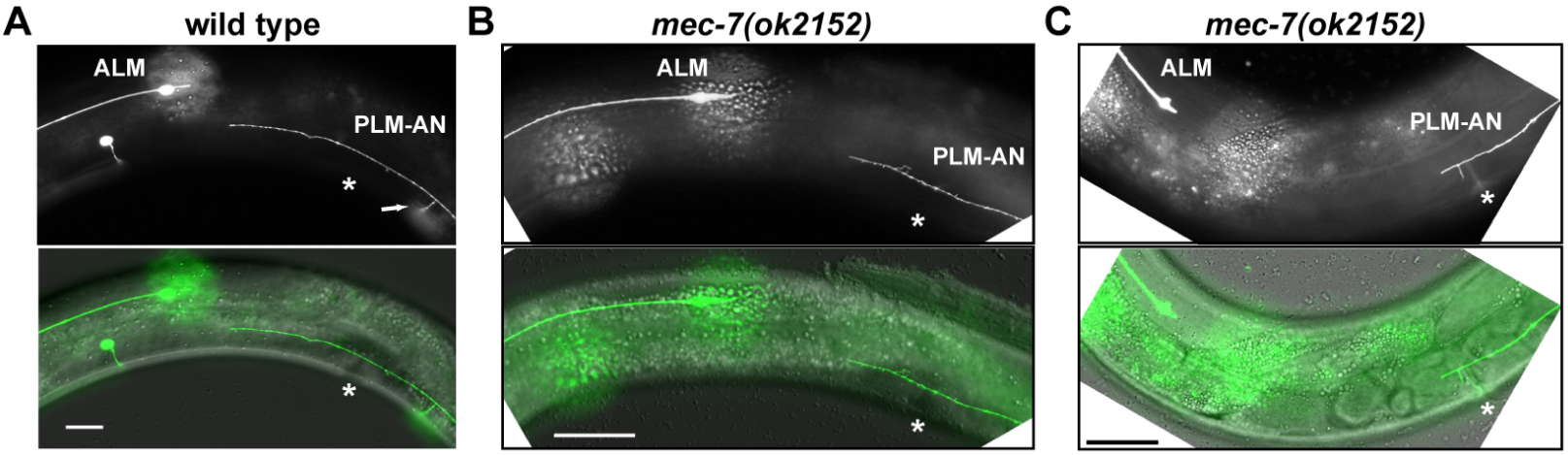
A
wild type
ALM
PLM-AN
*
*
B
mec-7(ok2152)
ALM
PLM-AN
*
*
C
mec-7(ok2152)
ALM
PLM-AN
*
*

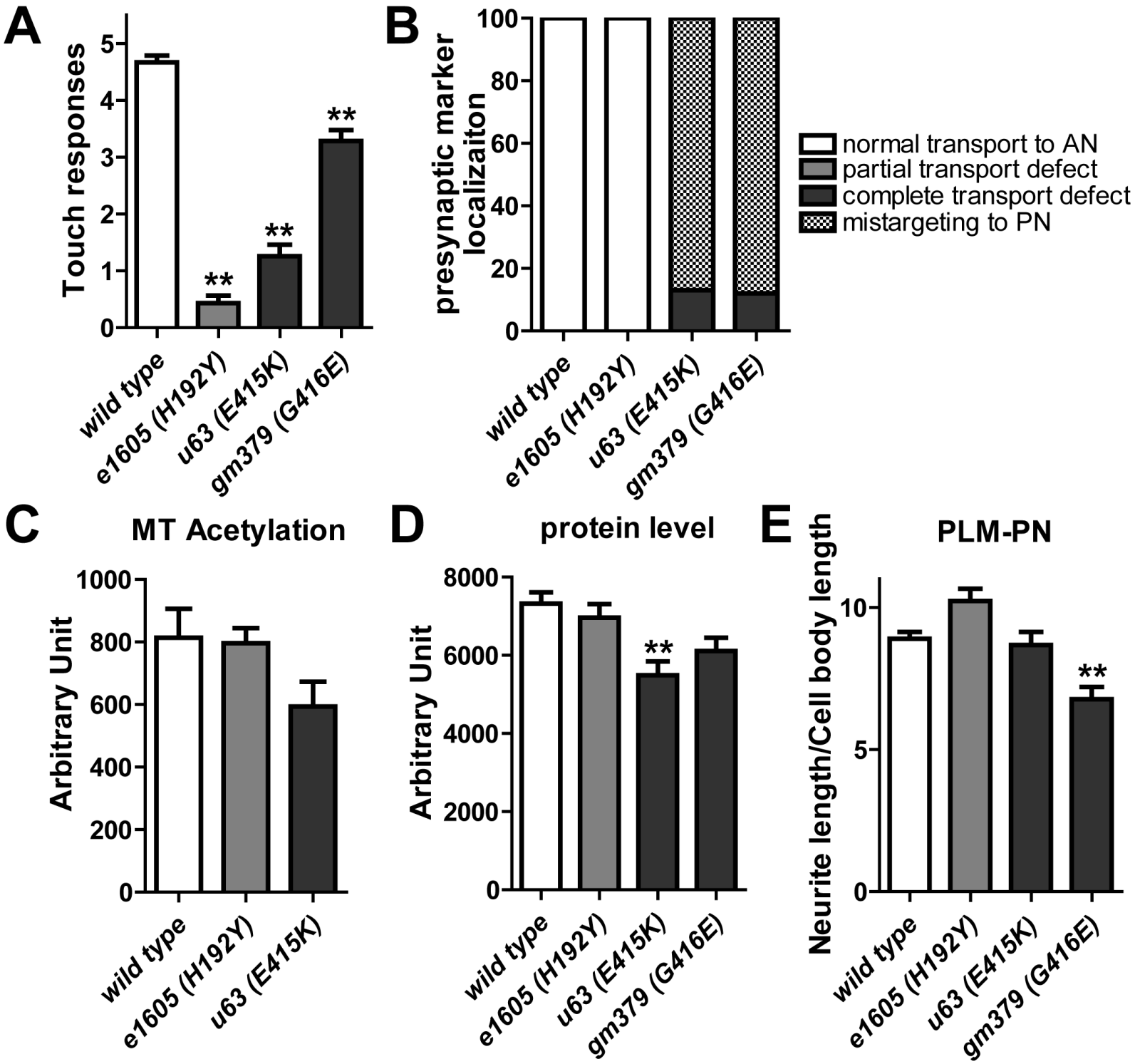
A
Touch responses
0
1
2
3
4
5
**
**
**
wild type
e1605 (H192Y)
u63 (E415K)
gm379 (G416E)
B
presynaptic marker localizaiton
0
20
40
60
80
100
normal transport to AN
partial transport defect
complete transport defect
mistargeting to PN
wild type
e1605 (H192Y)
u63 (E415K)
gm379 (G416E)
C
MT Acetylation
Arbitrary Unit
0
200
400
600
800
1000
wild type
e1605 (H192Y)
u63 (E415K)
D
protein level
Arbitrary Unit
0
2000
4000
6000
8000
**
wild type
e1605 (H192Y)
u63 (E415K)
gm379 (G416E)
E
PLM-PN
Neurite length/Cell body length
0
5
10
**
wild type
e1605 (H192Y)
u63 (E415K)
gm379 (G416E)

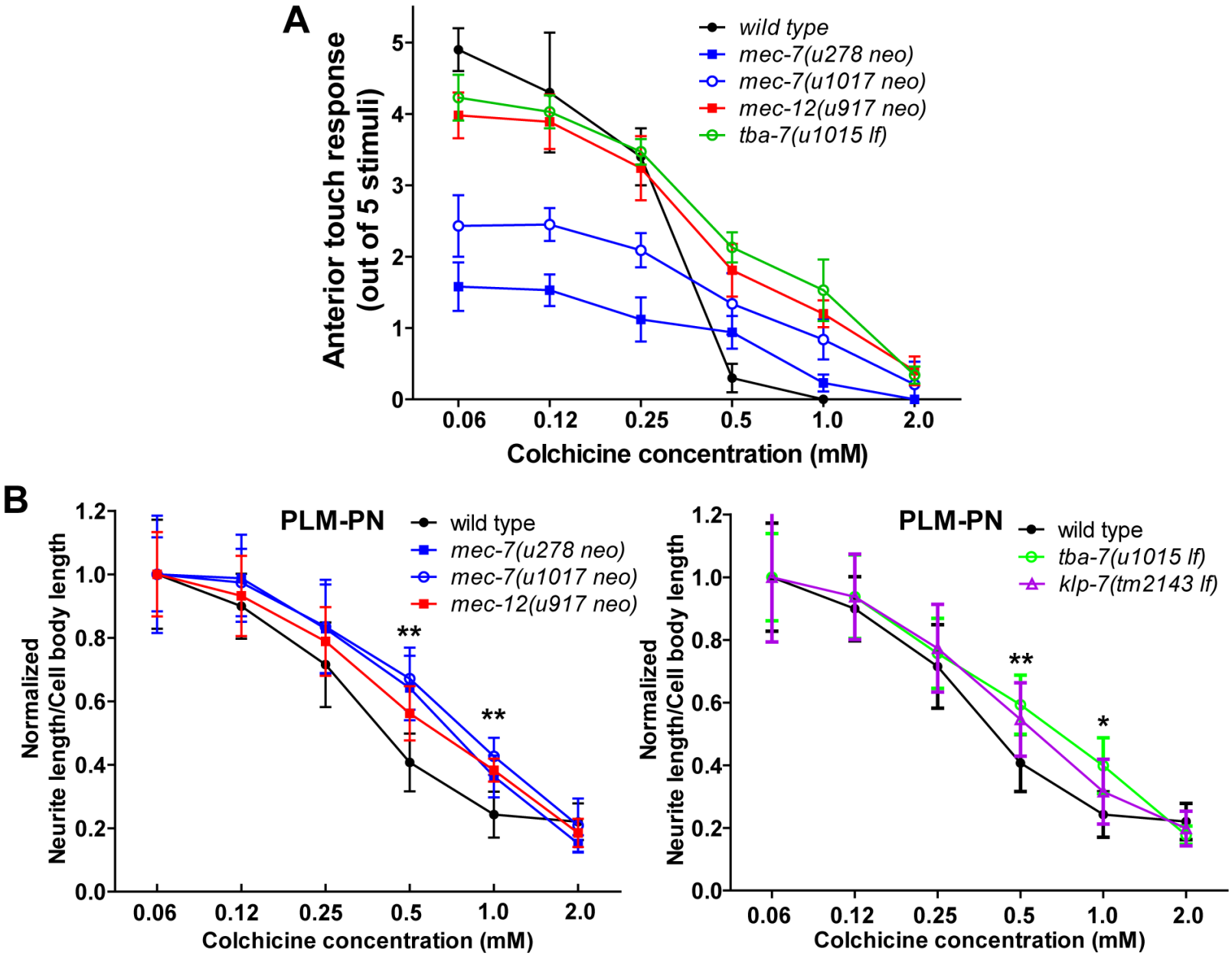
A
Anterior touch response
(out of 5 stimuli)
wild type
mec-7(u278 neo)
mec-7(u1017 neo)
mec-12(u917 neo)
tba-7(u1015 lf)
0
1
2
3
4
5
0.06
0.12
0.25
0.5
1.0
2.0
Colchicine concentration (mM)
B
PLM-PN
Normalized
Neurite length/Cell body length
wild type
mec-7(u278 neo)
mec-7(u1017 neo)
mec-12(u917 neo)
**
**
0.0
0.2
0.4
0.6
0.8
1.0
1.2
0.06
0.12
0.25
0.5
1.0
2.0
Colchicine concentration (mM)
PLM-PN
Normalized
Neurite length/Cell body length
wild type
tba-7(u1015 lf)
klp-7(tm2143 lf)
**
*
0.0
0.2
0.4
0.6
0.8
1.0
1.2
0.06
0.12
0.25
0.5
1.0
2.0
Colchicine concentration (mM)

A

```
Human TUBB3     1 MREIVHIQAGQCGNQIGAKFWEVISDEHGIDPSGNYVGDSDLQLERISVYYNEASSHKYVPRAILVDLEPGTMDSVRSGAFGHLFRPDNF 90
Human TUBB2B      MREIVHIQAGQCGNQIGAKFWEVISDEHGIDPTGSYHGDSDLQLERINVYYNEATGNKYVPRAILVDLEPGTMDSVRSGPFGQIFRPDNF
C.elegans MEC-7   MREIVHIQAGQCGNQIGSKFWEVISDEHGIDPSGQYVGDSDLQLERINVYYNEAGSNKYVPRAVLVDLEPGTMDSVRSGPFGQLFRPDNY
                  *****************:**************:*.* **********.****** ..******:*************** **::*****:
                   B1            H1                                                B2        H2
Human TUBB3    91 IFGQSGAGNNWAKGHYTEGAELVDSVLDVVRKECENCDCLQGFQLTHSLGGGTGSGMGTLLISKVREEYPDRIMNTFSVVPSPKVSDTVV 180
Human TUBB2B      VFGQSGAGNNWAKGHYTEGAELVDSVLDVVRKESESCDCLQGFQLTHSLGGGTGSGMGTLLISKIREEYPDRIMNTFSVMPSPKVSDTVV
C.elegans MEC-7   VFGQSGAGNNWAKGHYTEGAELVDNVLDVVRKEAESTDCLQGFQLTHSLGGGTGSGMGTLLISKIREEYPDRIMNTFSVVPSPKVSDTVV
                  :***********************.********.*. ****************************:**************:**********
                   B3                    H3                  B4                  H4                B5
Human TUBB3   181 EPYNATLSIHQLVENTDETYCIDNEALYDICFRTLKLATPTYGDLNHLVSATMSGVTTSLRFPGQLNADLRKLAVNMVPFPRLHFFMPGF 270
Human TUBB2B      EPYNATLSVHQLVENTDETYCIDNEALYDICFRTLKLTTPTYGDLNHLVSATMSGVTTCLRFPGQLNADLRKLAVNMVPFPRLHFFMPGF
C.elegans MEC-7   EPYNATLSVHQLVENTDSTFCIDNEALYDICFRTLKLTTPTYGDLNHLVSATMSGVTTCLRFPGQLNADLRKLAVNMVPFPRLHFFMPGF
                  ********:********.*:*****************:********************.******************************
                      H5          B6    H6                  H7                  H8          B7
Human TUBB3   271 APLTARGSQQYRALTVPELTQQMFDAKNMMAACDPRHGRYLTVATVFRGRMSMKEVDEQMLAIQSKNSSYFVEWIPNNVKVAVCDIPPRG 360
Human TUBB2B      APLTSRGSQQYRALTVPELTQQMFDSKNMMAACDPRHGRYLTVAAIFRGRMSMKEVDEQMLNVQNKNSSYFVEWIPNNVKTAVCDIPPRG
C.elegans MEC-7   APLTSRSNQQYRAITVPELTQQCFDAKNMMAACDPRHGRYLTAAAIFRGRMSMKEVDEQMLNIQNKNSSYFVDWIPNNVKTAVCDIPPRG
                  ****:*..*****:******** **:****************.*::*************** :*.*******:*******.*********
                                H9                  B8                  H10                 B9
Human TUBB3   361 LKMSSTFIGNSTAIQELFKRISEQFTAMFRRKAFLHWYTGEGMDEMEFTEAESNMNDLVSEYQQYQDATAEEEGEMYEDDEEESEAQGPK 450
Human TUBB2B      LKMSATFIGNSTAIQELFKRISEQFTAMFRRKAFLHWYTGEGMDEMEFTEAESNMNDLVSEYQQYQDATADEQGEFEEEEGEDEA----- 445
C.elegans MEC-7   LKMSATFIGNSTAIQELFKRISEQFTAMFRRKAFLHWYTGEGMDEMEFTEAESNMNDLVSEYQQYQEAAADEDAAEA-FDGE-------- 441
                  ****:*************************************************************:*:*:*:.     : *
                       B10           H11                                 H12
```

B

```
Human TUBA1A     1 MRECISIHVGQAGVQIGNACWELYCLEHGIQPDGQMPSDKTIGGGDDSFNTFFSETGAGKHVPRAVFVDLEPTVIDEVRTGTYRQLFHPE 90
C.elegans MEC-12  MREVISIHIGQAGVQIGNACWELYCLEHGIQPDGQMPSDKSLGGSDDSFSTFFSETGSGRHVPRAVMVDLEPTVIDEIRTGTYRSLFHPE
                  *** ****:*********************************::**.****.*******:*:******:***********:******.*****
                   B1            H1                                                B2        H2
human TUBA1A    91 QLITGKEDAANNYARGHYTIGKEIIDLVLDRIRKLADQCTGLQGFLVFHSFGGGTGSGFTSLLMERLSVDYGKKSKLEFSIYPAPQVSTA 180
C.elegans MEC-12  QLITGKEDAANNYARGHYTIGKEIIDLTLDRIRRLADNCTGLQGFLVFHSFGGGTGSGFTSLLMERLSVDYGKKAKLEFSIYPAPQVSTA
                  ****************************.*****:***:*************************************:***************
                   B3                    H3                  B4                  H4                B5
human TUBA1A   181 VVEPYNSILTTHTTLEHSDCAFMVDNEAIYDICRRNLDIERPTYTNLNRLIGQIVSSITASLRFDGALNVDLTEFQTNLVPYPRIHFPLA 270
C.elegans MEC-12  VVEPYNSILTTHTTLEHSDCSFMVDNEAIYDICRRNLDIERPSYTNLNRLIGQIVSSITASLRFDGALNVDLTEFQTNLVPYPRIHFPLA
                  ********************:*********************:**********************************************
                      H5          B6    H6                  H7                  H8          B7
human TUBA1A   271 TYAPVISAEKAYHEQLSVAEITNACFEPANQMVKCDPRHGKYMACCLLYRGDVVPKDVNAAIATIKTKRTIQFVDWCPTGFKVGINYQPP 360
C.elegans MEC-12  TFSPVISAEKAYHEQLSVAEITNMCFEPHNQMVKCDPRHGKYMAVCLLFRGDVVPKDVNAAIATIKTKRSIQFVDWCPTGFKVGINYQPP
                  *::******************** **** *************** ***:*********************:********************
                                H9                  B8                  H10                 B9
human TUBA1A   361 TATPNSQLATVDRAVCMLSNTTSIAEAWKRIDRKFDLMYAKRAFVHWYVGEGMEEGEFTEAREDLAALERDYIEVGADSYAEEEEF---- 451
C.elegans MEC-12  TVVPGGDLAKVPRAVCMLSNTTAIAEAWARLDHKFDLMYAKRAFVHWYVGEGMEEGEFSEAREDLAALEKDYEEVGVDSMEDNGEE-GDEY 450
                  *********** ******************************************************:**************:* :*** *:**
                       B10           H11                                 H12
```

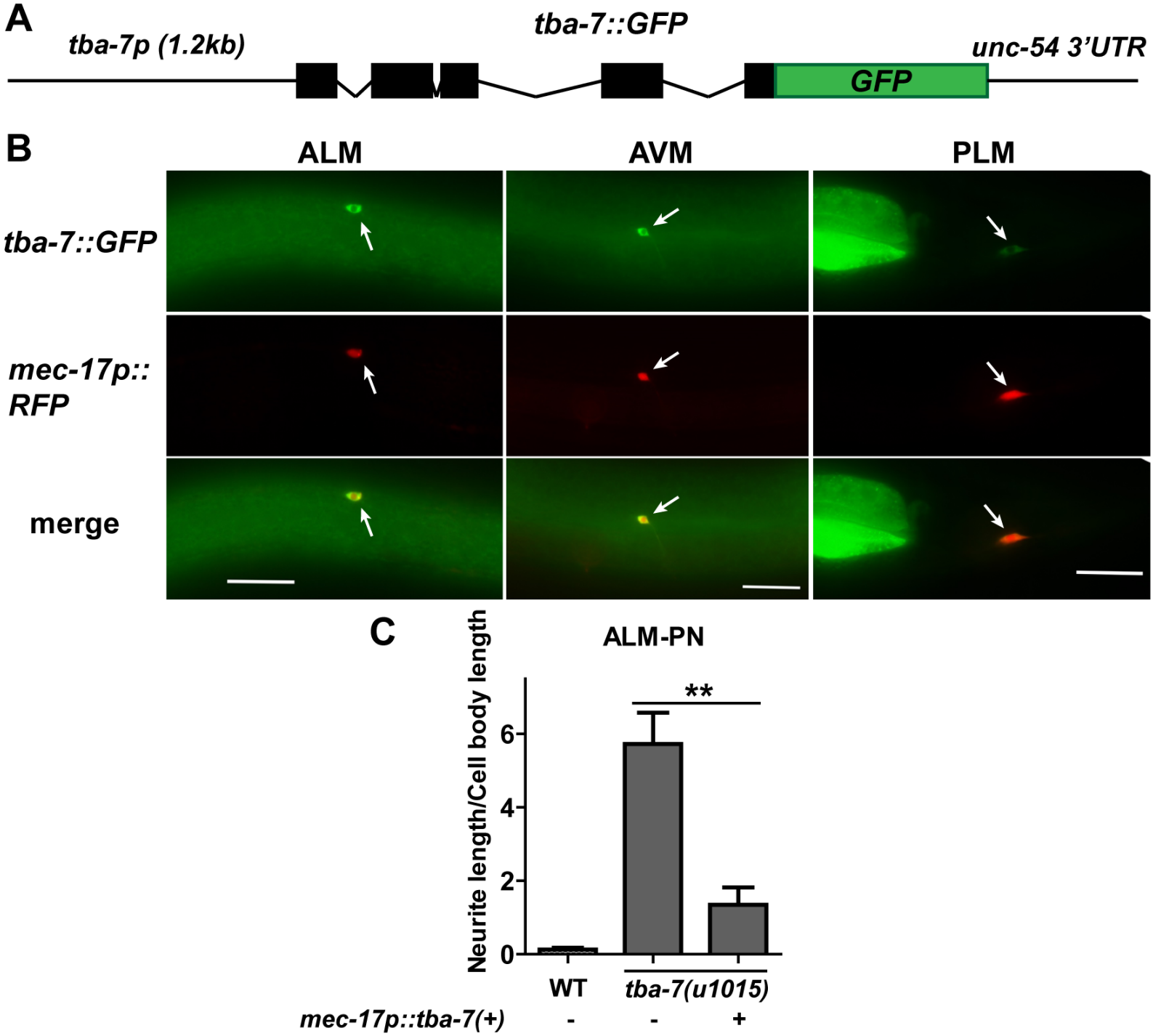
A
tba-7p (1.2kb)
tba-7::GFP
unc-54 3'UTR
GFP
B
ALM
AVM
PLM
tba-7::GFP
mec-17p::
RFP
merge
C
ALM-PN
Neurite length/Cell body length
**
0
2
4
6
WT
tba-7(u1015)
mec-17p::tba-7(+)
-
-
+

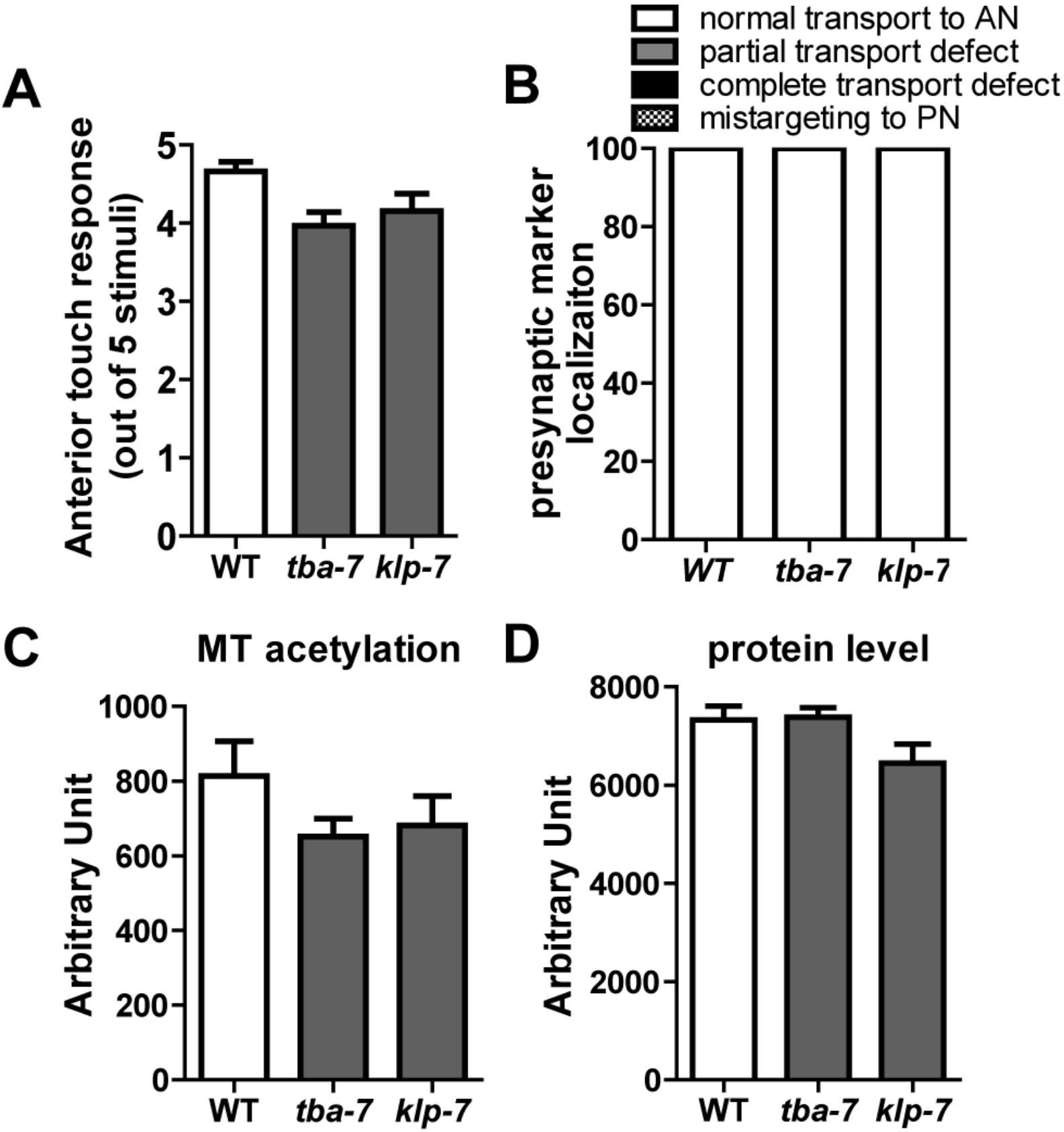
A
Anterior touch response (out of 5 stimuli)
5
4
3
2
1
0
WT
tba-7
klp-7
B
normal transport to AN
partial transport defect
complete transport defect
mistargeting to PN
presynaptic marker localizaiton
100
80
60
40
20
0
WT
tba-7
klp-7
C
MT acetylation
Arbitrary Unit
1000
800
600
400
200
0
WT
tba-7
klp-7
D
protein level
Arbitrary Unit
8000
6000
4000
2000
0
WT
tba-7
klp-7

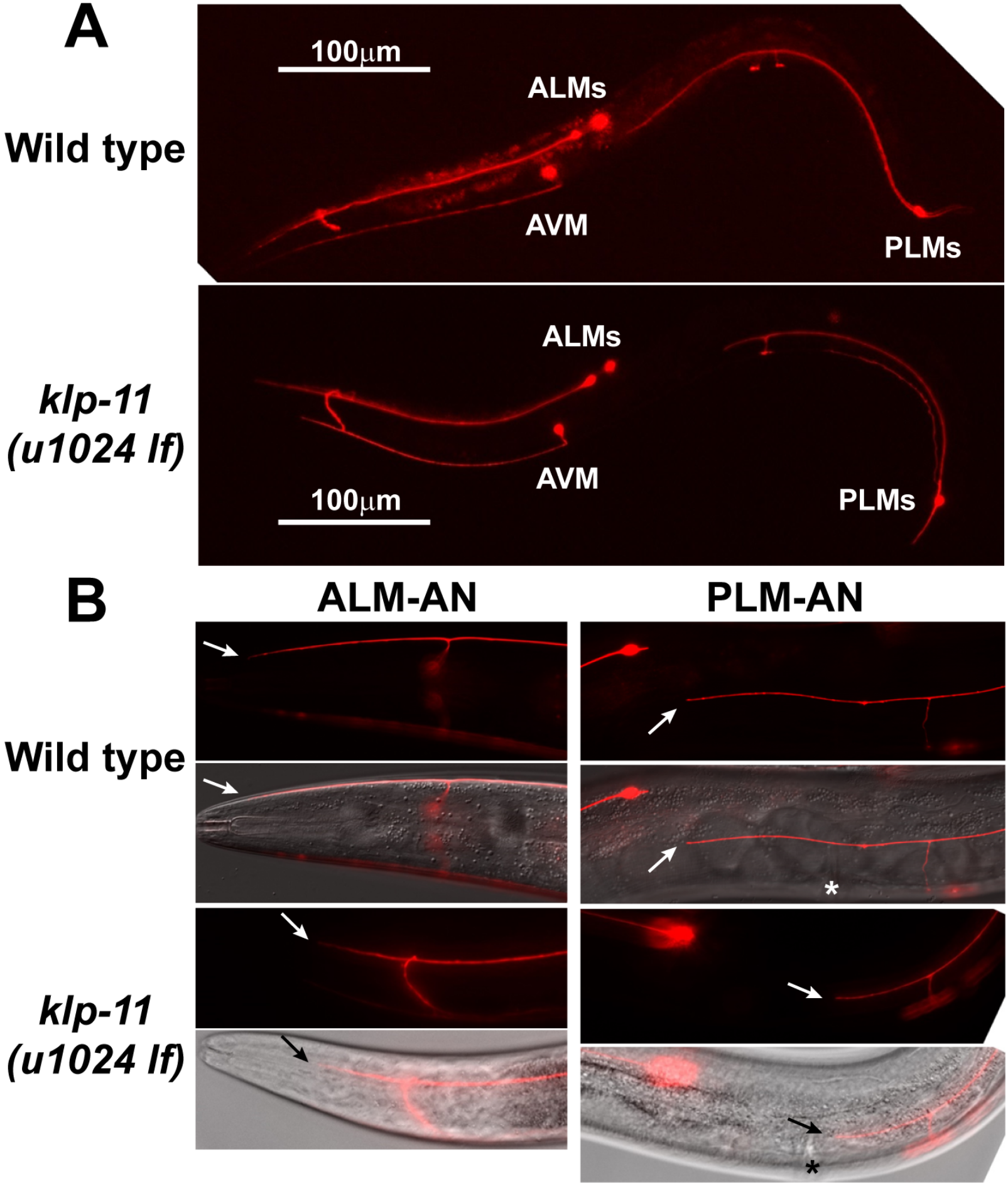
A
Wild type
100μm
ALMs
AVM
PLMs
klp-11
(u1024 lf)
ALMs
AVM
100μm
PLMs
B
ALM-AN
PLM-AN
Wild type
klp-11
(u1024 lf)
*
*

A

```
TBA-8     --MPSDGRECVSIHIGQAGAQIGNACWELYCIEHGLDEAGFLKEEEK-NKKQQSLQAFFS   57
TBA-6     MPQYKGSREVISIHVGQAGVQIGNACWELFCLEHGIQPDGYHVEDDTYDEETETINTFFA   60
TBA-5     ------MREIVSIHIGQAGVQIGNACWELYCLEHGITPDGLMPDDTSYGVEDQSYNTFFS   54
TBA-9     -MVNNRSREVISIHVGQAGVQMGNACWELYCLEHGIQPDGMINEEDSLGVDDDSFNTFFS   59
TBA-7     ------MREVISIHVGQAGVQIGNACWELYCLEHGILPDGTSME---PDGNSGSLGTFFS   51
MEC-12    ------MREVISIHIGQAGVQIGNACWELYCLEHGIQPDGQMPSDKSLGGSDDSFSTFFS   54
TBA-4     ------MREVISIHVGQAGVQIGNACWELYCLEHGIQPDGTMPSEQQNEG--GSFTTFFS   52
TBA-1     -MFVFNMREVISIHVGQAGVQIGNACWELYCLEHGIQPDGTMPSDQQADG--ESFTTFFS   57
TBA-2     ------MREVISIHVGQAGVQIGNACWELYCLEHGIQPDGTMPTQSTNEG--ESFTTFFS   52
                ** :***:****.*:*******:*:***:   *             :  :**:

TBA-8     EGEFMEARDDLAALEKDYAEVSRDTADLEEENDEF---------    452
TBA-6     EGEFSEAREDMAALEKDYEEIGEDELPDDIDDQSYRGRSSGSRY    464
TBA-5     EGEFSEAREDMAALEKDYEEVGVDSFDPNDEEY-----------    447
TBA-9     EGEFSEAREDLAALEKDYEEVGLDAGEPDEEDD-------YSHY    456
TBA-7     EGEFSEAREDLAALEKDYEEVGADSDANDNG---------DDEY    444
MEC-12    EGEFSEAREDLAALEKDYEEVGVDSMEDNG-EE-------GDEY    450
TBA-4     EGEFTEAREDLAALEKDYEEVGADSNEGL-EED-------GEEY    448
TBA-1     EGEFTEAREDLAALEKDYEEVGADSNEGGNEEE-------GEEY    454
TBA-2     EGEFTEAREDLAALEKDYEEVGADSNEGGEE-E-------GEEY    448
          **** ***:*:******* *:. *
```

B

```
TUBAL3    MRECLSIHIGQAGIQIGDACWELYCLEHGIQPNGVVLDTQQDQLENAKMEHTNASFDTFF   60
TUBA8     MRECISVHVGQAGVQIGNACWELFCLEHGIQADGTFDAQ-------ASKINDDDSFTTFF   53
TUBA3C    MRECISIHVGQAGVQIGNACWELYCLEHGIQPDGQMPSD-------KTIGGGDDSFNTFF   53
TUBA3D    MRECISIHVGQAGVQIGNACWELYCLEHGIQPDGQMPSD-------KTIGGGDDSFNTFF   53
TUBA3E    MRECISIHVGQAGVQIGNACWELYCLEHGIQPDGQMPSD-------KTIGGGDDSFNTFF   53
TUBA4A    MRECISVHVGQAGVQMGNACWELYCLEHGIQPDGQMPSD-------KTIGGGDDSFTTFF   53
TUBA1A    MRECISIHVGQAGVQIGNACWELYCLEHGIQPDGQMPSD-------KTIGGGDDSFNTFF   53
TUBA1B    MRECISIHVGQAGVQIGNACWELYCLEHGIQPDGQMPSD-------KTIGGGDDSFNTFF   53
TUBA1C    MRECISIHVGQAGVQIGNACWELYCLEHGIQPDGQMPSD-------KTIGGGDDSFNTFF   53
          *** :*:*:****:*:*:*****:******  :*                  . *: ***

TUBAL3    EEAEFLEAREDLAALERDYEEVAQSF------------     446
TUBA8     EEGEFSEAREDLAALEKDYEEVGTDSFEEENE--GEEF     449
TUBA3C    EEGEFSEAREDLAALEKDYEEVGVDSVEAEAEEG-EEY     450
TUBA3D    EEGEFSEAREDLAALEKDYEEVGVDSVEAEAEEG-EEY     450
TUBA3E    EEGEFSEAREDLAALEKDCEEVGVDSVEAEAEEG-EAY     450
TUBA4A    EEGEFSEAREDMAALEKDYEEVGIDSYEDEDEGEE---     448
TUBA1A    EEGEFSEAREDMAALEKDYEEVGVDSVEGEGEEEGEEY     451
TUBA1B    EEGEFSEAREDMAALEKDYEEVGVDSVEGEGEEEGEEY     451
TUBA1C    EEGEFSEAREDMAALEKDYEEVGADSADGE--DEGEEY     449
          **.** *****:****:* ***. .
```

Supplemental Tables

	Gene name	Allele name	Phenotype	Recessivity	Penetr-ance	Molecular Lesion	Reference
i	Mutations resulting in the absence of TRN maker						
	lin-32	*u909*	Lack of PLM, AVM, and PVM labeling	recessive	58%		Mitani et al., 1993
	cdk-4	*u948*	Lack of PLM, AVM, and PVM labeling	recessive	88%	Q18*	
	mec-4	*u947; u972*	Degeneration of TRNs	recessive	35% *(u947)*	A513T	
		u951	Degeneration of TRNs	dominant	65%	A713T	Driscoll and Chalfie, 1991
	mec-10	*u1025*	Degeneration of TRNs	recessive	10%	G312R	
ii	Mutations resulting in the expression of TRN markers in extra cells						
	egl-46	*u945*	Expression of TRN marker in FLPs	recessive	65%		Wu et al., 2001
	egl-44	*u965*	Expression of TRN marker in FLPs	recessive	79%		Wu et al., 2001
	pag-3	*u920; u949; u961*	Expression of TRN marker in BDUs	recessive	90% (*u920*)		Jia et al., 1996
	egl-13	*u964*	Expression of TRN marker in A/PQRs	recessive	68%	H389Y	Feng et al., 2013
iii	Mutations resulting in developmental defects in AVM/PVM						
	egl-20	*u999*	PVM is mispositioned anteriorly	recessive	82%	V92D	Harris et al., 1996
	unc-6	*u1018*	Ventral guidance defects for AVM neurites	recessive	61%	C346Y	Hedgecock et al., 1990

Table S1. Mutations that affect the expression pattern of TRN marker or the development of the postembryonic AVM and PVM cells. References indicate that similar mutant phenotypes for the gene were previously reported. *cdk-4* was not previously known to affect TRN development. Although they each have the same underlying defect, *u947* and *u972* were independently isolated. These two alleles and *mec-10(u1025)* identify novel changes that cause TRN degeneration.

	Gene name	Allele name	Recessivity	Penet-rance	Molecular Lesion	Reference
A	Mutations that shorten all TRN neurites					
	mec-7	*u910*	dominant	100%	P356L	
		u911	dominant		P171S	
		u955	dominant		A352T	
		u956	dominant		P358L	
		u957	dominant		P171L	
		u958	dominant		G244S	
	unc-51	*u1000*	recessive	80%	E188K	Du and Chalfie, 2001
B	Mutations that shorten the PLM-PN					
	mec-7	*u1020*	recessive		G34S	
	mec-12	*u1019*	dominant		G354E	
		u950	recessive		S140F	
		u1016	recessive		E97K	
		u1021	recessive		G144S	
	dsh-1	*u915*	recessive	95%	R165Stop	Zheng et al., 2015a
		u952	recessive		G512R	
		u953	recessive		R103Stop	
	tiam-1	*u914*	recessive	98%	R570Stop	Zheng et al., 2016
		u1003	recessive			
		u1004	recessive		R420Stop	
		u1005	recessive		Q846Stop	
		u1012	recessive		Q266Stop	
	egl-5	*u918; u966*	recessive	100%		Zheng et al., 2015b
	mua-3	*u973*	recessive	45%	C2191Y	
	sup-26	*u916*	recessive	81%	G95Stop	
C	Mutations that result in an ectopic ALM-PN					
	mec-12	*u917*	recessive	38%	V260I	
	mec-7	*u1017*	recessive	83%	L377F	
	tba-7	*u1015*	recessive	79%	G92D	
D	Mutations that shorten PLM-AN and elongate PLM-PN					
	lin-44	*u905; u906; u907; u959*	recessive	90% *(u905)*		Hilliard and Bargmann, 2006; Zheng et al., 2015a
	lin-17	*u919; u960; u962; u963*	recessive	75% *(u919)*		Hilliard and Bargmann, 2006; Zheng et al., 2015a
E	Mutations that shorten both PLM-AN and PLM-PN					
	mec-15	*u1008*	recessive	83%	Q194Stop	
F	Mutations that shorten ALM-AN and PLM-AN					
	unc-73	*u908*	recessive	85%	E1212K	Du and Chalfie, 2001; Zheng et al., 2016
	unc-53	*u913*	recessive	90%	Q261Stop	Hekimi and Kershaw, 1993
		u912; u946; u967; u968; u969; u970; u971; u974	recessive			
	klp-11	*u1024*	recessive	79%	Q53Stop	
G	Mutations that shorten ALM-AN but not PLM-AN					
	unc-23	*u1022*	recessive	82%	Q132Stop	

Table S2 Mutations that cause neurite outgrowth or guidance defects in TRNs. References indicate that the similar mutant phenotypes for the gene were either previously reported or we extensively characterized the mutants elsewhere.

Gene	**Allele**	**TRN morphology**
tba-1	*ok1123*	Normal
tba-1	*ok1135*	Normal
tba-1	*or346*	Normal
tba-1	*or594*	Normal
tba-2	*sb51*	Normal
tba-2	*sb25*	Normal
tba-5	*tm4200*	Normal
tba-7	*gk787939*	Ectopic ALM-PN
tba-7	*u1015*	Ectopic ALM-PN
tba-8	*tm4359*	Normal
tba-9	*ok1858*	Normal
ben-1	*e1880*	Normal
tbb-1	*gk207*	Normal
tbb-2	*t1623*	Normal
tbb-2	*gk130*	Normal
tbb-4	*sa127*	Normal
tbb-4	*ok1461*	Normal
tbb-6	*tm2004*	Normal

Table S3. Loss-of-function alleles of α and β tubulin genes (other than *mec-12* and *mec-7*) and their effects on TRN morphology.

Gene name	Mutation	Structural function	Corpus Callosum	Reference
TUBA1A	I5L	Tubulin folding	hypoplastic CC	Jansen et al., 2011
	E55K	Lumen-facing loop	partial ACC	Morris-Rosendahl et al., 2008
	T56M	Lumen-facing loop	complete ACC	Bahi-Buisson et al., 2014
	L70S	GTP binding	complete ACC	Cushion et al., 2013
	P72S	Intradimer interaction	hypoplastic CC	Bahi-Buisson et al., 2014
	L92V	Lumen-facing loop	complete ACC	Kumar et al., 2010
	N101S	GTP binding	complete ACC	Bahi-Buisson et al., 2014
	E113K	Lateral interaction	Normal	Bahi-Buisson et al., 2014
	R123C	Lateral interaction	Normal	Bahi-Buisson et al., 2014
	V137D	Tubulin folding	partial ACC	Kumar et al., 2010
	S158L	Tubulin folding	complete ACC	Bahi-Buisson et al., 2014
	Y161H	Lateral interaction	hypoplastic CC	Poirier et al., 2013
	I188L	Tubulin folding	partial ACC	Poirier et al., 2007
	Y210C	Intradimer interaction	hypoplastic CC	Jansen et al., 2011
	R214H	Intradimer interaction	complete ACC	Bahi-Buisson et al., 2014
	D218Y	Intradimer interaction	complete ACC	Kumar et al., 2010
	I219V	Intradimer interaction	partial ACC	Oegema et al., 2015
	V235L	Tubulin folding	hypoplastic CC	Poirier et al., 2013
	I238V	Tubulin folding	complete ACC	Fallet-Bianco et al., 2008
	D249H	Longitudinal interaction	complete ACC	Poirier et al., 2007
	P263T	MAP binding	complete ACC	Fallet-Bianco et al., 2008
	R264H	MAP binding	complete ACC	Bahi-Buisson et al., 2014
	R264C	MAP binding	Normal	Poirier et al., 2007
	A270T	Tubulin folding	complete ACC	Kumar et al., 2010
	L286F	Lateral interaction	complete ACC	Fallet-Bianco et al., 2008
	V303G	Tubulin folding	partial ACC	Lecourtois et al. 2010
	R320H	Tubulin folding	partial ACC	Bahi-Buisson et al., 2014
	K326N	Longitudinal interaction	complete ACC	Bahi-Buisson et al., 2014
	N329S	Longitudinal interaction	complete ACC	Kumar et al., 2010
	A333V	Longitudinal interaction	hypoplastic CC	Cushion et al., 2013
	V353I	Longitudinal interaction	partial ACC	Bahi-Buisson et al., 2014
	G366R	Lumen-facing loop	partial ACC	Okumura et al. 2013
	A369T	Lumen-facing loop	hypoplastic CC	Bahi-Buisson et al., 2014
	V371E	Lumen-facing loop	complete ACC	Bahi-Buisson et al., 2014
	M377V	Tubulin folding	partial ACC	Kumar et al., 2010
	A387V	MAP binding	hypoplastic CC	Romaniello et al., 2012
	R390C	MAP binding	complete ACC	Kumar et al., 2010
	R390H	MAP binding	partial ACC	Zanni et al. 2013
	D396Y	MAP binding	partial ACC	Bahi-Buisson et al., 2014
	L397P	MAP binding	partial ACC	Bahi-Buisson et al., 2008
	R402L	MAP binding	mild hypoplastic CC	Sohal et al., 2012
	R402C	MAP binding	normal	Kumar et al., 2010
	R402H	MAP binding	normal	Kumar et al., 2010
	V409A	MAP binding	complete ACC	Bahi-Buisson et al., 2014
	V409I	MAP binding	hypoplastic CC	Bahi-Buisson et al., 2014
	S419L	MAP binding	partial ACC	Poirier et al., 2007
	R422H	MAP binding	partial ACC	Kumar et al., 2010

	R422C	MAP binding	hypoplastic CC	Bahi-Buisson et al., 2008
	M425K	MAP binding	complete ACC	Kumar et al., 2010
	E429Q	MAP binding	complete ACC	Bahi-Buisson et al., 2014
	G436R	MAP binding	hypoplastic CC	Bahi-Buisson et al., 2008
TUBB2B	G13A	Tubulin folding	normal	Oegema et al., 2015
	G98R	GTP binding	complete ACC	Cushion et al., 2013
	L117P	Tubulin folding	normal	Guerrini et al., 2012
	G140A	GTP binding	complete ACC	Romaniello et al., 2012
	P171T	GTP binding	partial ACC	Bahi-Buisson et al., 2014
	S172P	GTP binding	complete ACC	Jaglin et al., 2009
	P173L	GTP binding	complete ACC	Bahi-Buisson et al., 2014
	I202T	Tubulin folding	partial ACC	Bahi-Buisson et al., 2014
	L207P	Tubulin folding	complete ACC	Cushion et al., 2013
	I210T	Tubulin folding	partial ACC	Jaglin et al., 2009
	L228P	Tubulin folding	complete ACC	Jaglin et al., 2009
	C239F	Intradimer interaction	complete ACC	Bahi-Buisson et al., 2014
	R241H	Intradimer interaction	normal	Bahi-Buisson et al., 2014
	A248T	Intradimer interaction	normal	Bahi-Buisson et al., 2014
	D249H	Intradimer interaction	complete ACC	Bahi-Buisson et al., 2014
	N256S	Intradimer interaction	hypoplastic CC	Guerrini et al., 2012
	F265L	Tubulin folding	partial ACC	Jaglin et al., 2009
	S278G	Lateral interaction	partial ACC	Bahi-Buisson et al., 2014
	T312M	Tubulin folding	hypoplastic CC	Jaglin et al., 2009
	G369V	Lumen-facing loop	partial ACC	Bahi-Buisson et al., 2014
	R380S	MAP binding	complete ACC	Cushion et al., 2013
	R380C	MAP binding	complete ACC	Cushion et al., 2013
	R380L	MAP binding	complete ACC	Amrom et al., 2014
	D417N	MAP binding	normal	Guerrini et al., 2012
TUBB3	R46G	Intradimer interaction	hypoplastic CC	Bahi-Buisson et al., 2014
	R62Q	Tubulin folding	normal	Tischfield et al., 2010
	G71R	Tubulin folding	partial ACC	Whitman et al., 2016
	G82R	Tubulin folding	partial ACC	Poirier et al., 2010
	G98S	Longitudinal interaction	hypoplastic CC	Whitman et al., 2016
	T178M	GTP binding	complete ACC	Poirier et al., 2010
	E205K	Tubulin folding	hypoplastic CC	Poirier et al., 2010
	R262C	MAP binding	partial ACC	Tischfield et al., 2010
	R262H	MAP binding	partial ACC	Tischfield et al., 2010
	E288K	Lateral interaction	hypoplastic CC	Oegema et al., 2015
	A302T	MAP binding	partial ACC	Tischfield et al., 2010
	A302V	MAP binding	hypoplastic CC	Poirier et al., 2010
	M323V	Intradimer interaction	partial ACC	Poirier et al., 2010
	P357L	Tubulin folding	normal	Oegema et al., 2015
	R380C	MAP binding	partial ACC	Tischfield et al., 2010
	M388V	MAP binding	complete ACC	Poirier et al., 2010
	E410K	MAP binding	partial ACC	Tischfield et al., 2010
	D417N	MAP binding	partial ACC	Tischfield et al., 2010
	D417H	MAP binding	N/A	Tischfield et al., 2010

Table S4. Missense mutations in human α and β tubulins that caused neurological disorders in heterozygous patients. 51 TUBA1A, 24 TUBB2B, and 19 TUBB3B mutations are listed. The mutated amino acids were mapped to the structural domains of α/β heterodimer and their potential structural functions were assigned according to Tischfield *et al.* (2011). Residues located in the interior of the structure were generally assigned to the category of "tubulin folding." Effects on the corpus callosum (CC) were used as an indicator of defects in axon growth and guidance. These phenotypes were extracted from the cited literature. ACC stands for agenesis of the corpus callosum.

References

Amrom D, Tanyalcin I, Verhelst H, Deconinck N, Brouhard GJ, Decarie JC, Vanderhasselt T, Das S, Hamdan FF, Lissens W et al. 2014. Polymicrogyria with dysmorphic basal ganglia? Think tubulin! *Clin Genet* **85**: 178-183.

Bahi-Buisson N, Poirier K, Boddaert N, Saillour Y, Castelnau L, Philip N, Buyse G, Villard L, Joriot S, Marret S et al. 2008. Refinement of cortical dysgeneses spectrum associated with TUBA1A mutations. *J Med Genet* **45**: 647-653.

Bahi-Buisson N, Poirier K, Fourniol F, Saillour Y, Valence S, Lebrun N, Hully M, Bianco CF, Boddaert N, Elie C et al. 2014. The wide spectrum of tubulinopathies: what are the key features for the diagnosis? *Brain* **137**: 1676-1700.

Cushion TD, Dobyns WB, Mullins JG, Stoodley N, Chung SK, Fry AE, Hehr U, Gunny R, Aylsworth AS, Prabhakar P et al. 2013. Overlapping cortical malformations and mutations in TUBB2B and TUBA1A. *Brain* **136**: 536-548.

Driscoll M, Chalfie M. 1991. The mec-4 gene is a member of a family of Caenorhabditis elegans genes that can mutate to induce neuronal degeneration. *Nature* **349**: 588-593.

Du H, Chalfie M. 2001. Genes regulating touch cell development in Caenorhabditis elegans. *Genetics* **158**: 197-207.

Fallet-Bianco C, Loeuillet L, Poirier K, Loget P, Chapon F, Pasquier L, Saillour Y, Beldjord C, Chelly J, Francis F. 2008. Neuropathological phenotype of a distinct form of lissencephaly associated with mutations in TUBA1A. *Brain* **131**: 2304-2320.

Feng G, Yi P, Yang Y, Chai Y, Tian D, Zhu Z, Liu J, Zhou F, Cheng Z, Wang X et al. 2013. Developmental stage-dependent transcriptional regulatory pathways control neuroblast lineage progression. *Development* **140**: 3838-3847.

Guerrini R, Mei D, Cordelli DM, Pucatti D, Franzoni E, Parrini E. 2012. Symmetric polymicrogyria and pachygyria associated with TUBB2B gene mutations. *Eur J Hum Genet* **20**: 995-998.

Harris J, Honigberg L, Robinson N, Kenyon C. 1996. Neuronal cell migration in C. elegans: regulation of Hox gene expression and cell position. *Development* **122**: 3117-3131.

Hedgecock EM, Culotti JG, Hall DH. 1990. The unc-5, unc-6, and unc-40 genes guide circumferential migrations of pioneer axons and mesodermal cells on the epidermis in C. elegans. *Neuron* **4**: 61-85.

Hekimi S, Kershaw D. 1993. Axonal guidance defects in a Caenorhabditis elegans mutant reveal cell-extrinsic determinants of neuronal morphology. *The Journal of neuroscience : the official journal of the Society for Neuroscience* **13**: 4254-4271.

Hilliard MA, Bargmann CI. 2006. Wnt signals and frizzled activity orient anterior-posterior axon outgrowth in C. elegans. *Developmental cell* **10**: 379-390.

Jaglin XH, Poirier K, Saillour Y, Buhler E, Tian G, Bahi-Buisson N, Fallet-Bianco C, Phan-Dinh-Tuy F, Kong XP, Bomont P et al. 2009. Mutations in the beta-tubulin gene TUBB2B result in asymmetrical polymicrogyria. *Nat Genet* **41**: 746-752.

Jansen AC, Oostra A, Desprechins B, De Vlaeminck Y, Verhelst H, Regal L, Verloo P, Bockaert N, Keymolen K, Seneca S et al. 2011. TUBA1A mutations: from isolated lissencephaly to familial polymicrogyria. *Neurology* **76**: 988-992.

Jia Y, Xie G, Aamodt E. 1996. pag-3, a Caenorhabditis elegans gene involved in touch neuron gene expression and coordinated movement. *Genetics* **142**: 141-147.

Kumar RA, Pilz DT, Babatz TD, Cushion TD, Harvey K, Topf M, Yates L, Robb S, Uyanik G, Mancini GM et al. 2010. TUBA1A mutations cause wide spectrum lissencephaly (smooth brain) and suggest that multiple neuronal migration pathways converge on alpha tubulins. *Hum Mol Genet* **19**: 2817-2827.

Lecourtois M, Poirier K, Friocourt G, Jaglin X, Goldenberg A, Saugier-Veber P, Chelly J, Laquerriere A. 2010. Human lissencephaly with cerebellar hypoplasia due to mutations in TUBA1A: expansion of the foetal neuropathological phenotype. *Acta Neuropathol* **119**: 779-789.

Mitani S, Du H, Hall DH, Driscoll M, Chalfie M. 1993. Combinatorial control of touch receptor neuron expression in Caenorhabditis elegans. *Development* **119**: 773-783.

Morris-Rosendahl DJ, Najm J, Lachmeijer AM, Sztriha L, Martins M, Kuechler A, Haug V, Zeschnigk C, Martin P, Santos M et al. 2008. Refining the phenotype of alpha-1a Tubulin (TUBA1A) mutation in patients with classical lissencephaly. *Clin Genet* **74**: 425-433.

Oegema R, Cushion TD, Phelps IG, Chung SK, Dempsey JC, Collins S, Mullins JG, Dudding T, Gill H, Green AJ et al. 2015. Recognizable cerebellar dysplasia associated with mutations in multiple tubulin genes. *Hum Mol Genet* **24**: 5313-5325.

Okumura A, Hayashi M, Tsurui H, Yamakawa Y, Abe S, Kudo T, Suzuki R, Shimizu T, Shimojima K, Yamamoto T. 2013. Lissencephaly with marked ventricular dilation, agenesis of corpus callosum, and cerebellar hypoplasia caused by TUBA1A mutation. *Brain Dev* **35**: 274-279.

Poirier K, Keays DA, Francis F, Saillour Y, Bahi N, Manouvrier S, Fallet-Bianco C, Pasquier L, Toutain A, Tuy FP et al. 2007. Large spectrum of lissencephaly and pachygyria phenotypes resulting from de novo missense mutations in tubulin alpha 1A (TUBA1A). *Hum Mutat* **28**: 1055-1064.

Poirier K, Saillour Y, Bahi-Buisson N, Jaglin XH, Fallet-Bianco C, Nabbout R, Castelnau-Ptakhine L, Roubertie A, Attie-Bitach T, Desguerre I et al. 2010. Mutations in the neuronal ss-tubulin subunit TUBB3 result in malformation of cortical development and neuronal migration defects. *Hum Mol Genet* **19**: 4462-4473.

Poirier K, Saillour Y, Fourniol F, Francis F, Souville I, Valence S, Desguerre I, Marie Lepage J, Boddaert N, Line Jacquemont M et al. 2013. Expanding the spectrum of TUBA1A-related cortical dysgenesis to Polymicrogyria. *Eur J Hum Genet* **21**: 381-385.

Romaniello R, Tonelli A, Arrigoni F, Baschirotto C, Triulzi F, Bresolin N, Bassi MT, Borgatti R. 2012. A novel mutation in the beta-tubulin gene TUBB2B associated with complex malformation of cortical development and deficits in axonal guidance. *Dev Med Child Neurol* **54**: 765-769.

Sohal AP, Montgomery T, Mitra D, Ramesh V. 2012. TUBA1A mutation-associated lissencephaly: case report and review of the literature. *Pediatr Neurol* **46**: 127-131.

Tischfield MA, Baris HN, Wu C, Rudolph G, Van Maldergem L, He W, Chan WM, Andrews C, Demer JL, Robertson RL et al. 2010. Human TUBB3 mutations perturb microtubule dynamics, kinesin interactions, and axon guidance. *Cell* **140**: 74-87.

Tischfield MA, Cederquist GY, Gupta ML, Jr., Engle EC. 2011. Phenotypic spectrum of the tubulin-related disorders and functional implications of disease-causing mutations. *Curr Opin Genet Dev* **21**: 286-294.

Whitman MC, Andrews C, Chan WM, Tischfield MA, Stasheff SF, Brancati F, Ortiz-Gonzalez X, Nuovo S, Garaci F, MacKinnon SE et al. 2016. Two unique TUBB3 mutations cause both CFEOM3 and malformations of cortical development. *Am J Med Genet A* **170A**: 297-305.

Wu J, Duggan A, Chalfie M. 2001. Inhibition of touch cell fate by egl-44 and egl-46 in C. elegans. *Genes & development* **15**: 789-802.

Zanni G, Colafati GS, Barresi S, Randisi F, Talamanca LF, Genovese E, Bellacchio E, Bartuli A, Bernardi B, Bertini E. 2013. Description of a novel TUBA1A mutation in Arg-390 associated with asymmetrical polymicrogyria and mid-hindbrain dysgenesis. *Eur J Paediatr Neurol* **17**: 361-365.

Zheng C, Diaz-Cuadros M, Chalfie M. 2015a. Dishevelled attenuates the repelling activity of Wnt signaling during neurite outgrowth in Caenorhabditis elegans. *Proceedings of the National Academy of Sciences of the United States of America* **112**: 13243-13248.

-. 2015b. Hox Genes Promote Neuronal Subtype Diversification through Posterior Induction in Caenorhabditis elegans. *Neuron* **88**: 514-527.

-. 2016. GEFs and Rac GTPases control directional specificity of neurite extension along the anterior-posterior axis. *Proceedings of the National Academy of Sciences of the United States of America* **113**: 6973-6978.